EUKARYOTIC FLAGELLAR ASSEMBLY: INSIGHTS LEARNED FROM INTRAFLAGELLAR TRANSPORT (IFT) AND SMALL GTPASE ARL3

A Dissertation

by

XUE JIANG

Submitted to the Office of Graduate and Professional Studies of
Texas A&M University
in partial fulfillment of the requirements for the degree of

DOCTOR OF PHILOSOPHY

Chair of Committee,	Hongmin Qin
Committee Members,	Arne Lekven
	James Smith
	Tina Gumienny
Head of Department,	Tom McKnight

May 2017

Major Subject: Microbiology

ABSTRACT

Eukaryotic cilia/flagella are the evolutionary conserved microtubule-based organelles. Projecting away from the cell surface, they perform a variety of sensing, signaling, and motility-based functions. In humans, defective cilia lead to an array of pleiotropic disorders, which are collectively referred to as ciliopathies. The aim of my study is to identify and characterize the factors that play roles in the ciliary/flagellar assembly by using a simple model organism, *Chlamydomonas*.

This study focuses on three flagellar assembly mutants, *ift57-1*, *ift56-2*, and *arl3*, which are identified from a mutant library using a PCR-based method called restriction enzyme cassette mediated PCR. *ift57-1* and *ift56-2* carry mutations in two subunits of intraflagellar transport complex B (IFT-B), IFT57 and IFT56, respectively. In many ciliopathies, mutations have been identified in components of IFT complexes, which are mainly used for delivering cargos in and out of cilia. The *ift57-1* mutant expresses a reduced amount of IFT57 (≤5%) and assembles short motility-defective flagella with variable lengths. Although IFT57 is proposed to play an essential role in bridging two IFT-B subcomplexes, IFT-B1 and IFT-B2, our results show that IFT57 is not essential for the IFT-B assembly but rather functions to prevent IFT-B from degradation. Moreover, IFT57 may deliver specific motility-related cargos including an inner dynein arm subunit IC97. On the other hand, the null mutant *ift56*-2 possesses evenly shortened flagella. We verify that IFT56 is a *bona fide* IFT-B subunit. However, it is neither

essential for the IFT-B assembly nor for the stability. Possible reasons leading to the shorter flagellar length in *ift56* mutants, including precursor pool size, axonemal disassembly rate, and known length regulators, are explored but are found to play insignificant roles.

Recently, several small GTPases are reported to be involved in ciliogenesis. The small GTPase ARL3 mutant *arl3* presents a variety of subtle flagellar defects. The mutant cells expressing the GTP-dominant form of ARL3 possess significantly shortened flagella, indicating that GTPase activity of ARL3 is involved in flagellar length control. Previous studies propose that ARL3 is important for the flagellar transport of lipid-modified peripheral membrane proteins. Our data show that a myristoylated protein CrPKG is likely to be affected in *arl3*. Using isolated pure flagella, we found that the amount of a few hydrophobic proteins, probably membrane proteins, are altered in the *arl3* flagella, suggesting that ARL3 is involved in transport or retention of certain flagellar membrane proteins.

DEDICATION

This dissertation is dedicated to my awesome parents for their love, support, and encouragement in all my life.

This dissertation is also dedicated to my loving and caring husband for his endless love and remarkable patience.

ACKNOWLEDGMENTS

I would like to give thanks to the individuals that help me a lot during my study. First of all, I would like to thank Dr. Hongmin Qin, my supervisor, for her guidance and support. She is always there and willing to help whenever there are challenges throughout the course of my research. Her mentoring and encouragement help a lot.

I also want to thank my committee members, Dr. Tina Gumienny, Dr. Arne Lekven, and Dr. James Smith, for their guidance and support. Their valuable suggestions and encouragement are important for the dissertation completion.

Thanks to Dr. Karl Aufderheide for his help in experiments and the chance to be his teaching assistant, which I enjoyed a lot.

Thanks to Dr. Beiyan Nan, Dr. Rene Garcia, and their lab members for their assistance in some experiments.

Special thanks to the past and present lab members from Dr. Hongmin Qin's lab: Elizabeth, David, and Jie, for their valuable suggestions and for making the lab have fun. Also, I would like to thank Xinhe, Catherine, Daniel, and Jessica, who had worked with me and contributed to the project.

Thanks also go to my friends and colleagues and the department faculties and staffs for making the whole journey more easy and enjoyable.

Finally, thanks to my parents and my husband for their endless love and support.

CONTRIBUTORS AND FUNDING SOURCES

Contributors

This work was supervised by a dissertation committee consisting of Dr. Hongmin Qin, and Drs. Arne Lekven and James Smith of the Department of Biology and Dr. Tina Gumienny of the Department of Biology at Texas Women's University.

The data for making Figure 3-1 E was partly conducted by Catherine Hernandez. Figure 3-9 A-D was generated by Dr. Hongmin Qin. The data for making Figure 3-10 D and E was conducted by Zhaolan Ding of the Department of Biology. Figure 5-7 B was generated by Jessica Bhandari.

All other work conducted for the dissertation was completed independently by the student.

Funding Sources

This work was made possible in part by National Science Foundation (NSF) under Grant Number MCB-0923835.

Its contents are solely the responsibility of the authors and do not necessarily represent the official views of the NSF.

NOMENCLATURE

ARL3	ADP-ribosylation factor-like 3
AtpB	Beta-subunits of ATP synthase (Anti–β-F_1-ATPase)
DIC	Differential interference contrast
GAP	GTPase activating protein
GEF	Guanine nucleotide exchange factors
IFT	Intraflagellar Transport
IFT-A	Intraflagellar Transport Complex A
IFT-B	Intraflagellar Transport Complex B
PKD2	Polycystin 2
RP2	Retinitis Pigmentosa
TAP	Tris-acetate-phosphate medium
TIRF	Total Internal Reflection Fluorescence

TABLE OF CONTENTS

Page

Page

LIST OF FIGURES

Page

Page

LIST OF VIDEOS

Video 3-1: Real-time video of the wild-type *cc125*.

Video 3-2: Real-time video of the mutant *ift57-1*.

Video 3-3: Real-time video of the rescue strain *ift57-1-rescue*.

Video 3-4: High-speed video of the wild-type cell *cc125.*

Video 3-5: High-speed video of the mutant cell *ift57-1*.

Video 3-6: High-speed video of the mutant cell *ift57-1*.

Video 3-7: High-speed video of the mutant cell *ift57-1*.

Video 3-8: Fluorescent video microscopy of KAP-GFP in flagella of *fla3-1b*:: KAP-GFP.

Video 3-9: Fluorescent video microscopy of KAP-GFP in flagella of *fla3-1b ift57-1*:: KAP-GFP.

Video 4-1: Real-time video of the wild-type *cc125*.

Video 4-2: Real-time video of the mutant *ift56*-2.

Video 4-3: High-speed video of the wild-type cell *cc125*.

Video 4-4: High-speed video of the mutant *ift56*-2 (moving cells).

Video 4-5: High-speed videos of the mutant *ift56-2* (paralyzed cells).

Video 4-6: High-speed video of the mutant *ift56*-1 (moving cells).

Video 5-1: High-speed video of the wild-type cell *cc125*.

Video 5-2: High-speed video of the mutant *arl3*.

CHAPTER I

INTRODUCTION

Introduction

Cilia, a conserved organelle with multiple functions

Cilia and flagella are hair-like structures extending from the surface of most eukaryotic cells. The words “flagella” and “cilia” refer to ultrastructurally identical organelles and can be used interchangeably. Centriole-based basal bodies serve as the templates to nucleate microtubules forming a cylinder-like structure called axoneme. The axoneme is surrounded by a ciliary membrane, which is continuous with the plasma membrane but has significantly distinct protein and lipid composition [1-3]. Cilia are some of the most ancient eukaryotic organelles. Based on their motility, cilia can be categorized into two types: motile cilia and non-motile cilia (primary cilia). Although their basic structures are similar to each other, generally, their microtubule organization in axonemes can help differentiate them. Most motile cilia have a typical “9×2+2” axoneme structure, which contains nine outer doublet microtubules and two central singlet microtubules. Appended to these microtubules are some specific structures including outer dynein arms, inner dynein arms, radial spokes, and nexin links, which are used for ciliary motility. The dynein arms are the motors that cause the sliding of the axonemal microtubules and produce the force for motility; radial spokes regulate the activity of the dynein. In most cases, the primary cilia only have nine outer doublet microtubules (referred to as “9×2+0”), and they are devoid of dynein arms. Thus, the primary cilium is

restricted to being a sensory organelle, and it is relatively rich in signaling proteins. There are, however, exceptions. For example, the nodal cilia lack the central singlet microtubules but are motile [4]. On the other side, the olfactory cells have non-motile cilia that show the "9×2+2" axoneme structure at their base [5].

Cilia can serve multiple functions in different organisms/cell types depending on their protein compositions. These functions include: propelling the cell, moving fluid or mucus over the cell surface, sensing, and signaling. In addition, cilia play vital roles in the developmental regulation of multicellular organisms. Although the functions of cilia are remarkably diverse, the structure and the basic mechanisms are conserved among different ciliated organisms.

Cilia and human diseases

In humans, cilia can be found on almost all differentiated cells. Motile cilia are less widely distributed than the primary cilia. They are only found in certain types of cells in our body. Functions of motile cilia mainly depend on their motility. Examples of motile cilia include sperm cells, epidermis cells in the trachea, ependymal cells in the brain and spinal cord, and the node cells. Spermatozoa use their cilia to move through the female reproductive tract. The ones with defective cilium fail to do so, and lead to male infertility. The tracheal epithelium is covered with rows of cilia, which can do directional movement. Together, they sweep mucus and dirt out of the lungs. Defects in tracheal cilia can lead to respiratory diseases. The ventricles in the adult brain and the central canal of the spinal cord are lined up with multi-ciliated ependymal cells. These

motile cilia beat coordinately to circulate the cerebrospinal fluid (CSF). The beating is also presumed to assist the distribution of chemical messengers including neurotransmitters to neurons. Defects in the motility of ependymal cilia lead to impaired CSF movement and cause neurological deficits [6, 7]. The node of the vertebrate embryo is an important structure that specifies development. The rotational movement of the nodal cilia generates the unidirectional flow, which is essential for the further development of the left-right asymmetry. Abnormal nodal cilia lead to wrong placement of organs relative to the left-right body axis [4].

Non-motile cilia are much more widespread in our body; they can be found in many different types of cells. Usually, one cell has a single primary cilium. In the kidney collecting duct and tubule, cilia can detect fluid flow. They bend in response to the fluid flow. The bending generates calcium influx, which is important for normal kidney function. Defects in these cilia are a leading cause of polycystic kidney disease [8]. Specialized primary cilia can be found in human sensing organs, such as the eyes and the nose. The outer segments of the photoreceptors in our retina, which is critical for light perception, are considered to be modified primary cilia. Light-sensing molecules are delivered and concentrated there. Defects in these modified cilia can lead to retinal degeneration and blindness [9]. Olfactory cilia are enriched with odorant receptor proteins. Thus, they are critical for detecting chemicals in the environment. Abnormal cilia can cause impaired olfactory function [10]. Primary cilia also play a crucial role in the development of multiple organs. It is particularly due to the essential role of cilia in Hedgehog (Hh) signaling and possible roles of cilia in other signaling pathways [11].

Mounting evidence has linked ciliary dysfunction to a broad spectrum of human genetic diseases, collectively referred to as ciliopathies [12, 13]. Due to the widespread distribution of cilia in the human body, cilia-related diseases often have multiple symptoms. Research on ciliogenesis and ciliary function will help us answer a series of questions, such as how the dysfunction of specific cilia causes related symptoms, which factors (genetic mutation, pharmacological agents, and extracellular environmental stimuli) are involved in the dysfunction of cilia, and how ciliary assembly and its functions are tightly controlled. The answers to these critical questions will help elucidate the pathophysiological mechanisms that are responsible for causing the ciliopathies and develop novel strategies for the treatment of ciliopathies.

Chlamydomonas as a model organism

Since the basic structure and mechanisms in cilia/flagella are conserved among ciliated organisms, model organisms are valuable tools for us to get a better understanding of this organelle. *Chlamydomonas* is an extensively used model for studying the ciliary assembly and functions. It is a type of unicellular green algae with two motile flagella protruding from the anterior end. As an established model organism, *Chlamydomonas* has several advantages over other ciliated organisms. First, *Chlamydomonas* is a haploid organism, in which all the mutations are “dominant” and readily to be analyzed by standard genetic techniques. The downside of using a haploid organism is that it is difficult, if not impossible, to study lethal mutations in haploid cells. However, mutations that affect the flagellar assembly and motility are not lethal in *Chlamydomonas* and can be isolated. Second, the two motile flagella are used for

swimming. Defects in flagellar assembly or motility can be simply identified by observing the cell motility. Third, *Chlamydomonas* flagella can be easily visualized and measured under optical microscopes, and the flagellar assembly can be easily manipulated. For example, *Chlamydomonas* cells treated with the pH shock, mechanical force, or specific chemicals can lose their flagella and start to generate new ones. Also, some chemicals can be used to trigger the elongation or shortening of the flagella. Fourth, *Chlamydomonas* can be easily grown in a large volume of synchronously dividing cultures, and its flagella can be easily isolated and purified to get sufficient high-quality samples for biochemical analyses. Fifth, over decades of efforts, there has been a large collection of pre-existing flagellar mutants, which could facilitate flagella-related experiments. For instance, using a conditional kinesin II mutant (*fla10ts*), the IFT machinery, which is critical for delivering a subset of ciliary precursors to ciliary tip, can be tightly controlled by changing environmental temperature. Moreover, double mutants are easy to generate through a standard cross to find the relationship between genes. Lastly, cilia are conserved, having similar structures and using similar mechanisms for various functions across species. In particular, the intraflagellar transport (IFT) system, which is essential for the flagellar assembly and maintenance, is composed of the same set of homologous proteins between humans and *Chlamydomonas* [14].

Using *Chlamydomonas*, many breakthroughs in the field of cilia research were made. For example, *Chlamydomonas* contributed a lot in the studies of IFT, which is an essential cargo delivery system in ciliogenesis. The first description of the IFT system came from *Chlamydomonas.* Using differential interference contrast (DIC) microscopy,

Kozminski and his colleagues observed some granule-like particles that rapidly move along the flagella in both directions [15]. Then a series of findings of IFT were reported in the *Chlamydomonas* field: A) the microtubule motor proteins are found to be necessary for IFT particles movement [16, 17]. B) The major components of IFT particles have been isolated and identified by exploiting the *fla10-1* temperature sensitive mutant [18, 19]. C) Then the IFT subunit was shown to be responsible for delivering specific cargos [20].

In conclusion, *Chlamydomonas* is an attractive model organism for studying the mechanisms of the ciliary/flagellar assembly, and it also can be valuable in the large-scale chemicals screening for the cilia diseases treatment.

Chlamydomonas flagellar regeneration

Flagellar regeneration is an important process for studying the defects of the flagellar assembly. When *Chlamydomonas* loses its flagella, either amputated or resorbed, it will re-assemble its flagella in favorable conditions. This process is called flagellar regeneration. During regeneration, cilia/flagella grow fast. Thus, if there are ciliary/flagellar assembly defects in the strains, they are easier to identify. In *Chlamydomonas,* a wide range of events or stimuli can trigger flagellar regeneration. *Chlamydomonas* will resorb their flagella just before dividing and after mating. In harsh conditions, either chemical or physical stimuli will induce *Chlamydomonas* to shed its flagella. After transferring the deflagellated cells into a stress-free environment, the cells will assemble new flagella. Using this behavior of the *Chlamydomonas*, multiple

methods, such as pH shock and mechanical force, are applied in laboratories to induce deflagellation. Generally, at around 10 minutes after deflagellation, the flagella emerge and start to extend rapidly. They will reach their full-length within two hours (Figure 1-1) [21], and by then they can perfectly perform their functions of motility or sensing. It means that all structural and functional subunits need to be delivered and positioned in different parts of cilia/flagella appropriately in less than two hours.

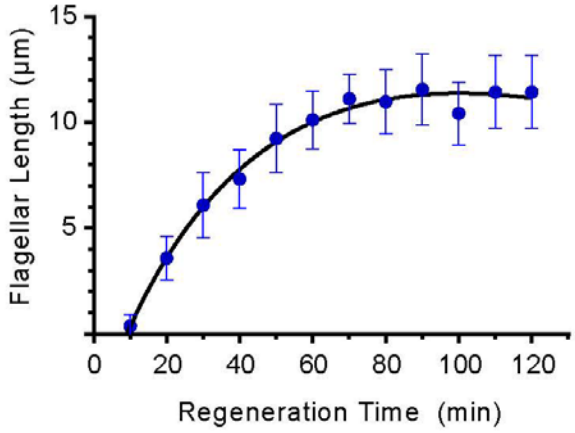

Figure 1-1. Flagellar regeneration curve of *Chlamydomonas reinhardtii.*
Flagella emerge at around 10 minutes after deflagellation and extend at extremely fast at the beginning. The first-half is assembled in about 30 minutes, and then the assembly will slow down. The whole process will be finished in about 90-120 minutes. Different strains and culture conditions may cause some variance.

Cilia/Flagella are the organelles that protrude from the cell body, and there is no protein synthesis machinery in cilia/flagella. Moreover, the protein composition of flagella is unique [1-3, 22]. Thus, the flagellar proteins need to be prepared and sent from the cell body through highly regulated delivery processes. A proteomic study of flagella in

Chlamydomonas showed that there are more than six-hundred types of proteins in *Chlamydomonas* flagella [22]. Moreover, some specific subunits, such as tubulin and dynein arms, are in high demand during flagellar regeneration. We use tubulin, the major structural subunit in the assembly of the flagellar axoneme, as an example. Around 1400,000 tubulin dimers are required for assembling a pair of full-length flagella [23].

Additionally, the whole flagellar regeneration process is under tight regulatory control. It has been shown that when the *Chlamydomonas* cells are deflagellated, genes encoding a large set of flagellar components are upregulated immediately [24-26], and protein syntheses are enhanced [25, 27]. When the flagella reach their full-length, flagellar protein syntheses decrease gradually and return to pre-deflagellation level. Moreover, the progress of the flagellar assembly is tightly controlled. The flagella extending is rapid at the beginning, and then the process keeps slowing down until full-length flagella are assembled. Then the flagella will be in a steady state until it receives other stimuli for deflagellation or resorption.

It is fascinating that such a large amount of diverse proteins are prepared, delivered into right places, and ready to work in an ordered manner in such a short period. It raises the question about how cells deliver specific proteins into their cilia/flagella efficiently.

Transport to flagella

As mentioned above, the cilium/flagellum has distinctive protein and lipid content, which helps enable its specific functions. Proteins that are closely related to ciliary

function are highly concentrated in cilia, such as the motility-related proteins and sensing or signaling-related proteins [28]. Although the cilia protrude from the surface of the cell body, they are not completely separated from the cell body by membranes but connect with cell body through a region called transition zone. At transition zone, the ciliary membrane is continuous with the plasma membrane, and the continuity between cytosol and flagellar matrix remains. Then how are the unique proteins targeted and retained in the flagella without complete separation? Flagellar proteins can be categorized into two groups, membrane proteins and soluble proteins. In the case of soluble protein, it has been shown that there is a size-dependent diffusion barrier at the transition zone. The smaller molecules can pass the barrier freely while the larger molecules remain excluded [29-31]. The larger size proteins require active transport for the entry into the cilia. Active transport is also necessary for the proteins that are highly concentrated in the cilia (e.g., tubulin) for efficient delivery. In the case of the membrane proteins, studies show that a diffusion barrier, which contains septin and B9 complex, exists in the transition zone. It restricts the lateral protein diffusion between the plasma membrane and ciliary membrane [32, 33]. Thus, the ciliary membrane proteins need to be targeted to flagella by active transport and then retained there. Among multiple means of active transports that are involved in cilia, IFT is the best studied.

Intraflagellar transport machinery

During flagellar assembly, it has been shown that axoneme precursors are delivered to flagella tip [34, 35] at a remarkably high speed. In *Chlamydomonas*, before the flagella reach their half-length, the assembly rate is more than 0.2μm/min. To meet such a high

loading requirement for transportation, an efficient system, intraflagellar transport (IFT), is used for ciliogenesis. IFT was first observed in *Chlamydomonas* and was shown to be indispensable for cilia assembly and maintenance [15, 36]. IFT is a bidirectional movement of large protein complexes along the axonemal microtubules and is powered by motor proteins (Figure 1-2). The movement from the cell body to the flagellar tip is called anterograde IFT and is driven by the motor protein kinesin-2 at around 2.0μm/s. The opposite direction, known as retrograde IFT, is powered by the cytoplasmic dynein 1b/2 at around 3.5μm/s [15]. The additional motor may exist in certain types of organisms. It has been shown that two motors, kinesin-II and osmotic avoidance defective (OSM)-3 kinesin, team up in the anterograde transport for a more efficient transport in *C.elegans* [37, 38]. However, this unique IFT system has not been proved in other organisms.

The whole IFT functions like a double-track railway system. Microtubule doublets in axoneme serve as the bidirectional double-track railway. B-microtubules and A-microtubules are used for anterograde and retrograde trains, respectively, to avoid collisions [39]. The IFT motors function as wheels on the track. The IFT trains operate as trains. Many different cargos (structural and functional subunits) are delivered towards or away from the cilia tip by this delicate transport system [40-43]. IFT trains are expected to have different regions that fit for different cargos due to the diversity of cargo. IFT trains are polymers of IFT particles. The IFT particles are large protein complexes that are composed of two functionally and biochemically separated sub-complexes IFT-A and IFT-B, which contain at least 6 and 16 polypeptides, respectively

[36, 44]. These subunits contribute in keeping the structural stability of the particle, delivering specific sets of cargos, or both. Bioinformatic analysis of IFT protein shows that IFT proteins are rich in well-known protein-protein interaction motifs [45]. A significant amount of these domains provides a solid foundation for the assembly of IFT complexes and their versatile functions.

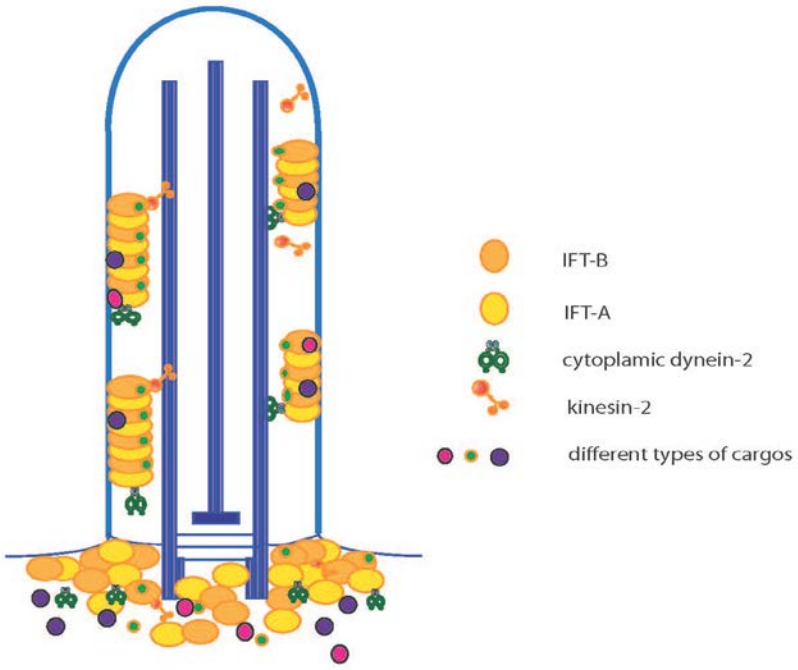

Figure 1-2. Schematic presentation of a cilium and IFT trains.
The cilium is a microtubule –based organelle projecting away from the cell surface. The axoneme, which is composed of multiple microtubules and MAP, extends from the basal body and covered by a ciliary membrane. IFT is a bi-directional transport system that delivers different types of cargos into and out of cilia. The anterograde movement (from the cell body to cilia) is driven by kinesin-2 while cytoplasmic dynein-2 powers the retrograde transport (from cilia to cell body). IFT complex, which comprises IFT-A and IFT-B, is responsible for carrying cargos.

The architecture of IFT complexes

The research in the past decade has made great advances in the architecture of the IFT complexes.

IFT-A is formed by six polypeptides including IFT43, IFT121, IFT122, IFT139, IFT140, and IFT144 [46, 47]. It has been shown that three IFT-A subunits IFT122, IFT140, IFT144 can form a stable heterotrimeric complex without the other subunits. The other subunit IFT121 may play a role in assembling IFT43 and IFT139 onto the heterotrimeric complex because the absence of IFT121 completely removes these two subunits from IFT-A [48].

Compared to IFT-A, IFT-B complex has a less stable structure and can be broken down into a core complex and some peripheral proteins by increasing ionic strength [49]. Work in Dr. Lorentzen's lab presented a biochemical dissection of the molecular interaction in the IFT-B core complex [50]. The IFT-B core could be divided into two stable subcomplexes consisting of IFT88/70/52/46 and IFT81/74/27/25. IFT52 is the backbone for the subcomplex IFT88/70/52/46. The C-terminal of IFT52 and IFT46 interact with each other and play an essential role in combining two subcomplexes [45, 50, 51]. The proposed model well explained the observation that mutant *ift52*, *ift46*, and *ift88* have different levels of defects in the IFT-B assembly. The absence of IFT52 and IFT46 cause significant defects in IFT-B core assembly while the absence of IFT88 has little effect [52]. Although IFT56 was not included in the structure map, it was confirmed as a bona fide IFT core protein [53]. It interacts with another IFT-B core

protein IFT46 [54]. Recent studies found that the peripheral proteins are not just loosely attached onto the IFT-B core complex but rather form a distinct complex [54, 55]. The core complex, which includes IFT22, IFT25, IFT27, IFT46, IFT52, IFT56, IFT70, IFT74, IFT81, and IFT88, is renamed as IFT-B1. The peripheral complex, which is formed by IFT20, IFT54, DYF-3/Cluap1, IFT57, IFT80, and IFT172, is called IFT-B2. IFT52/IFT88 in IFT-B1 and two subunits, IFT57 and DYF-3/Cluap1, were proposed to play a crucial role in bridging IFT-B1 and IFT-B2 together [54, 55].

Function of IFT particle subunits

IFT trains serve as cargo adaptors. They assist in delivering cargos towards or away from the ciliary/flagellar tip. Multiple proteins and protein complexes have been confirmed to be the cargos of IFT system (reviewed in [44]), and much more are expected to be found in the future. Generally, IFT-B is considered to be responsible for carrying cargos into cilia while IFT-A is specifically involved in the retrograde intraflagellar movement. IFT-B mutants usually cause more severe defects in cilia assembly than IFT-A mutants, and the identified cargo binding sites are mainly located at IFT-B subunits [20, 44, 56]. IFT-A mutants usually display a characteristic bulge at their flagellar tips, in which IFT-B is accumulated [46, 57]. Also, IFT-A mutants have significantly defective retrograde ciliary transport while the anterograde transport is not affected [57, 58]. However, there are a few exceptions. It has been shown that IFT-A is essential for ciliary entry of Tubby-like protein 3 (TULP3) and indirectly affects the trafficking of a set of the G-protein-coupled receptor (GPCR) [59]. Additionally, an IFT-B subunit IFT27 is reported to be involved in BBsome export [60, 61]. Thus, although

these two IFT complexes mainly deliver in one direction, they can be involved on the other side.

Studies also show that the cargo loading of IFT trains is tightly regulated. During ciliary/flagellar assembly, lots of structural proteins are loaded onto the IFT trains. However, these types of cargos are rare when the cilia/flagella are in their steady states [23, 62]. The experiment also shows that if only one flagellum is amputated while the other one remains intact in a *Chlamydomona*s cell, much more tubulin will be loaded and transported into the newly assembled flagella [23]. Although it is possible that the loading priority is simply regulated by the cargo supply, it is also possible that the IFT trains themselves are involved in the regulatory process.

The function of IFT complexes is a collective output of all IFT proteins. Researchers dedicate to study about contributions of individual IFT proteins. Each subunit plays unique roles in the complexes structure, function or both [44, 63]. Mutagenesis and other methods are used to determine how these subunits affect the others and what are their influences on the whole IFT system. However, the study is hindered by the fact that null mutants of many IFT subunits completely abolish the ciliogenesis due to their roles in IFT complex stability. Thus, their specific contributions other than keeping complex assembly are masked. In these cases, analyzing the IFT mutants with a reduced expression level or destroy specific domain of the studied IFT protein may help settle problems.

Despite the fact that the functions of many subunits have not been confirmed yet, significant progress is made in past decades. Based on previous studies, IFT subunits play different roles in complex stability, cargo delivery, and IFT regulation.

IFT subunits that are involved in the IFT complex assembly and stability

IFT subunits play important roles in complex assembly and stability. Functions of a few subunits have been confirmed. A typical example is IFT52. The structural and biochemical analyses showed that IFT52 is essential for the assembly and stability of IFT-B by connecting two stable subcomplexes, IFT88/70/52/46 and IFT81/74/27/25 [50-52], in IFT-B1. Also, it plays a vital role in bridging IFT-B1 and IFT-B2 together [54, 55]. IFT88 also functions in connecting IFT-B1 and IFT-B2 [54, 55], though it is not essential for the IFT-B1 assembly and stability [52]. It also has been shown that the carboxyl-terminal of IFT46 is critical for stabilizing IFT-B [20, 51, 52], and it is proposed to help IFT56 assemble onto the IFT-B [54]. Recently, IFT74 was reported to play a similar role in stabilizing IFT-B [64]. Additionally, in IFT-A complex, IFT121 is essential for the assembly of IFT139 onto IFT-A [48].

IFT subunits that are involved in cargo delivery

IFT particles are believed to serve as adaptors to bridge flagellar precursors and IFT motors. Although many proteins are shown to be IFT cargos, little is known about their binding sites in IFT particles [44]. So far, IFT46, IFT74, and IFT81 are the only IFT particle subunits that have been confirmed to transport specific sets of cargos. IFT46 is responsible for delivering the preassembled outer dynein arms into flagella through an

adaptor ODA16 [20, 65]. Studies show that the IFT74 and IFT81 are crucial for tubulin delivery. The N-termini of these two subunits, together, form a tubulin binding module, while the absence of either of them lead to a significantly decreased tubulin delivery rate [56, 66]. There are also some IFT subunits are proposed to assist specific cargo delivery. IFT25/IFT27 has been implicated in the export of BBSomes from cilia, and in return affects the ciliary localization of a specific set of membrane protein [67]. IFT70/Fleer/DYF-1 is involved in polyglutamylation of axonemal tubulin [68, 69], but it remains unclear whether IFT70 directly binds to a tubulin glutamylase. Moreover, the absence of IFT56 results in a significant reduction of a specific set of inner dynein arms [53]. These results hint that individual IFT proteins are likely to play distinct roles in delivering specific cargos.

IFT subunits with other functions

Some IFT subunits have functions other than keeping IFT complexes stability and cargo delivery. A typical example here is IFT172. IFT172 is an unusual IFT subunit. Although it is an IFT-B subunit, the phenotype of its mutant is similar to the IFT-A mutants, which have an accumulation of IFT proteins at their ciliary tips [70]. IFT172 is proposed to play a crucial role in IFT particles turnaround at the ciliary tip by interacting with a microtubule plus-end tracking protein EB1 [71-73]. Recently, it has been shown that IFT-A subunits IFT43 and IFT140 are involved in transporting ciliary components in the cytoplasm to the peri-basal body region [74].

IFT and ciliary length control

Flagellar length control is an active research area. Many studies show that the length of flagella is tightly controlled, and flagella only function well with the right length. Motile cilia rely on “just right” length to generate effective beat force, which is critical to propel the movement of the cell itself or generate a fluid flow. Consequently, both long and short flagella are function defective, which is best characterized by using mutants of *Chlamydomonas*. In humans, motile cilia with abnormal length cause symptoms such as infertility and chronic respiratory disease [75]. The right length is also essential for primary cilia to function as a sensory hub [76, 77]. The abnormal length of primary cilia is always correlated with human diseases or injury of tissue [78-80]. For example, the altered dynamic of cilia assembly in *bbs-4* is associated with renal cystic disease [81].

Due to the importance of having functional cilia, the ciliated organisms have to set up a ciliary length control system. Based on early observations, the system has several characteristics. First, it can control when to assemble/disassemble cilia. Second, the assembly rate of cilia is dynamic and length dependent. Third, it should “know” the length of its existing cilia. At last, it should “know” the “just right” length for cilia and stop at the right point.

Over many years, researchers have gained a much better understanding of the system. Some chemicals are identified to have an effect on ciliary length. Therefore, the ciliary length can be manipulated. When cells are cultured in a medium with low concentration

of lithium [82], the cilia become longer. In contrast, shortening of cilia can be induced by sodium pyrophosphate (NaPPi) or isobutyl methyl -xanthine (IBMX) [27].

On the other hand, genetic studies identified some valuable mutants with defects in ciliary length control. Five long-flagella mutants, which harbor mutations in LF1 to LF5, are identified and detailed analyzed [83-85]. Three of them are kinases. LF2 shares sequence similarity with members of cyclin-dependent kinase family. LF2, together with two accessory proteins, LF1 and LF3, forms a cytosol protein complex called length regulatory complex (LRC) [86]. By analyzing different alleles of LF2, Tam *et al.* showed that the activity of LF2 is tightly regulated to set flagellar length. The absence of LF2 kinase activity results in mutant cells with short and unequal-length flagella. Conversely, low level of LF2 activity in some mutants induces the assembly of extremely long flagella [86]. However, LF1, LF2, and LF3 are *Chlamydomonas* specific proteins and are not found in other ciliated organisms. They might be involved in a mechanism specifically exist in *Chlamydomonas*. In contrast, the other two kinases, LF4 and LF5, are conserved across ciliated organisms. LF4 encodes a MAP kinase whose sequence is similar with MAPK MOK, while LF5 encode a CDKL kinase that share a high similarity with CDKL5. Both of them could enter flagella [87, 88].

It also has been shown that flagellar length can be affected by limited structural precursors. When the protein synthesis is blocked by treating cells with a protein synthesis inhibitor cycloheximide before deflagellate them, cells can only regenerate short-length flagella [21]. Some other evidence came from Lorentzen and Yoder labs.

Lorentzen's lab shows that the IFT particle proteins IFT74 and IFT81 bind tubulin and are essential for ciliogenesis [66]. Using pharmacological treatment, Sharma *et al*. showed that cilia length is influenced by the dynamic of the cytoskeleton, which is related to the level of soluble tubulin [89]. Therefore, precursor pool size is a key factor in ciliary length control system.

Based on these studies, different theoretical models were established. As research technology continues to develop, and more details were examined, the ciliary length control model continually improved. It seems that the ciliary length control is even more delicate than we imagine.

The early length control model proposed that a length sensor is involved in ciliary length regulation. The sensor activates a signaling pathway that modulates ciliary assembly/disassembly in response to ciliary length in a feedback control pathway. The problem is such specific molecules had not been identified at that time.

After the characterization of IFT machinery, a simple but versatile model "balance-point" was set up. Because flagellar components are constantly turning over, the flagellar length must be set by the assembly rate and the disassembly rate. The key point of the model is that there is no need for a sensor or regulator for flagellar length control. The flagella reach their full-length when the assembly rate is balanced by the disassembly rate [90]. The disassembly rate is not length-dependent [91], while the assembly rate keeps changing depending on flagellar length. This model proposes that

the total amount of IFT proteins is length independent. The factor that mediates length-dependent assembly rate is IFT train size. Experiments results supporting this model include the regenerating short flagella have a high relative concentration of IFT particle proteins, and the size of individual IFT trains scales inversely with ciliary length [90]. According to this model, IFT train size is tight linked to ciliary length. However, there was little clue to explain what regulates IFT train size. Later on, Ludington et al. provide a possible explaination. By comparing newly growing flagella and steady-state flagella, which have large, infrequent injections and small, frequent injections, respectively, they found that more IFT material accumulates at the base of the regenerating flagella. They proposed that the IFT injections result from avalanche-like releases of accumulated IFT material at the flagella base, and the cell could control their flagellar length by regulating the accumulation of IFT material at the flagellar base [92]. However, it raises another question why more IFT particles are accumulated at the base of regenerating flagella.

In “balance-point” model the disassembly rate was thought to be independent of length. Also, the cargo-loading efficiency is not considered. To “balance-point” model, some researchers have somewhat different opinions. “It seems that little or no regulation of assembly and disassembly is required per se to maintain wild type ciliary length. However, the existence of mutations that alter the ciliary length, especially long-cilia mutant suggests that the proper function of these mutated components is to regulate ciliary length, possibly by regulating the rates of assembly and/or disassembly.” [93]. By treating *Chlamydomonas* cell with Nappi, Pan *et al*. [94] found that once flagella shortening is triggered, the number of entering IFT train increased two to four folds,

however, with much less anterograde cargos. Quarmby's lab found that a null mutant *cnk2* has defects in resorbing their flagella when flagella shortening are induced. Also, the double mutant *lf4 cnk2* has longer flagella than an *lf4* single mutant, indicating that the NIMA-related kinase CNK2 helps cilia reach their perfect size by activating disassembly when the cilia beyond its normal length [93, 95]. Recently, by imaging single molecules of a labeled axonemal component DRC4-GFP, Wren *et al*. [62] showed that although the amount of IFT complexes is fixed, cargo transport frequency is variable during ciliary growth. The cargo transport frequency is much lower in steady-state flagella than in newly growing flagella. As the flagellar length increases, the cargo transport frequency decreases proportionately with length. Also, it has been shown that the cargo availability is not the limiting factor of the decreased cargo transport frequency. However, whether the train size mentioned in "balance-point" correlates with cargo transport frequency remains unknown.

Although some length effectors have already been identified, the answer of "how does the IFT system know the length of the existing cilia" remains unknown. A study from Pan Junmin's lab shed light on the question. They found that the phosphorylation state of an aurora-like kinase (CALK) closely correlates with flagellar length [96, 97]. It may work as an indicator to "show" the cell the length of existing flagella [98]. Then cell will "decide" how to response. For example, the cell may increase or decrease the cargo loading efficiency according to the "report". If indicator is affected or altered, the whole system might be reprogrammed.

Given that all, cilia length is under control of a complicated IFT-centered multi-layer system. Many regulators may be involved in length control by tightly regulating the IFT system. However, many details remain unclear.

CHAPTER II

IDENTIFICATION OF THE TWO *CHLAMYDOMONAS* IFT SUBUNIT MUTANTS BY RESTRICTION ENZYME CASSETTE MEDIATED PCR

Introduction

Mutations in the intraflagellar transport (IFT) system can cause defects in ciliogenesis and ciliary function, which can lead to an array of ciliopathies, including polycystic kidney disease (PKD) [99], Bardet-Biedl syndrome [100], nephronophthisis [101], and Huntington's disease [102]. Although we are beginning to know the components and the basic mechanisms of the IFT system, many missing pieces hinder us from fully understanding the whole system.

The IFT system contains motors, IFT trains, cargos, and axoneme. IFT trains play a critical role in connecting motors and the delivered cargos. The IFT trains are the polymers of IFT particles, which comprise two functionally and biochemically separated sub-complexes IFT-A and IFT-B. In general, IFT-B is responsible for anterograde transport. Moreover, compare to IFT-A, mutations in IFT-B usually cause more severe phenotypes. The same as IFT-A, IFT-B is composed of multiple subunits. If we know the specific function of each subunit, it will facilitate our comprehensive understanding of the IFT-B and the whole IFT complex.

Mutagenesis is essential for the forward genetics. Specific phenotypes of the mutants help us understand functions of the causative mutated genes. Mutants-related studies

contribute a lot in dissecting functions of different IFT complex subunits. We have already learned that different IFT subunits play different roles in the IFT complex structure, function, or both [44, 63] because mutations in different subunits have varied phenotypes ranging from completely abolished ciliogenesis to malfunctions in full-length cilia. Although considerable effort has been invested, and substantial progress has been made, the functions of many subunits remained unknown.

In this chapter, we took advantage of an established insertional *Chlamydomonas* mutant library, which is composed of mutants with flagellar defects, to screen out the mutants with mutations in IFT-B subunits. The flagellar defects were observed, and their insertion sites were analyzed using an enzyme cassette mediated method. A set of mutants has been identified, including three IFT subunit mutants.

Results

The mutants used in this study were generated by transforming *Sca*I linearized *pHyg3* plasmid, which contains a hygromycin resistant gene, into a wild-type strain *cc125*. Then the generated mutants were screened by their capability of displaying phototaxis. Only phototaxis negative mutants were preserved [103]. Because most of known IFT-B subunit mutants cannot assemble flagella or only assemble short flagella, we focused on mutants that are bald (non-flagellated) or with short flagella. A set of mutants were selected for further analysis, including three promising IFT-B bald mutants that were screened out previously using western blot (Figure 2-1, cited from [103]) and some short-flagella mutants.

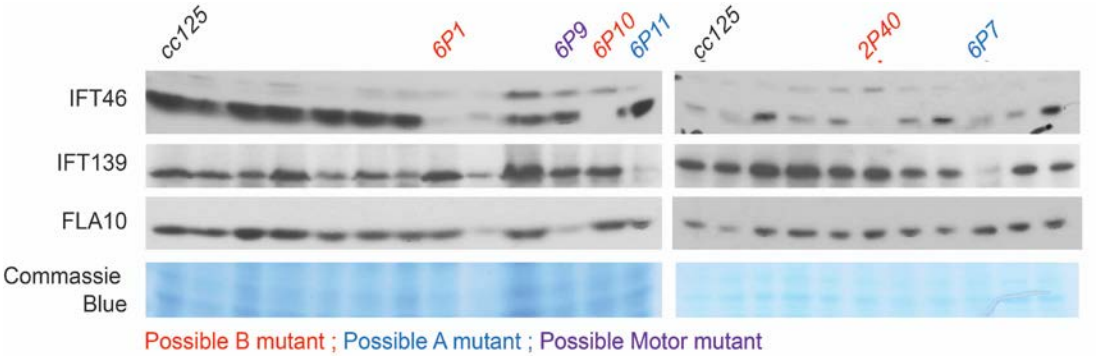

Figure 2-1. Western blots of whole cell extracts revealed potential IFT mutants. Strains *6P1*, *6P10*, and *2P40* are possible IFT-B mutants. These strains reduced the expression of IFT-B protein IFT46 while maintain or increase the expression of IFT-A protein IFT139. *6P11* and *6P7* are potential IFT-A mutants, having a reduction in expression of IFT-A protein IFT139 while maintaining the expression of IFT-B protein IFT46. *6P9* may be a motor protein since it has a decrease in a motor protein FLA10, but not in IFT139 or IFT46 expressions. Coomassie staining gels are used as loading controls. (This figure is reprinted from [103] with permission).

Restriction enzyme cassette - mediated PCR

To localize the region where the linearized vector integrated into mutants, I modified a method from Takara LA PCR in vitro Cloning Kit to adapt it to *Chlamydomonas*. All the related operations and primers are summarized in Figure 2-2 and Table 2-1, respectively. Briefly, the genomic DNA from a mutant strain was extracted and then digested with a set of restriction enzymes, respectively. This set of enzymes (*Hin*dIII, *Pst*I, *Sac*II, *Nco*I and *Apa*L1) was chosen because their cutting sites are abundant in the *Chlamydomonas* genome, which makes them highly possible to locate closely enough to the insertion site. However, those enzymes whose cutting sites have excessive frequency were avoided due to the production of tiny digestion fragments, which are challenging for purification. Then the digested fragments were purified separately and ligated to respective cassettes, which contain the same restriction enzyme cutting site and a short-designed sequence.

During PCR, the amplification would occur between primers that are specific for marker DNA and the primers that are specific for designed sequence in the cassette. Nested amplification was utilized to increase the efficiency and specificity of the amplification.

Usually, after three rounds of nested PCR, the specificity and quantity of amplified products are good enough for sequencing. The size of most of the amplified bands ranges from 300bp to 1.5kb, a range that is good for sequencing (Figure 2-3). Using this method, we identified three IFT-B subunit mutants: an *ift57* mutant *2P40*, an *ift56* mutant *3P3*, and an *ift81* mutant *6P1*.

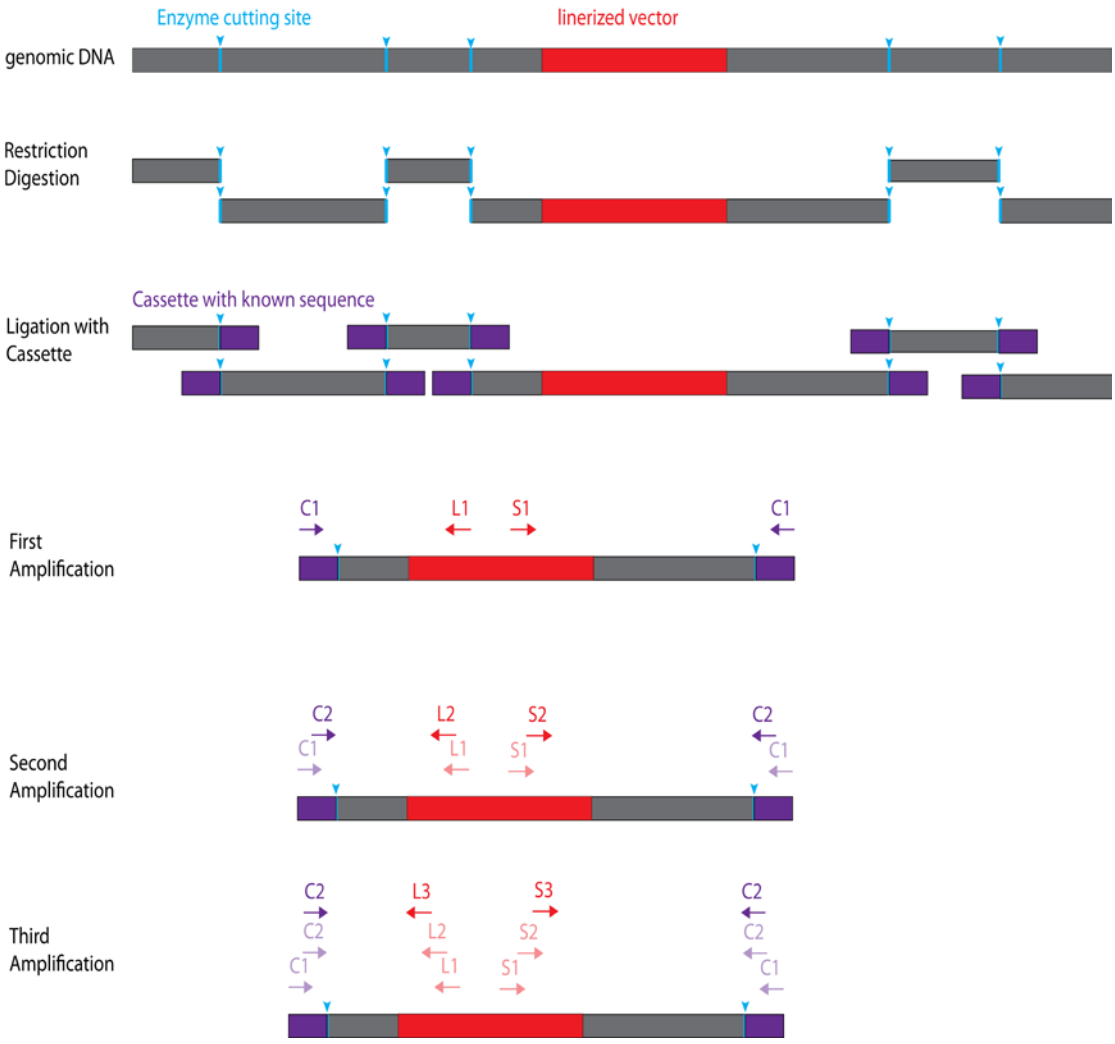

Figure 2-2. Schematic diagram of the restriction enzyme cassette - mediated PCR steps.

Cassettes are double-strand DNA fragments that contain a restriction enzyme cutting site and a short-designed sequence. The cassettes are ligated to fragmented *Chlamydomonas* genomic DNA, which is digested using the corresponding restriction enzyme. Then the ligation products were used as templates for three rounds of net PCR. The 1st round PCR is performed by primer C1 and L1/S1. Primer C1 contains the designed sequence in the cassettes while the L1/S1 contains the sequence in linearized vector, which is inserted into the strain by random insertional mutagenesis. The 1st round product is then used as the template for the 2nd round of PCR. Then amplified products are utilized for the final round. The sequences of cassettes and primers are shown in Table 2-1.

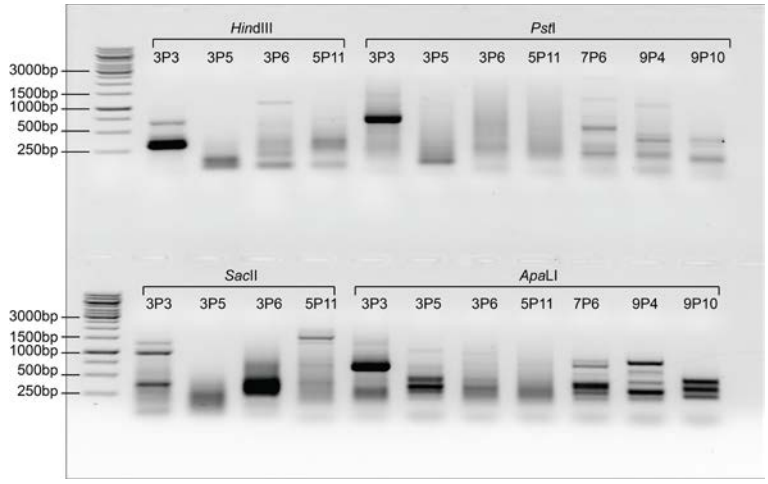

Figure 2-3. Examples of the Restriction Enzyme cassette mediated.
Cassettes *Hin*dIII, *Pst*I, *Sac*II, and *Apa*L1 are used in seven insertional *Chlamydomonas* mutants. Bands that have high intensity and suitable size (300bp-1500bp) were sent for sequencing. Bands from strains *3P3*, *3P5*, *3P6*, *9P4*, and *9P10* got positive results.

IFT57 is an IFT-B peripheral protein that has been linked to Huntington's disease and unclassified oral-facial-digital syndrome [102, 104-106]. Here, the *2P40* mutant, a possible *ift57* mutant, forms pamelloid in TAP medium; only few cells assemble motile flagella that are varied in length (Figure 2-4 A). However, even the flagellated cell cannot swim fluently as wild-type cells. The sequencing result of the amplified fragment showed that the sequence besides the linearized insertion vector perfectly matched a part of the *IFT57* gene (91bp-246bp), indicating that the vector is inserted before nucleotide 91 of the *IFT57* gene (Figure 2-4 B). The first exon of *IFT57* starts from nucleotide 166. Thus, the vector is inserted into the 5'UTR of the gene. Sequencing results from the other side of the insertion also revealed that the insertion is at nucleotide 91(Figure 2-4 C).

To confirm the insertion site, we synthesized a pair of primers *IFT57*-51-69-F and *IFT57*-515-535-R depend on sequences at 51bp-69bp and 515bp-535bp, respectively. PCR results showed that a specific band with expected size was amplified from *cc125* genomic DNA. However, that band was completely missing in *2P40*, indicating that *IFT57* was indeed disrupted at this region (Figure 2-4 D). The fact that primer *IFT57*-51-69-F paired with another primer from insertion vector (hygromycin-R) amplified a specific band from the *2P40* mutant but not from the *cc125*, further confirmed the insertion site (Figure 2-4 E). The whole cell lysate WB also showed that *2P40* has a drastically reduced level of IFT46, which is a typical phenotype of an IFT-B subunit mutant (Figure 2-1, cited from [103]). Thus, *2P40* is a real *ift57* mutant. However, due to the insertion is in the 5'UTR, whether *IFT57* transcription is entirely abolished needs to be examined in the future.

DYF-13 is a putative IFT subunit. Although it was not isolated and identified as an IFT subunit through the standard approach in the first attempt [18], mounting evidence shows that DYF-13 is involved in ciliogenesis [107-110]. The *3P3*, which is a putative *dyf-13* mutant, only assembles short length flagella in TAP medium (Figure 2-5 A). The swimming speed of the cells is much slower than wild-type cells, which may be due to the shorter flagellar length. No diseases related to mutations in the human ortholog have been reported so far. The sequencing result showed that the linearized vector is inserted before nucleotide 1690 in *CrDYF-13*, indicating that the insertion is in the 3rd intron (1241bp-1780bp).

Figure 2-4. *2P40* is a putative IFT57 mutant.

A. The *2P40* mutant cells displayed flagellar assembly defects. In TAP medium, the control wild-type *cc125* cells were rarely seen in clusters. However, most cells were seen in clumps; few can assemble flagella. **B**. The sequencing result of the fragment, which is amplified using C1, C2, C3, L1, L2, and L3. **C**. The sequencing result of the fragment, which is amplified using C1, C2, C3, L1, L2, L3, and L4. **D**. *IFT57* is disrupted between 51-535 nucleotides in *2P40* mutant. PCR was performed using primers *IFT57*-51-69-F and *IFT57*-5-5-535-R. Wild-type *cc125* is used as a control. **E**. In the mutant *2P40*, a linearized vector containing hygromycin is inserted in *IFT57*. PCR was performed using primers *IFT57*-51-69-F and hygromycin-R*. 2P40-1* and *2P40-2* are two isolated colonies of *2P40.* The lane labeled as blank was another control using water as the template in PCR.

A

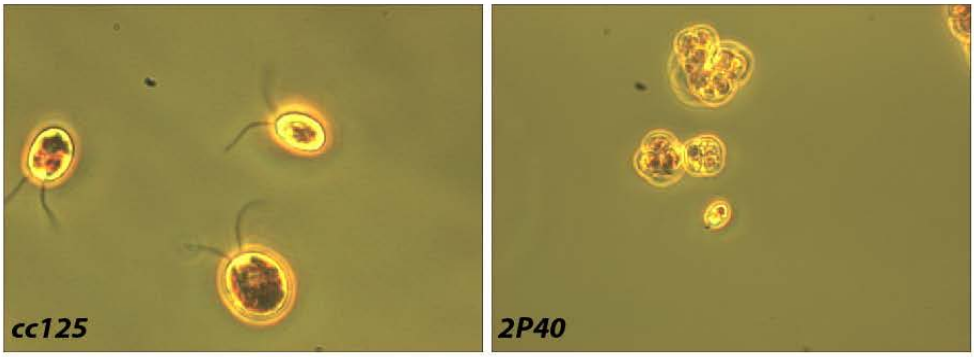

B

(2692)GCANGAGTGGGTTACATCGAACTGGATCTCAACAGCGGTAAGATCCTTGAGAGTTTTCGCCCCGAAGAAC
GTTTTCCAATGATGAGCACTTTTAAAGTTCTGCTATGTGGCGCGGTATTATCCCGTATTGACGCCGGGCAAGAGCA
ACTCGGTCGCCGCATACACTATTCTCAGAATGACTTGGTTGAGT(2881)TATCCGGTAACTATCGTCTTGAGTCCAA
CCCGGTAAGACACGACTTATCGCCACTGGCAGCAGCCACTGGTAACAGGATTAGCAGAGCGAGGTATGTAGGCG
GTGCTACAGAGTTCTA(91)CCCAGCGAGCCGCGCTCCTTGCCACATGTCCTGCTAGCTTCTGGTTTACACCGTAGAT
TCATTTAAGCGAGAGACATGAGCAGCAAGCGGGTGCGTACGGGTCTGCGCGGGCTGCACGAAGGACAGGCCGG
GTGACCTTGTGGCGCGTCTTCTGCA(246)GTCTCCCTATAGTGAGTCGTATTACGCGTTCTAACGA

Hygromycin Insertion; Uknown- no regions identified using chlamy center; IFT57 Genomic Sequence Overlap; Primer C2

C

TNC(84)TNGGANC(91)(354)GGGCTGCANGGGCGCTCCGATGCCGCTCCAGGGCGAGCGCTGTTTAAATAGCCA
GGCCCCCGATTGCAAAGACATTATAGCGAGCTACCAAAGCCATATTCAAACACCTAGATCACTACCACTTCTACAC
AGGCCACTCGAGCTTGTGATCGCACTCCGCTAAGGGGGCGCCTCTTCCTCTTCGTTTCAGTCACAACCCGCAAACA
TGACACAAGAATCCCTGTTACTTCTCGACCGTATTGATTCGGATGATTCCTACGCGAGCCTGCGGAACGACCAGNN
ATTCTGG(643)A

Hygromycin Insertion; IFT57 Genomic Sequence Overlap

D

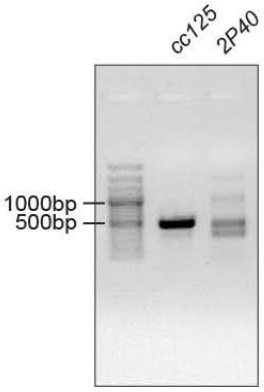

E

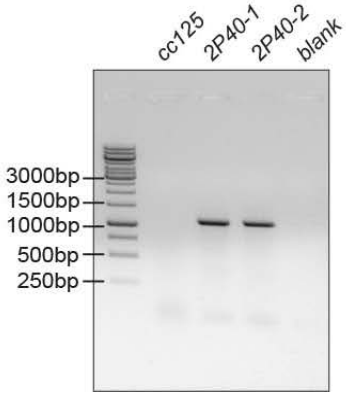

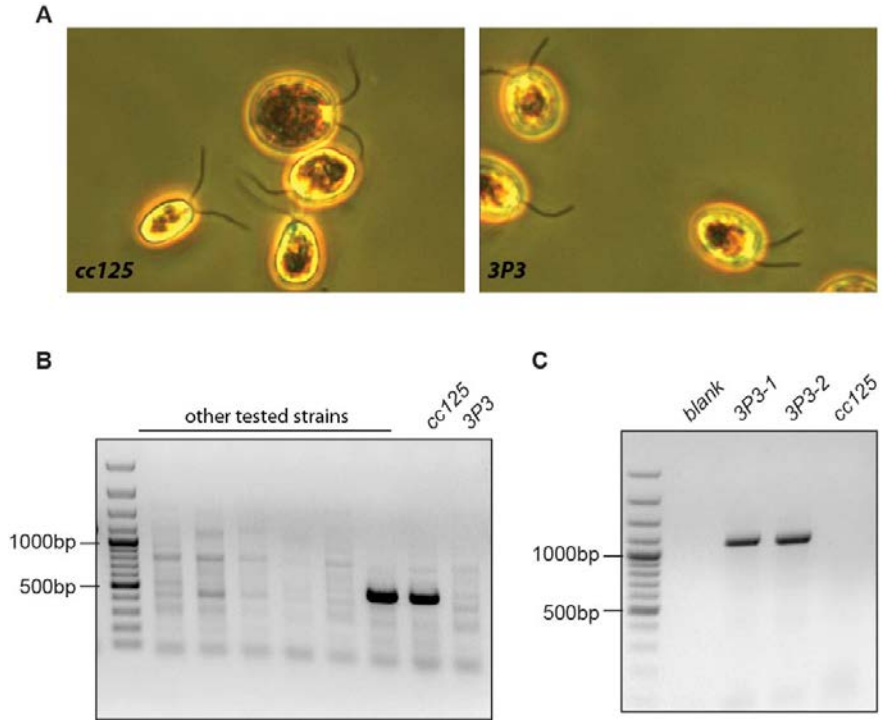

Figure 2-5. *3P3* is a putative *CrDYF-13* mutant
A. The *3P3* assembles short flagella though it can disperse well in TAP medium. **B**. *CrDYF-13* is disrupted between 1598-2089 nucleotides in *3P3* mutant. PCR was performed using primers *IFT56-1598-1622*-F and *IFT56*-2065-2089-R. Wild-type *cc125* is used as a control. **C**. In the mutant *3P3*, a linearized vector containing hygromycin is inserted in *CrDYF-13*. PCR was performed using primers *IFT56-742-760-R* and L3*. 3P3-1* and *3P3-2* are two isolated colonies of *3P3.* The lane labeled as blank was another control using water as the template in PCR.

To confirm the insertion site fragments 1598-1622 and 2065-2089 were used for designing primers *IFT56*-1598-1622-F and *IFT56*-2065-2089-R. A specific band of right size was amplified from the wild-type cell *cc125* but not from the *3P3* mutant (Figure 2-5 B). Another primer *IFT56*-742-760-R, together with an L3 primer from the linearized vector, was also used to confirm the insertion site. A specific band showed from the *3P3* mutant but was missing from *cc125* as expected (Figure 2-5 C). However, according to whole cell lysate WB, the level of IFT46 is not significantly reduced in the *3P3* mutant

(Data not shown). Also, the insertion is in an intron. Whether or not the *IFT56 (CrDYF13)* expression is affected need to be confirmed by further tests.

IFT81 is an IFT-B core protein and is associated with ciliopathies [111]. The putative IFT81 mutant *6P1* does not assemble any flagellum in TAP medium (Figure 2-6 A). Sequencing results showed that the insertion is in the 7^{th} intron. The insertion was confirmed by PCR using primers IFT81-2747-2766-F and IFT81-2918-2939-R. Primer IFT81R 2918-2939 with another primer from the linearized vector (Hygromycin-F) was also used (Figure 2-6 B) to verify the results.

Besides these IFT subunits mutants, strains with mutations in other genes, such as Casein kinase II (CK2) and tropomyosin, were also identified in this screen.

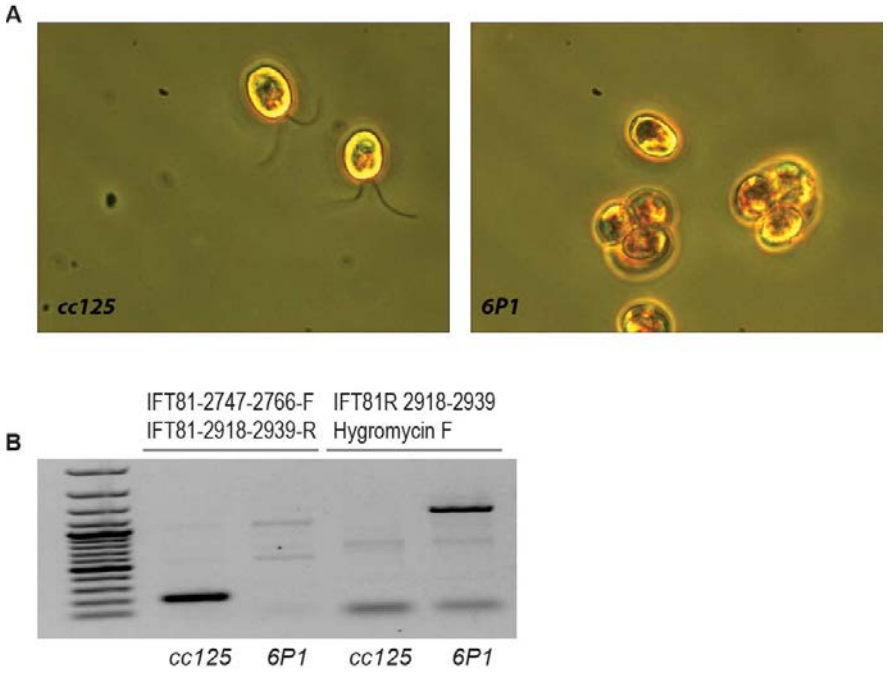

Figure 2-6. *6P1* is a putative *IFT81* mutant
A. The *6P1* mutant cannot assemble flagella. **B**. *IFT81* is disrupted by the hygromyin insertion between 2747-2939 nucleotides in *6P1* mutant. PCR was performed using two sets of primers *IFT81-2747-2766*-F/*IFT81-2918-2939*-R and IFT81-2918-2939-R/Hygromycin F. The wild-type *cc125* is used as a control.

Discussion

As one of the best mutagenesis methods, random insertional mutagenesis is widely used for generating mutant libraries Although it is not flawless (for example, the possible influences of integration site may affect the phenotype) it has a huge advantage of having a known sequence in the region of insertion, which helps identify disrupted genes. Multiple methods have been created to identify the insertion sites. The restriction enzyme cassette mediated PCR method used here has both obvious advantages and disadvantages compared to other methods. Compared to purely PCR-based methods, the

major limitation of this approach is that it is time consuming and not suitable for use on a large scale. Methods such as restriction enzyme site-directed amplification PCR (RESDA-PCR) are better choices in a large-scale screening [112]. The prominent advantage of this approach is it could endure some degree of contamination, and the result is highly reliable. Thus, it is an excellent choice for a limited number of mutants. In this project, we started with RESDA method; however, we faced contamination issues, and troubleshooting did not resolve technical problems. When we switched to the restriction enzyme cassette mediated PCR, we got satisfying results.

The success of the restriction enzyme cassette mediated PCR relied on both the quantity of the genomic DNA and the Taq polymerase used for amplification. Some widely used DNA extraction protocols, which only work well for PCR, such as Chelex-100 extraction method [113], are not suitable for this method. Also, probably due to the high GC level (65%) of the *Chlamydomonas* genome, the general Taq polymerase only works for short fragment (≤500bp) amplification and does not work well for longer fragment amplification, which may be required in this method. Thus, a more robust and reliable Taq Polymerase gives a better result.

In recent years, with the rapid progress in techniques, more and more attractive methods for identifying mutation sites have been created and tested in the *Chlamydomonas* field, such as next-generation sequencing. It provides an alternative way to find mutation sites in *Chlamydomonas*. The whole genomes of mutants can be sequenced to identify the mutations [114-117]. However, sequence alignments and identification of the causative

mutation from multiple non-causative mutations remained challenging [117]. In the near future, the sequencing-based method still will be limited to mutations without a marker inside. As mentioned above, some purely PCR-based methods, such as RESDA, are suitable for large-scale screening.

When my study was close to completion, a genome-wide insertion mutant library for the *Chlamydomonas* was released. More than 20,000 mutants, which cover 58% of the *Chlamydomonas* genome, are contained in this library. Thousands of more mutants will be continuously added to the library. The library will be a powerful complement to resources that are currently available. This project could be much easier if this library were available at the time. Even if the desired mutants could not be found in the library, other methods, which could precisely edit the genome, such as CRISPR/Cas, could be exploited.

In recent years, the CRISPR/Cas9 system [118], which is developed from a prokaryotic immune system [119], is widely used for genome editing due to its simplicity and high efficiency in multiple organisms. The CRISPR/Cas9 system was proved function properly in *Chlamydomonas* [120]; after a few adjustments, the low-efficiency issue, which may be due to toxicity caused by the continuous expression of Cas9, was solved; the mutagenic efficiency and specificity in *Chlamydomonas* were improved dramatically [121]. Further development of the method related to CRISPR/Cas system would allow this method to be more attractive and robust in *Chlamydomonas* field.

Even though multiple alternative methods are available, this restriction enzyme cassette mediated method is still a valuable tool in some circumstances. Both the mutant library and CRISPR/Cas system are favorable in reverse genetics. However, some projects, such as finding out the unknown players in a specific pathway, may still need to use forward genetics by screening mutants. Although the insertional sites of these mutants in the library, which is mentioned above, had already been identified, it is not suitable for large-scale screening for a specific trait due to the high cost and the strain handling process. The CRISPR/Cas also could not give much help unless the candidate genes are limited. In forward genetics, if a dozen or tens of mutants were screened out by a specific trait, this method is an excellent choice due to its high reliability, low price, and a relatively high success rate. Also, lots of generated insertional mutants with interesting phenotype were preserved in past years. This method could also be used for identifying the insertional site of a specific mutant.

Methods and Materials

Strains culture conditions

Strains were streaked from stock slants onto fresh TAP agar plates for one week. The newly recovered strains were used for inoculating 20mL TAP medium in 50mL flasks. The flasks were kept on a shaker (125rpm) for 2-3 days until the cultures reached the dark green. During the process, the strains and cultures were maintained at room temperature with continuous light.

Restriction enzyme cassette mediated PCR

Cassette preparation

Took 5μL of each cassette-1 and cassette-2 (stock concentrations are 80nM), then mixed them together thoroughly. After that, the short double-strand cassettes were created using program: 94°C, 8 minutes; 92.5°C - 31°C (each minute let the temperature decrease 1.5°C), 4°C in hold.

DNA extraction

Fresh cell cultures that reach dark green were used for DNA extraction. Cells were collected at 3000rpm for 5 minutes. Then the cells were washed with fresh TAP medium and harvested by centrifugation The DNA was either extracted using Genomic DNA Purification Kit (Thermo) or following the protocol below:

The DNA quality and concentration were examined on 1% agarose gel if the DNA extraction were conducted using the protocol above.

Digestion

The extracted genomic DNA of each strain was divided into several parts depend on how many cassettes were used in each strain. The digestion system was set up as specific enzyme 5μL, 10×enzyme buffer 10μL, genomic DNA; then the volume was adjusted to 50μL using sterile water. The digestion tubes were kept at 37°C for 4 hours to overnight.

Ligation with cassette

Digested products were purified by ethanol precipitation and then ligated with corresponding cassettes. The ligation system was set as below, digested products 5μL, cassette 10μL, T4 Ligase 2μL, 10×T4 ligase buffer 3uL. The sterile water was added to reach 30μL. The ligation step took 4 hours to overnight.

PCR program

The ligation products were purified by ethanol precipitation, and the final volume was adjusted to 5μL using sterile water. One microliter purified ligation product was used for first round PCR. Two pairs of primers (C1 paired with L1 and S1, respectively) were used for each ligation products. Then amplification was conducted using program: 94°C 3 minutes, 94 °C 30 seconds 55°C 30 seconds 72°C 2 minutes 35 cycles, 72°C 10 minutes. Then 1μL of amplified product from first round PCR was used for the second round. Primer C2/L2 and C2/S2 were used for second round amplification. Third round PCR used the second-round PCR product (1μL) as a template. The final products were amplified using primers C2/L3 and C2/S3. In a rare case, the fourth-round PCR were used to increase the quality and quantity of the amplified fragment for ideal sequencing results.

The Gotaq® DNA polymerase (Promega) was used in the experiment. A suitable amount of $MgCl_2$ and DMSO were added to facilitate amplification of fragments with high GC content.

Sequencing results analysis

The sequencing results were analyzed using software Sequencher from Gene Codes Corporation.

Table 2-1 Primers used for restriction enzyme cassette mediated PCR and strain verification.

Primer names	**Sequences**
Primers for restriction enzyme cassette mediated PCR	
*Hin*dIII cassette-1	5' – GTA CAP ATT GTC GTT AGA ACG CGT AAT ACG ACT CAC TAT AGG GAG A – 3'
*Hin*dIII cassette-2	5' – AGC TTC TCC CAT TAG TGA GTC GTA TTA CGC GTT CTA ACG ACA ATA TGT AC – 3'
*Pst*I Cassette-1	5' – GTA CAT ATT GTC GTT AGA ACG CGT AAT ACG ACT CAC TAT AGG GAG ACT GCA – 3'
*Pst*I Cassette-2	5' – GTC TCC CTA TAG TGA GTC GTA TTA CGC GTT CTA ACG ACA ATA TGT AC – 3'
*Sac*II cassette-1	5' – GTA CAT ATT GTC GTT AGA ACG CGT AAT ACG ACT CAC TAT AGG GAG ACC GC – 3'
*Sac*II Cassette-2	5' – GGT CTC CCT ATA GTG AGT CGT ATT ACG CGT TCT AAC GAC AAT ATG TAC – 3'
*Nco*I Cassette-1	5' – GTA CAT ATT GTC GTT AGA ACG CGT AAT ACG ACT CAC TAT AGG GAG AC – 3'
*Nco*I Cassette-2	5' – CAT GGT CTC CCT ATA GTG AGT CGT ATT ACG CGT TCT AAC GAC AAT ATG TAC – 3'
*Apa*l Cassette-1	5' – GTA CAT ATT GTC GTT AGA ACG CGT AAT ACG ACT CAC TAT AGG GAG AGG GCC – 3'
*Apa*l Cassette-2	5' – CTC TCC CTA TAG TGA GTC GTA TTA CGC GTT CTA ACG ACA ATA TGT AC – 3'
Cassette Primer C1	5' – GTA CAT ATT GTC GTT AGA ACG CGT AAT ACG ACT CA – 3'
Cassette Primer C2	5' – CGT TAG AAC GCG TAA TAC GAC TCA CTA TAG GGA GA – 3'

Table 2-1 Continued

Primer names	**Sequences**
Left direction L1	5' – GCA ACT TTA TCC GCC TCC ATC CAG TCT AT – 3'
Left direction L2	5' – CGC TCG TCG TTT GGT ATG GCT TCA – 3'
Left direction L3	5' – GGC GAG TTA CAT GAT CCC CCA TGT T – 3'
Left direction L4	5' – GAT CGT TGT CAG AAG TAA GTT GGC – 3'
Right direction S1	5' – AAG AGT ATG AGT ATT CAA CAT TTC CGT GTC GCC – 3'
Right direction S2	5' – AGA AAC GCT GGT GAA AGT AAA AGA TGC TGA AG – 3'
Right direction S3	5' – AAG ATG CTG AAG ATC AGT TGG GTG C – 3'
Right direction S4	5' – CGT TTT CCA ATG ATG AGC ACT – 3'
Primers used for strain verification	
IFT57-51-69-F	5' – AGG CCA GCC TTC CAA CTT – 3'
IFT57-515-535-R	5' – AAA TTC TCA CCA TGC ACA CGT – 3'
IFT56-1598-1622-F	5' – CAT CCG CAA TGG CAC TGG TCT CCA T – 3'
IFT56-2065-2089-R	5' – CTC GCT ATC CCC ATC CCA GTC CTT T – 3'
IFT56-742-760-F	5' – GGA TCC ATG TTC TAC AGC AAG TCC AGA C – 3'
IFT81-2747-2766-F	5' – CTG CAG ACG TCG TAC CAG GA – 3'
IFT81-2918-2939-R	5' – CAG CCA ACC GGC TAG TTA AG – 3'
Hygromycin-F	5' – CGG TGG ATG GAA GAT ACT GC – 3'
Hygromycin-R	5' – GGT TAG CTC CTT CGG TCC TC – 3'

CHAPTER III

IFT57 STABILIZES ASSEMBLED INTRAFLAGELLAR TRANSPORT COMPLEX AND MEDIATES TRANSPORT OF MOTILITY-RELATED CARGO*

Introduction

Eukaryotic cilia/flagella project from the surface of almost all interphase cells where they perform a variety of signaling and motility-based functions [36]. The assembly and function of the cilium rely on intraflagellar transport (IFT), which is a bi-directional traffic of linear trains of IFT particles along the axoneme [122]. Ciliary defects, including those caused by IFT deficiencies, are linked to ciliopathies, such as polycystic kidney disease (PKD) and Bardet-Biedl syndrome (BBS) [123].

The IFT particle is composed of two biochemically separable complexes, IFT-A and IFT-B, which contain 6 and 16 subunits, respectively [36]. The research in the past decade has made significant advances in the architecture of the IFT complexes, especially the IFT-B complex [55, 124, 125]. The IFT-B complex contains a salt-resistant-core-complex and several peripheral proteins [126]. An earlier yeast two-hybrid assay shows that the peripheral proteins IFT57 and IFT20 directly interact [127], providing the first clue that the peripheral proteins may not just loosely stick onto the IFT-B core complex, but rather form complexes. Indeed, two very recent comprehensive mappings of interactions among all IFT-B subunits demonstrate all peripheral proteins,

---

*Reprinted with permission from "IFT57 Stabilizes Assembled Intraflagellar Transport Complex and Mediates Transport of Motility-Related Flagellar Cargo" by Xue Jiang, Daniel Hernandez, Catherine Hernandez, Zhaolan Ding, Beiyan Nan, Karl Aufderheide, Hongmin Qin. *J Cell Sci* doi: 10.1242/jcs.199117

IFT20, IFT54, DYF-3/Cluap1, IFT57, IFT80, and IFT172, form a distinct biochemical complex which is now called IFT-B2. The core complex, IFT22, IFT25, IFT27, IFT46, IFT52, IFT56, IFT70, IFT74, IFT81, and IFT88, is renamed as IFT-B1 [55, 125].

Several subunits play prominent roles in IFT-B assembly. IFT52 is the backbone for the IFT-B1 subcomplex IFT88/70/52/46 [50, 52]. IFT52 is also essential for the overall stability of IFT-B1 because it mediates the binding of the subcomplex IFT88/70/52/46 with the other subcomplex IFT81/74/27/25/22 [50, 51]. Recently, the Lorentzen and the Nakayama laboratories, using expressed *Chlamydomonas* and human/mouse proteins, respectively, have biochemically mapped the subunits at the interface between IFT-B1 and IFT-B2 [55, 125]. IFT57 and DYF-3/Cluap1 in IFT-B2 and IFT52/IFT88 in IFT-B1 are the ones bridging the two subcomplexes together to form a complete IFT-B complex. Consistently, the IFT-B complex completely fails to assemble in the *bld1*/*ift52* mutant, while IFT-B2 proteins dissociate from the IFT-B1 complex in the *ift88* mutant in *Chlamydomonas* [52]. The essential role of DYF-3/Cluap1 in IFT-B assembly has also been verified by the cultured Cluap1$^{-/-}$ MEF cell line [125]. Currently, among the four interface subunits, only the impact of IFT57 on the *in vivo* assembly of the IFT-B complex has not been examined.

It is unknown whether individual subunits of IFT57 and DYF-3/Cluap1 are sufficient for the interaction with IFT88/52. The Nakayama group, through the use of visible immunoprecipitation (VIP) assays, shows that IFT57 and DYF-3/Cluap1 are essential for mediating the binding between the two IFT-B subcomplexes [125]. However, since IFT57 and DYF-3/Cluap1 could only be purified as a single complex, whether individual

subunits or both are necessary for the interaction with IFT88/52 still needs to be determined [55]. Moreover, the work from the Lorentzen group uses purified proteins from *E. coli* [55], while the interaction mapped by Nakayama and colleagues is through exploration of an artificial overexpression system [125]. Ideally, the role of IFT proteins in IFT complex assembly should be addressed through an organism with functional IFT.

In most ciliated organisms, the heterotrimeric kinesin-2 motor drives the anterograde transport of IFT particles carrying cargo proteins to the flagellar tip, and the cytoplasmic dynein-1b returns particles carrying turnover products to the base [18, 128-131]. Since the IFT particle relies on the proper association of multi-subunits, the loss of any one of IFT particle proteins could have a disastrous effect on the structure of the IFT particle, leading to defects in ciliary assembly and function. Obviously, the subunits in the interface between IFT-B1 and IFT-B2, IFT52, IFT88, DYF-3/Cluap1, and IFT57, are likely critical for the integrity of the IFT-B complex. On the other hand, several IFT particle proteins are shown to bind to specific flagellar precursors directly. For example, IFT46 directly interacts with ODA16, which facilitates the outer arm dynein transport [20, 65, 132]. By dimerization, IFT74 and IFT81 cooperatively transport tubulin for cilia assembly [56, 66]. IFT56/DYF-13 appears to carry a set of proteins involved in motility [53]. Consistent with being an IFT particle protein, IFT57 has been shown to be essential for ciliogenesis in several model organisms, including *Caenorhabditis elegans* [133, 134], zebrafish [135], and mice [136]. However, the exact role of IFT57 in the IFT-B complex assembly and cargo transportation is unknown.

In this study, we isolated a mutant, which contains a hypomorphic allele of *IFT57*, in *Chlamydomonas* and analyzed the specific contributions of IFT57 in flagellar assembly and function. The mutant expresses a significantly reduced amount of IFT57. Concomitantly, the amounts of some other IFT-B core proteins decrease dramatically as well. Surprisingly, although IFT57 lies at the interface between IFT-B1 and IFT-B2 [55, 125], the depletion of IFT57 affects neither the assembly of IFT-B nor the flagellar entry of IFT particles. We also show that even though a percentage of the *ift57* mutant cells assemble flagella, these flagella have motility defects and display abnormal waveforms. Analysis of the mutant flagellar protein composition shows certain axonemal proteins are drastically changed, suggesting that IFT57 is involved in transporting a specific set of motility-related cargoes.

Results

The ift57-1 mutant expresses a trace amount of IFT57 due to an insertion at 5'UTR of IFT57 gene

We generated *C. reinhardtii* mutants by random insertional mutagenesis and first screened for phototaxis defective mutants. Flagellar assembly mutants were found by microscopic observation [137]. We further screened a set of mutants with severe flagellar assembly defects by immunoblotting whole cell extracts with a strong IFT-B antibody anti-IFT46 [20]. One strain *2P40* was found expressing a highly-reduced level of IFT46 and contained a complete hygromycin-resistant gene cassette in the 5' UTR of *IFT57* loci (Figure 3-1 A). We renamed the mutant *2P40* as *ift57-1* after backcrossing three times. Since the coding sequence of *IFT57* remained intact, we hitherto evaluated

the effect of the insertion by measuring the protein and mRNA abundance of *IFT57* in *ift57-1*. The mutant cells expressed about 5% of wild-type amount of *IFT57* at both the mRNA (Figure 3-1 D) and protein level (Figure 3-1 B, C). Therefore, the insertion at the 5'UTR did not completely abolish the expression of *IFT57* but rather reduced its transcriptional efficiency or transcripts' stability. After transforming a 7.2-kb genomic fragment containing *IFT57* gene into the *ift57-1* genome, *IFT57* expression at both the protein and mRNA level was recovered (Figure 3-1 B-D). Moreover, accompanied by the expression of *IFT57*, the flagellar defects associated with *ift57-1* were rescued as well (Figure 3-3 B, C).

Depletion of IFT57 reduces the stability of IFT-B1

The effects of the IFT-B2 protein IFT57 depletion on other IFT particle proteins were examined by immunoblotting assays. Previously characterized IFT-B1 mutants, *bld1/ift52*, *ift46*, and *ift88* were included for comparisons. Similar to IFT-B1 mutants, *ift57-1* had a normal to a slightly elevated cellular level of the complex A protein IFT122 but substantially reduced levels of complex B1 proteins, IFT46, IFT74, and IFT81 (Figure 3-1 E). However, despite the fact that IFT57 and IFT20 are in the same IFT-B2 subcomplex and directly interact biochemically [55, 125], IFT20 was not reduced but rather increased in *ift57-1* (Figure 3-1 E). Since the IFT20 level was not adversely affected by the depletion of the IFT-B complex, the biochemical stability of IFT20 is independent of the presence of either the IFT-B1 or IFT-B2 subcomplexes.

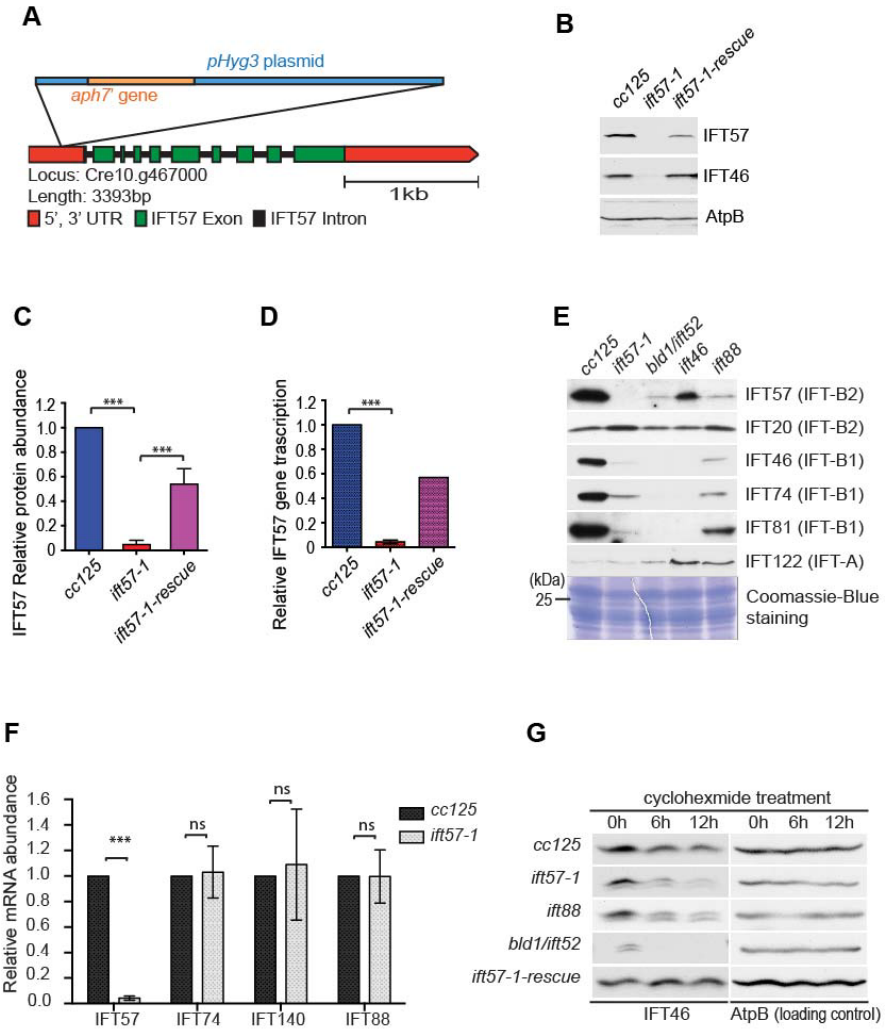

Figure 3-1. Characterization of the *ift57*-1 mutant.
A. A hygromycin resistant gene *aph7'* was inserted to the 5'UTR after nucleotide 91 of the *IFT57* gene. **B**. The *IFT57* expression at the protein level was reduced in the *ift57-1* mutant. Whole cell lysates from the wild-type *cc125* and the mutant *ift57-1* were probed with antibodies against IFT57 and IFT46. Beta subunit of ATP synthase (AtpB) was used to show equal loadings. The *ift57-1* mutant cells had ~ 5% of wild-type amount of *IFT57* at the protein (panel **C**) and mRNA level (panel **D**). IFT57 was recovered to ~ 50% of wild-type level in the *ift57-1-rescue* strain. The relative IFT57 abundances were plotted based on the intensity of the bands on immunoblots. The mRNA of *IFT57* was measured by qPCR. Data were collected from three independent experiments. **E**. The levels of the IFT-B proteins were severely reduced in *ift57-1*. Whole cell lysates from *cc125*, *ift57-1*, and three known IFT-B mutants (*bld1*/*ift52*, *ift46,* and *ift88*) were probed with antibodies against IFT complex proteins. **F**. IFT genes (*IFT74*, *IFT140,* and *IFT88*) were expressed at similar levels in *cc125* and *ift57-1*. The graph was generated from three independent qPCR results. **G.** The stability of IFT46 was reduced in *ift57-1*. A 12-hour-time-course treatment with cycloheximide was used to examine degradation rates of existing proteins. Whole-cell extracts were probed against anti-IFT46. AtpB was used to ensure equal loadings. In all panels, the error bars represent standard deviations (s.d.).

We then measured mRNA levels and turnover rates of IFT proteins in *ift57-1* to determine if reduced cellular levels of IFT-B1 proteins were caused by transcriptional inhibition or increased protein degradation. The qPCR results showed that the transcriptional levels of *IFT74* (IFT-B1), *IFT88* (IFT-B1), and *IFT140* (IFT-A) in *ift57-1* were comparable to those of wild-type cells (Figure 3-1 F). Apparently, the depletion of *IFT57* mRNA did not affect the gene transcriptions of IFT particle proteins. Then we conducted a time-course cycloheximide treatment to measure the degradation rate of IFT46, which is critical for the stability of IFT-B [20, 52], in *ift57-1*. Similar to previous results, IFT46 was very stable in wild-type cells (Figure 3-1 G), showed a slight decrease in stability in the *ift88* mutant and a dramatic reduction in the *bld1/ift52* mutant [52]. In the *ift57-1* mutant, IFT46 exhibited a decreased stability, indicating IFT57 is important for preventing degradation of IFT complex B proteins. Moreover, when *ift57-1* mutant cells reached the stationary growth phase, the IFT-B complex was quickly degraded (Figure 3-2). These results are in agreement with IFT57 as an integral component of the IFT-B complex, and IFT57 depletion results in the destabilized IFT-B complex (Figure 3-1 G).

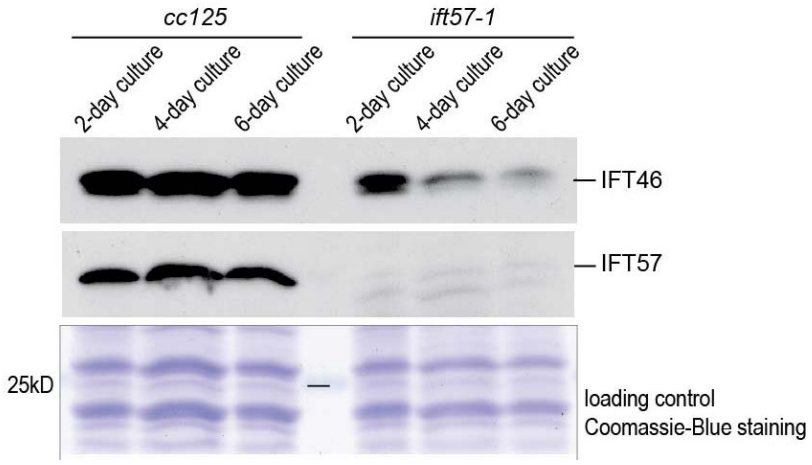

Figure 3-2. The amount of IFT particle proteins decreases when the *ift57-1* mutant cell culture reaches the stationary stage.
After the cells had been transferred from TAP plates to liquid media, the cultures were in the exponential growth stage in the first two days and then entered the stationary stage on day 3 or day 4. Immunoblots of whole cell lysates from 2-day, 4-day, and 6-day cultures were probed with antibodies, anti-IFT46 and anti-IFT57. Stained gels were used to ensure equal loadings. The amount of IFT46 and IFT57 in wild-type cells always remained constant throughout the six-day culture period no matter whether the cells kept dividing or not. In contrast, the level of IFT46 was reduced gradually after the *ift57-1* cells shifted from the exponential growth to the stationary phase. The total cellular amount of IFT46 is influenced by two factors: one is the rate of new protein synthesis, and the other is the rate of protein degradation. A previous study shows that the transcription of IFT particle protein genes is cell cycle regulated. IFT protein mRNAs are expressed during the S and the M phase but are inhibited in the G1 phase [138]. When *ift57-1* cell culture reached the stationary stage, cell division was halted which in turn inhibited the production of new IFT46 mRNA and protein. At the same time, without IFT57 the assembled existing IFT-B complex was unstable and quickly degraded, resulting in a low amount of IFT46. These results supported the fact that IFT57 is important for maintaining the stability of the IFT-B complex.

The flagellar assembly is compromised when IFT57 is depleted

As the depletion of IFT57 caused a reduction of IFT particles, we asked how the flagellar assembly is affected in *ift57-1* mutant cells. Unlike wild-type *cc125* that contained individual cells with two long flagella (mean length=10.55 ±1.11 μm) (Figure 3-3 A-C), about 80% of *ift57-1* total cell population were clusters of four or eight cells

encased in mother cell walls (Figure 3-3 A, B). Close microscopic analyses revealed that at least some cells trapped inside the mother cell walls assembled short flagella (Figure 3-3 A). The release of daughter cells from mother cell walls depends on a proteolytic enzyme secreted by the flagella of the daughter cells [139]. Apparently, *ift57-1* flagella were incapable of secreting a sufficient amount of the enzyme to digest mother cell walls. Moreover, most of the small percentage of liberated individual cells in the *ift57-1* culture were bald; a few cells assembled flagella (2.3%). Occasionally, a cell with near full-length flagella could be observed (Figure 3-3 A-C). Obviously, the flagellar assembly of *ift57-1* was greatly compromised. These results are consistent with IFT57 being critical for ciliogenesis in other ciliated organisms [133-136].

Autotrophic condition promotes the flagellar assembly and IFT particle protein expression

There are two common media for *Chlamydomonas* culture, TAP and M1. The main difference between them is the TAP provides carbon nutrients, while the M1 does not. Consequently, the cell growth is entirely dependent on photosynthesis. *Chlamydomonas* cells grow much faster in TAP media. However, the cells, especially the flagellar defective mutants, flagellate much better when cultured in M1 media. Therefore, M1 media is often used to encourage flagellar assembly. When *ift57-1* grew in M1 media, cell clumps seen in TAP media largely disappeared (Figure 3-4 A). Moreover, about 75% of cells assembled relative long flagella ($\geq$ 6 μm). Obviously, when the *ift57-1* cells were cultured autotrophically in M1 media, the flagellar assembly was much less adversely affected.

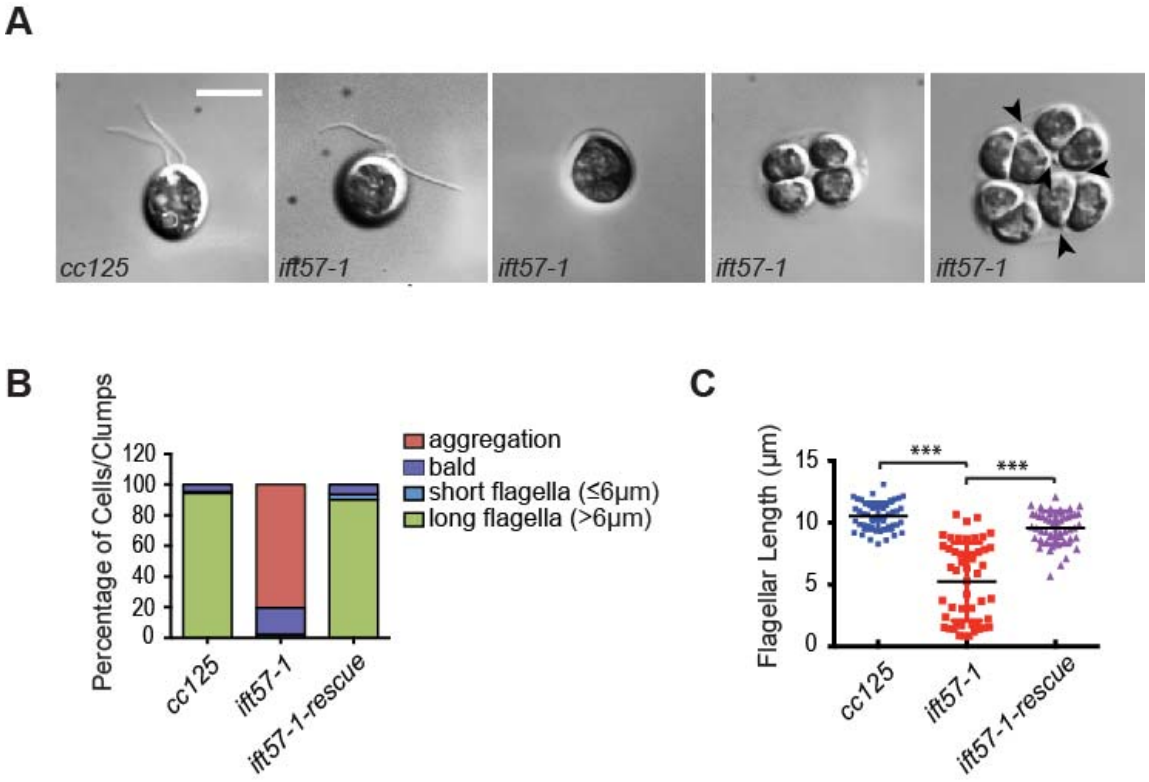

Figure 3-3. IFT57 depletion causes flagellar assembly defects.
A. The *ift57-1* mutant cells displayed a range of flagellar assembly defects. The control wild-type *cc125* cells were rarely seen in clusters, and over 90% of cells had full-length flagella. When *ift57-1* cultured in TAP media, most cells were seen in clumps. Hatched individual cells assembled no or short flagella. Tiny flagella were occasionally observed on cells trapped inside mother cell walls (highlighted by black arrowheads). The scale bar equals 10μm. **B.** Three hundred randomly picked cells or cell clumps from each strain were analyzed. The graph shows the percentage of cells or cell clumps that: a) assembled long flagella (>6μm); b) assembled short length flagella, (≤ 6μm); c) were bald; or d) were in aggregates. One representative result is shown here. Similar results were observed in many repeats. **C.** Fifty flagellated cells from each culture were randomly selected for length measurement. The average flagellar length of *ift57-1* mutant cells (5.25 ± 3.15 μm) was shorter than that of wild-type cells (10.55 ± 1.11μm). The defect was partially recovered in the rescue strain *ift57-1-rescue* (9.58 ± 1.34μm).

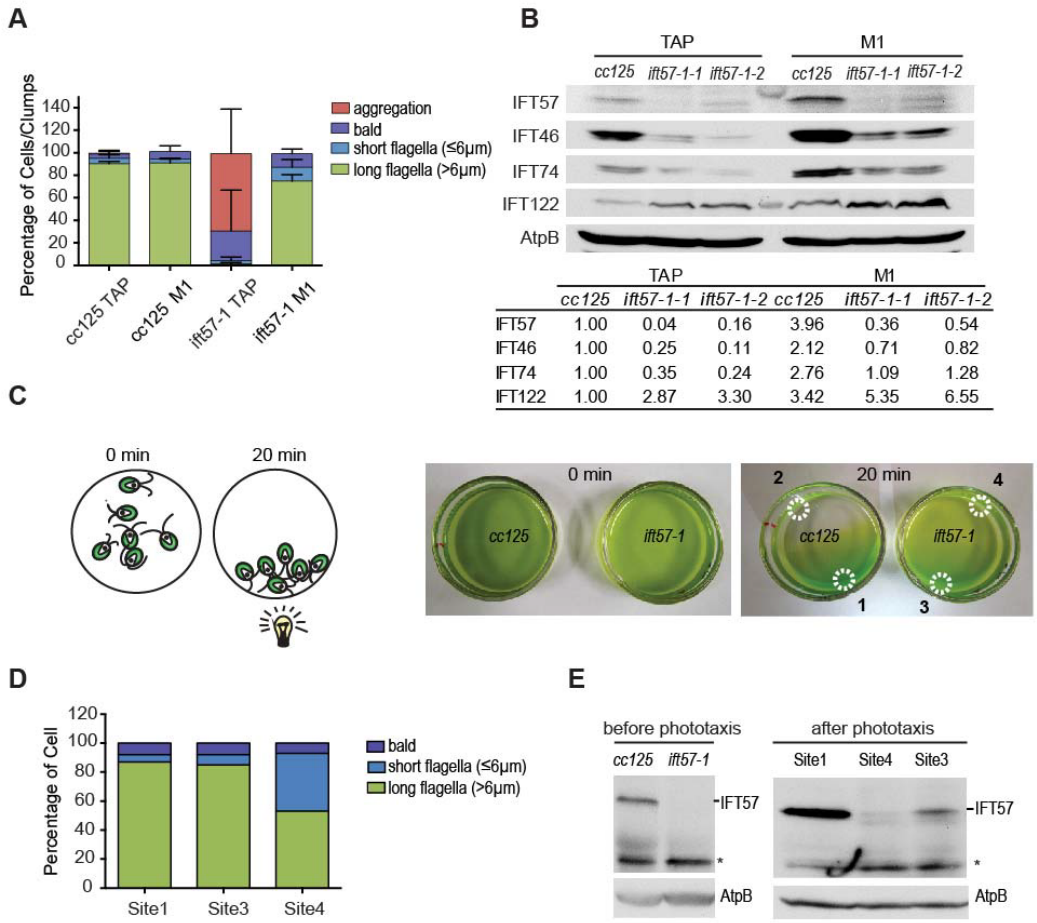

	TAP			M1		
	cc125	*ift57-1-1*	*ift57-1-2*	*cc125*	*ift57-1-1*	*ift57-1-2*
IFT57	1.00	0.04	0.16	3.96	0.36	0.54
IFT46	1.00	0.25	0.11	2.12	0.71	0.82
IFT74	1.00	0.35	0.24	2.76	1.09	1.28
IFT122	1.00	2.87	3.30	3.42	5.35	6.55

Figure 3-4. Autotrophic condition promotes flagellar assembly of *ift57-1*.
The *ift57-1* mutant cells were flagellated better in M1 than in TAP. Data were collected from three independent experiments (total n=300, individual cells plus cell clumps per experiment). Error bars represent s.d.. **B.** Immunoblots of whole cell lysates from cells cultured in TAP or M1 media probed with antibodies against IFT particle proteins as indicated. Lanes between the "TAP" and "M1" samples were molecular weight markers. The samples "*ift57-1*-1 and *ift57-1*-2" were duplicates of whole-cell extracts of *ift57-1*. The table showed the relative protein abundances were based on the intensity of the bands on immunoblots. The bands in the lane "*cc125* TAP" were assigned as "1.00". AtpB bands were used to normalize the variations caused by loadings. **C.** Using the photoaccumulation assay, the wild-type *cc125* or the mutant *ift57-1* cells were separated into two groups; one that swam to light (1 and 3), and the other group failed to swim towards the light source (2 and 4). **D.** Cells taken from sites 1, 3, and 4 (n=300) were observed under the microscope. The graph shows the percentage of cells that were bald, with short flagella, or with long flagella. Site 2 was devoid of cells because of strong phototaxis effects. The result from one experiment is shown here. Similar results were obtained from three repeats. **E.** Immunoblots of whole-cell lysates showed cells from site 3 expressed a higher level of IFT57 than those from site 4. Antibody AtpB was used to ensure equal loadings. Similar results were observed in three repeats. The nonspecific bands on anti-IFT57 immunoblots were labeled with "*".

Immunoblotting results showed that both the wild-type and the *ift57-1* mutant cells clearly expressed a higher amount of IFT particle proteins when the cells cultured in M1 were compared to those in TAP media (Figure 3-4 B). Therefore, the autotrophic culture condition increased the cellular concentrations of IFT particle proteins in general, which led to the improved flagellar assembly of *ift57-1* cells cultured in M1 media.

We then asked whether *ift57-1* cells with long flagella contain more IFT particles than those with short/no flagella. Because only the cells bearing long flagella swam effectively towards light while the ones with short/no flagella could not (Figure 3-4 C, D), we were able to separate them by photoaccumulation. Immunoblotting analysis revealed that cells with longer flagella indeed had a higher *IFT57* expression, while the ones with shorter or no flagella had a much lower amount of IFT57 (Figure 3-4 E). To summarize, these results provide lines of evidence that in *ift57-1* cells the *IFT57* expression positively correlates with the status of flagellar assembly.

In *Chlamydomonas*, gametes possess longer flagella than vegetative cells. We want to test whether IFT proteins are more abundant in gametes. Additionally, we showed that cells cultured in M1 have a higher concentration of IFT than cells cultured in TAP. The major difference between cells cultured in these two conditions is the length of the cell cycle; cells have a longer cell cycle in M1. Gametes, compared to vegetative cells, have an even longer cell cycle, which may lead to even higher concentration of IFT. To test this hypothesis, we examined the level of IFT proteins in gametes, M1 cultured cells, and TAP cultured cells in both wild-type *cc125* and *ift57*. Results showed that in both

strains, gametes have the highest level of IFT proteins whereas the TAP cultured cell has the lowest, which is correlating with their length. It indicates that the level of IFT plays a role in regulating the flagellar length. The better flagellation in autotrophic condition is likely due to the slower cell cycle in M1 medium, which results in an accumulation of IFT (Figure 3-5).

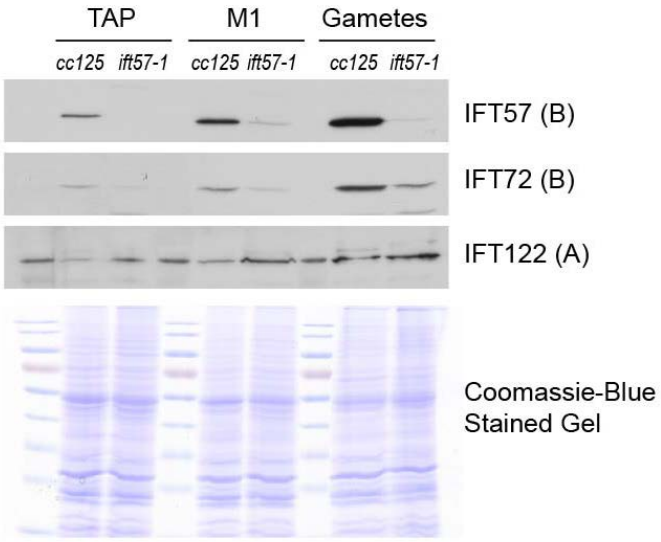

Figure 3-5. Gametes have a higher concentration of IFT particle proteins than the vegetative cells.
TAP cultured cell, M1 cultured cell, and gametes were collected from both the wild-type *cc125* and the mutant *ift57-1*. Immunoblots of the whole cell were probed with antibodies, anti-IFT57 (IFT-B), anti-IFT72 (IFT-B), and anti-IFT-122 (IFT-A). A Coomassie-Blue stained gel was used to ensure equal loadings. The bands showed in lanes between samples on the IFT122 panel are caused by the protein marker.

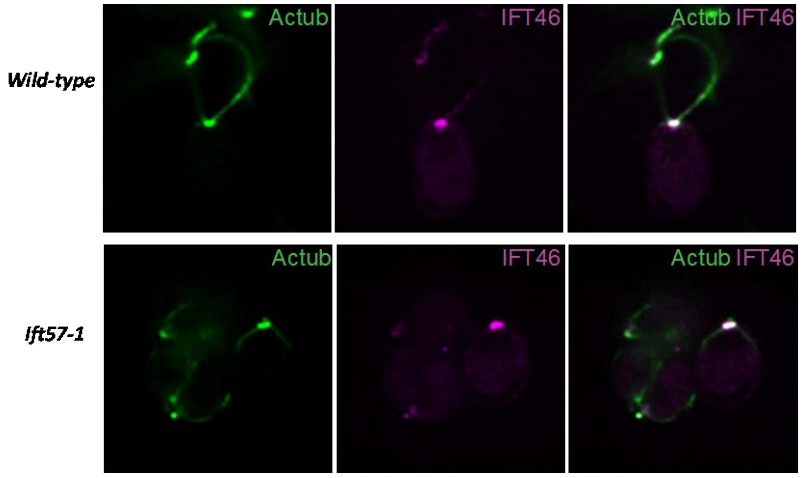

Figure 3-6. Effects of IFT57 reduction on cellular localization of IFT-B subunit IFT46.
Immunofluorescent stainings of the wild-type *cc125* and the mutant *ift57*-1. Antibodies against IFT46 were used in the stainings. Acetylated tubulin was used as a basal body marker.

IFT particle proteins localize to the basal body in ift57-1 mutant cells

To examine whether the IFT-B complex still localized to the basal body in *ift57-1*, we checked the cellular distribution of a few IFT proteins by indirect immunofluorescence staining (Figure 3-6 and Figure 3-7). The anterograde motor subunit FLA10 and acetylated tubulin were used as a basal body marker [18, 52, 140]. We chose the cells cultured in TAP media and that had tiny/no flagella for staining. These cells presumably had a low level of *IFT57* expression (Figure 3-1 B, C). Results showed that in both wild-type and the *ift57-1* mutant cells, the IFT-A protein IFT139 co-localized with FLA10 at the basal body. Thus, the IFT-A was not affected by the depletion of IFT57. In contrast, changes were noticed for IFT-B proteins. In *cc125*, all three IFT-B proteins co-localized with IFT122 (IFT-A) and FLA10. In the mutant *ift57-1*, IFT46 (IFT-B1) was clearly

localized to the basal body. IFT81 (IFT-B1) and IFT172 (IFT-B2) were also consistently found at the basal body. However, the labeling of IFT81 (IFT-B1) was more dispersed, similar to the background dots in wild-type cells. In contrast, although only a small proportion of IFT172 reached the basal body, most IFT172 did not disperse throughout the cell but rather accumulated just beneath the basal body. This cellular distribution pattern of IFT172 was also observed in other IFT-B mutants (Figure 3-8). Overall, the localization of IFT particle proteins, as well as the IFT motor FLA10, appeared to be normal.

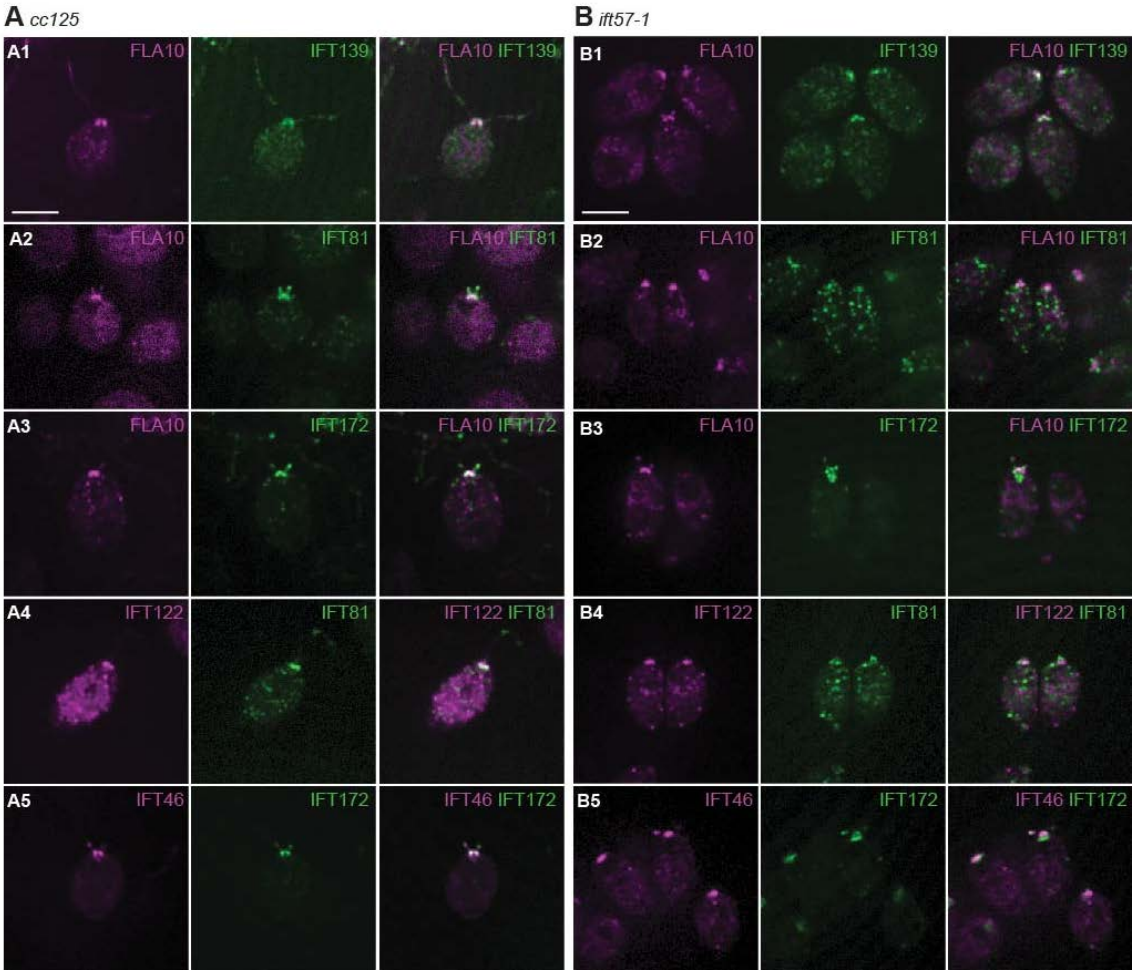

Figure 3-7. Effects of IFT57 reduction on cellular localization of IFT-B proteins.
Immunofluorescent stainings of the wild-type *cc125* (**A**) and the mutant *ift57*-1 (**B**). Antibodies against IFT proteins, IFT139 (A), IFT122 (A), IFT172 (B), IFT81 (B), IFT46 (B), and FLA10, were used in the stainings. All analyzed cells showed consistent localization patterns as depicted in Panel A1, B1, A2, B2, A4, and B4. The IFT172 accumulation beneath the basal body (depicted as in B3 and B5) was often detected in *ift57-1* mutant cells (49 out of 61), while it was rarely seen in *cc125* (2 out of 25). Scale bars equal 10μm.

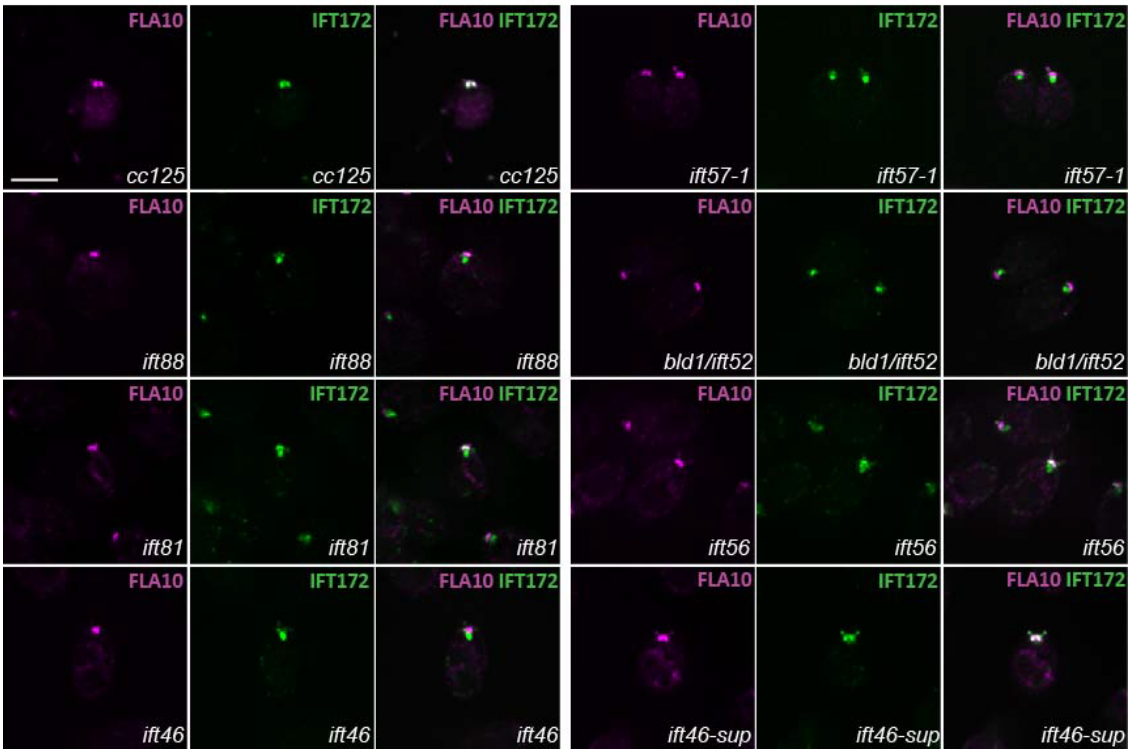

Figure 3-8. Localization of IFT172 in IFT-B mutants.
Immunofluorescent staining revealed the localization patterns of IFT172 in *cc125*, *ift57-1*, and several known IFT-B mutants including *ift88*, *ift52*, *ift81*, *ift56*, *ift46*, and *ift46* suppressor (*ift46-sup*). IFT172 mostly accumulated beneath basal bodies in *bld1/ift52* and *ift88* mutants. In *ift57-1* and *ift46*, a small amount of IFT172 localized to basal bodies while the rest concentrated just beneath basal bodies. The *ift46* suppressor (*ift46-sup*) partially or completely rescued the mislocalization of IFT172. The mutant *ift81* and *ift56* had relatively mild defects in IFT172 mislocalization. FLA10 was used as a marker for basal bodies. The scale bar equals 10μm. Although IFT172 accumulation beneath the basal body has a subtle degree of variation in the population, it was very obvious in mutant cells (*dyf-13*, 13 out of 15 cells; *ift46*, 17 out of 18; *ift46-sup*, 10 out of 21; *ift52*, 18 out of 18; *ift81*, 7 out of 11; and *ift88*, 16 out of 16). However, it is rarely seen in wild-type *cc125* (2 out of 25). Images that can present the majority of the cells were chosen in this figure.

CrDYF-3 is an IFT particle protein of Chlamydomonas and co-purifies with IFT57

IFT57, together with CrDYF-3, plays a crucial role in IFT-B1 and IFT-B2 connection through contacts with IFT52/88 [55, 125]. We generated polyclonal anti-CrDYF-3 antisera

to detect the endogenous CrDYF-3 on Western blots. The antibody recognized a single band, which is slightly smaller than IFT57 of flagellar extracts (Figure 3-9 A).

The flagellar entry of IFT particles solely depends on the anterograde motor kinesin-II [16]. The mutant *fla10-1* harbors a point mutation in the kinesin-II motor subunit FLA10, and is functionally normal in flagellar assembly at the permissive temperature (18°C) but abolishes the anterograde IFT at the non-permissive temperature (32°C) [18, 141]. Similar to IFT particle subunits IFT139 and IFT74, the amount of CrDYF-3 was significantly decreased in the flagella of the *fla10-1* mutant at 32°C (Figure 3-9 B). This result revealed that, like other IFT proteins, the entrance of CrDYF-3 into flagella is FLA10 dependent.

We then utilized sucrose density gradient centrifugation to determine the sedimentation pattern of CrDYF-3 (Figure 3-9 C, D). On the gradient, CrDYF-3 co-peaked with IFT57 in the 16S fractions. The corresponding band from the Coomassie-Blue stained gel (Figure 3-9 D) was analyzed by mass spectrometry. Only two proteins, IFT57 and CrDYF-3, were identified from the band (data were not shown), confirming the identity of CrDYF-3. Moreover, we noticed that IFT-B1 and IFT-B2, the two subcomplexes of IFT-B, did not completely co-sediment on gradients (Figure 3-9 C). IFT-B1 subcomplex proteins IFT81 and IFT70 co-peaked at the fractions 8 and 9, while IFT-B2 subunits IFT57 and CrDYF-3 concentrated at the fractions 9 and 10. Therefore, IFT-B1 and IFT-B2 were biochemically separated on gradients. These results suggested that the

association and disassociation between IFT-B1 and IFT-B2 could be subjected to regulation *in vivo*.

The purification of recombinant CrDYF-3 protein alone is difficult since the protein appears to be structurally unstable and is prone to form aggregates. DYF-3 becomes soluble only when it co-expressed with IFT57 [55]. Indeed, a few attempts to purify the soluble CrDYF-3 protein alone from *E. coli* were unsuccessful. However, when we mixed the two crude *E. coli* extracts which contained the expressed tagged CrDYF-3 and IFT57 proteins, respectively, we were able to co-purify CrDYF-3 and IFT57 (Figure 3-9 E). This result supports that CrDYF-3 and IFT57 directly interact.

Figure 3-9. CrDYF-3 is an IFT-B2 protein in *Chlamydomonas*.
A. The size of CrDYF-3 was slightly smaller than that of IFT57 based on two immunoblots of a single membrane. The membrane was first probed with anti-CrDYF-3 (a rabbit antibody), and then with anti-IFT57 (a mouse monoclonal antibody). **B.** Immunoblots of flagellar extracts showed that CrDYF-3 disappeared along with IFT139 and IFT74 from *fla10-1* flagella at 32°C. Axonemal protein IC69 was used as an equal loading control. **C.** CrDYF-3 co-migrated with IFT57 on sucrose density gradients. Immunoblots of gradient fractions showed that the sedimentation peaks of IFT-A protein IFT139, IFT-B proteins IFT81, IFT70, IFT57, and CrDYF-3. Arrows highlighted the peak fractions of each labeled protein. **D.** The upper panel is a Coomassie-Blue stained gel of gradient fractions showing protein bands of IFT particle proteins. Grey arrows highlighted the fractions of IFT-A and IFT-B, respectively. The lower panel showed the positions of IFT57 and CrDYF-3 along with a few other IFT-B proteins. **E.** CrDYF-3 interacts with IFT57. MBP-tagged IFT57 and GST-tagged CrDYF-3 were expressed in *E.coli* and used for in vitro binding assay. The left panel (Coomassie-Blue stained gel) showed that immobilized MBP-IFT57 pulled down CrDYF-3 protein. Immunoblots probed with antibodies against IFT57 and CrDYF-3 on the right panel showed that immobilized GST-CrDYF-3 retained IFT57 protein. The Coomassie-Blue stained gel at the bottom was used to show the proteins in the input for pull-down analysis.

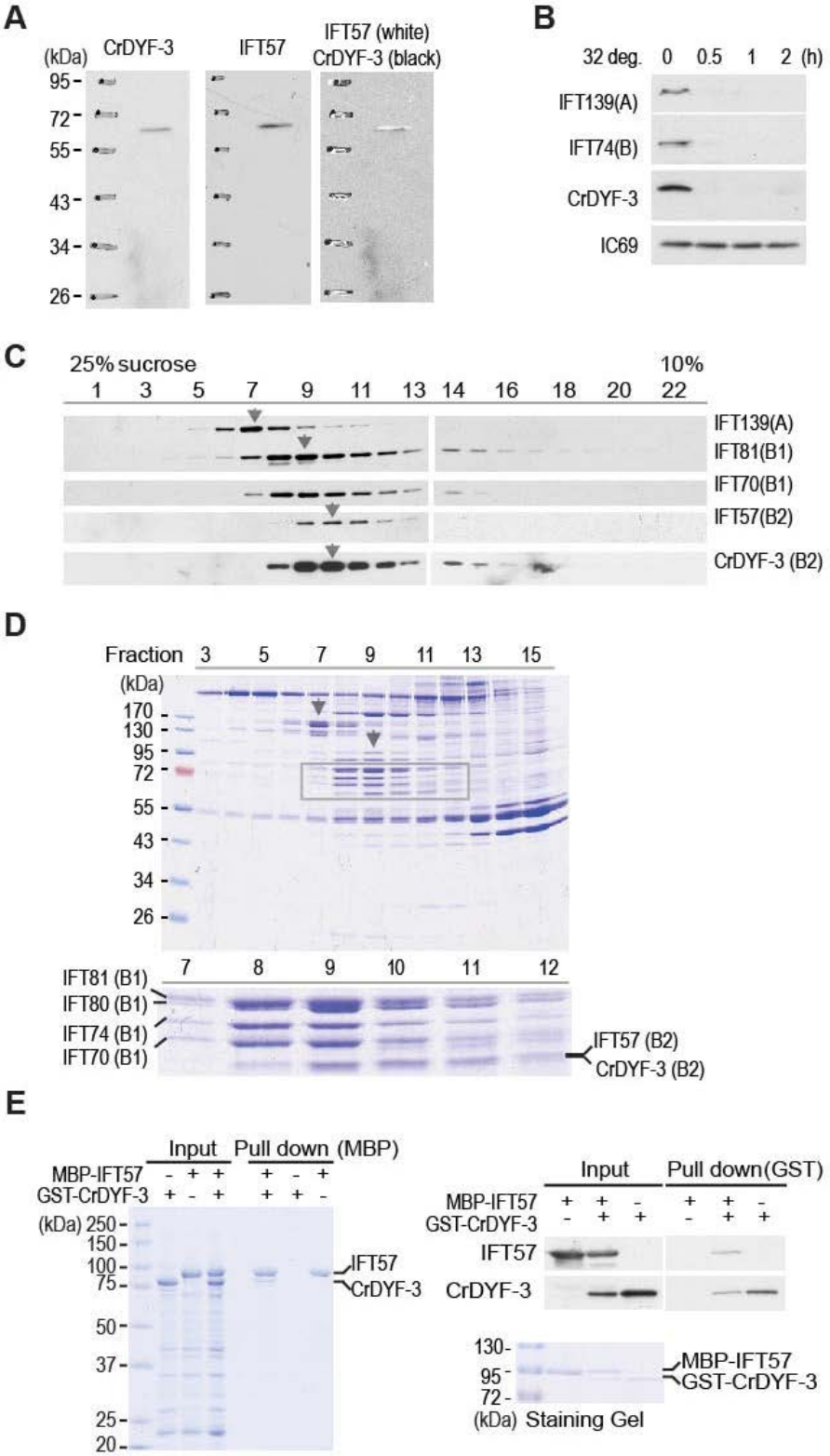
A
(kDa)
CrDYF-3
IFT57
IFT57 (white)
CrDYF-3 (black)
95
72
55
43
34
26
B
32 deg.
0
0.5
1
2 (h)
IFT139(A)
IFT74(B)
CrDYF-3
IC69
C
25% sucrose
10%
1 3 5 7 9 11 13 14 16 18 20 22
IFT139(A)
IFT81(B1)
IFT70(B1)
IFT57(B2)
CrDYF-3 (B2)
D
Fraction 3 5 7 9 11 13 15
(kDa)
170
130
95
72
55
43
34
26
7 8 9 10 11 12
IFT81 (B1)
IFT80 (B1)
IFT74 (B1)
IFT70 (B1)
IFT57 (B2)
CrDYF-3 (B2)
E
Input
Pull down (MBP)
MBP-IFT57
GST-CrDYF-3
(kDa)
250
150
100
75
50
37
25
20
IFT57
CrDYF-3
Input
Pull down(GST)
MBP-IFT57
GST-CrDYF-3
IFT57
CrDYF-3
130
95
72
(kDa)
Staining Gel
MBP-IFT57
GST-CrDYF-3

IFT57 depletion does not affect the flagellar entry of IFT particles and the assembly of IFT-B complex

To address how the depletion of IFT57 affects the distribution of IFT particles to flagella, we checked the levels of IFT57 as well as several subunits of IFT-A and IFT-B in isolated *ift57-1* flagella (Figure 3-10 A, B). *Ift57-1 flagella* showed a reduced level of IFT57 compared to wild-type *cc125*. Two complexes, IFT-A and BBSome, remained at wild-type levels. Strikingly, the flagellar content of IFT-B2 proteins CrDYF-3 and IFT172 as well as IFT-B1 subunits IFT46, IFT56 and IFT81 was not reduced. This result revealed that, in *ift57-1* mutant flagella, IFT57 was at a sub-stoichiometric level relative to the rest IFT-B proteins (Figure 3-10 A, B). The IFT-B complex assembly appeared to be normal in *ift57-1* (Figure 3-10 C). We also examined the movement of IFT trains in *ift57-1* mutant flagella with total internal reflection fluorescence (TIRF) microscopy followed by kymograph analysis [90, 142, 143]. The KAP-GFP-fusion protein underwent robust anterograde IFT with similar speeds as in wild-type *cc125* (Figure 3-10 D, E and Video 3-8, Video 3-9), indicating that the IFT movement is likely unaffected in *ift57-1* flagella. Therefore, despite the fact that IFT57 sits at the interface between the IFT-B1 and IFT-B2 complexes [55, 125], these results collectively showed that IFT57 is not essential for the assembly of IFT-B, nor required for the flagellar entry of IFT particles. Because CrDYF-3 presented at the wild-type level in *ift57-1* mutant flagella, we postulated that CrDYF-3, the other interface subunit of IFT-B2, is sufficient to mediate the binding between IFT-B1 and IFT-B2.

IFT57 is required for establishing normal flagellar waveforms

While performing the photoaccumulation experiments, we noticed that within the population of *ift57-1* cells that failed to swim towards the light source, about 50% percent of cells assembled flagella longer than 6 μm (Figure 3-4 D). We thought that their failure to swim towards the light might due to motility defects. We checked the swimming patterns of wild-type and *ift57-1*. Most wild-type cells swam in a relatively continuous smooth path (Figure 3-11 A1 and Video 3-1 Video 3-4). However, the trajectories of *ift57-1* cells revealed that they either frequently stopped or exhibited a spiral pattern, leading to a decreased forward motion (Figure 3-11 A2-A4 and Video Video 3-2, Video 3-5, Video 3-6, Video 3-7). These movements were not seen in wild-type cells. Using different batches of *ift57-1*, the severity of swimming defects was variable (Figure 3-11 A). The swimming paths of wild-type cells were always consistent, indicating that their flagella were well equipped to tolerate fluctuating environmental changes. The defects were recovered in rescued strain (Video 3-3).

Figure 3-10. IFT57 is not essential for IFT complex B assembly, its entry to flagella or its motility inside flagella.

A. Immunoblots of isolated flagella from *cc125* and *ift57-1* showed that although the level of IFT57 was dramatically reduced in *ift57-1* flagella, the levels of other IFT proteins and BBS4, one subunit of BBSome, were comparable to those in *cc125*. Ponceau stained tubulin was used as the equal loading control. **B**. Quantitative analysis of IFT protein levels in *cc125* and *ift57-1*. The graph was generated from 4 independent experiment results. **C.** Immunoblots showed that the sedimentation peaks of both IFT-A (IFT122) and IFT-B (IFT46 and IFT81) proteins were the same on sucrose density gradients from the control *cw92* and the mutant *ift57-1* whole-cell extracts. FLA10 (at 10S) and Rubisco (at 19S) were used as references to ensure the gradients were prepared identically. Peaks of Rubisco (at 19S) were indicated with arrows. **D.** Kymographs revealed the motility of KAP-GFP in flagella of *cc125* and *ift57-1.* **E.** The mean speed of KAP-GFP showed the anterograde IFT movement in *ift57-1* was normal. In all panels, the error bars represent standard deviations (s.d.).

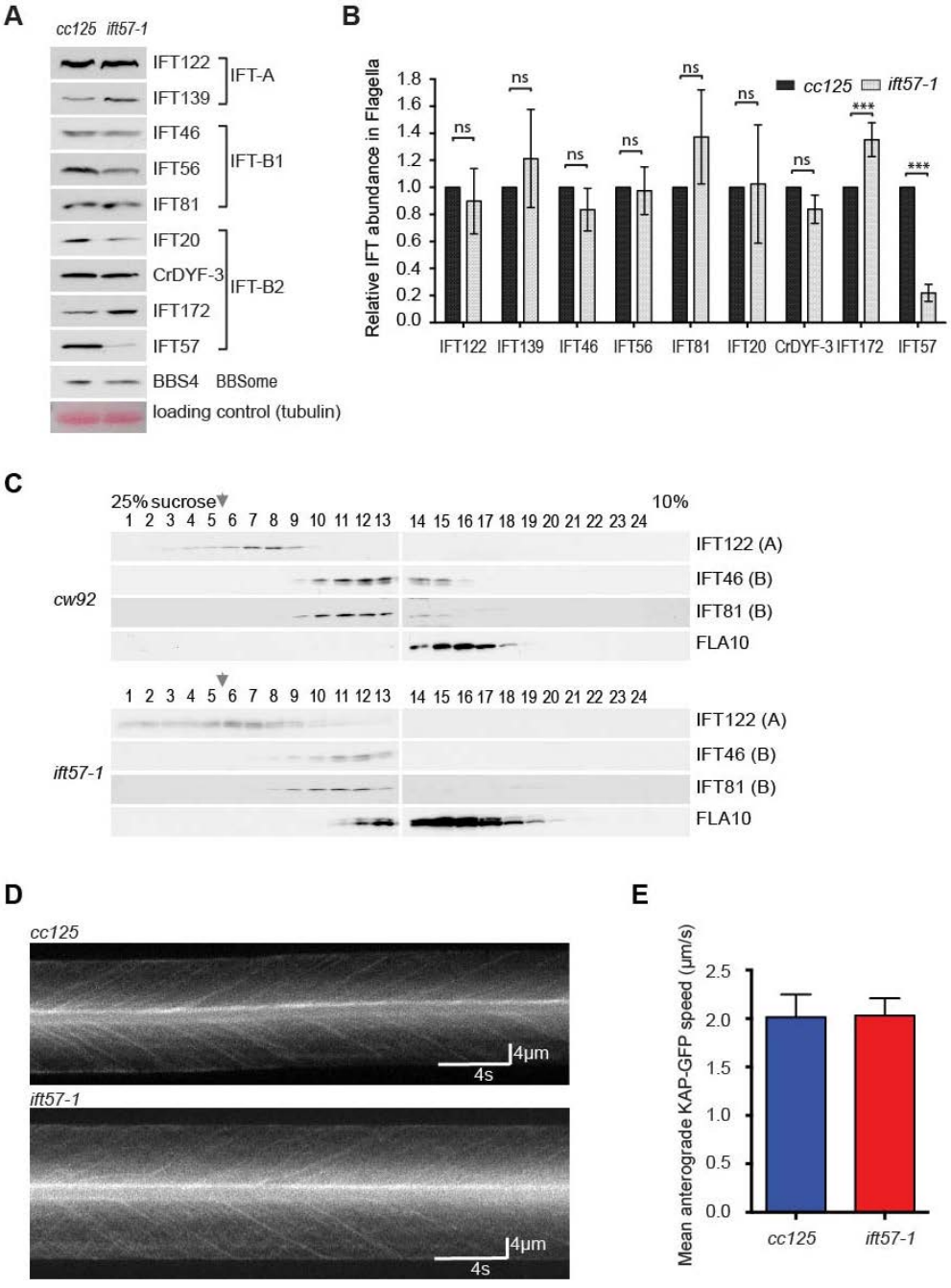
A
cc125 ift57-1
IFT122
IFT139
IFT-A
IFT46
IFT56
IFT81
IFT-B1
IFT20
CrDYF-3
IFT172
IFT57
IFT-B2
BBS4
BBSome
loading control (tubulin)
B
Relative IFT abundance in Flagella
cc125
ift57-1
ns
***
IFT122 IFT139 IFT46 IFT56 IFT81 IFT20 CrDYF-3 IFT172 IFT57
C
25% sucrose
10%
1 2 3 4 5 6 7 8 9 10 11 12 13 14 15 16 17 18 19 20 21 22 23 24
cw92
IFT122 (A)
IFT46 (B)
IFT81 (B)
FLA10
ift57-1
D
cc125
ift57-1
4μm
4s
E
Mean anterograde KAP-GFP speed (μm/s)
cc125
ift57-1

To closely watch flagellar waveforms, we recorded single cell movements in wild-type and *ift57-1*. Consistent with previous reports, wild-type cells swam forward using an asymmetrical flagellar waveform (Figure 3-11 B1 and Video 3-4). One beating cycle of wild-type flagella consisted a recovery stroke (Figure 3-11 B1 frame 1-6) followed by a power stroke (Figure 3-11 B1 frame 7-12). However, the waveform was abnormal, and the beatings of the two flagella of *ift57-1* cells were uncoordinated (Figure 3-11 B2, B3**,** and Video 3-5, Video 3-6, Video 3-7). The abnormal waveform caused the cells to restlessly tumble at the same spot, move around in circles, or spiral paths (Figure 3-11 A). In the *ift57-1-rescue* strain, both the swimming path and the flagellar waveform were back to normal (data were not shown).

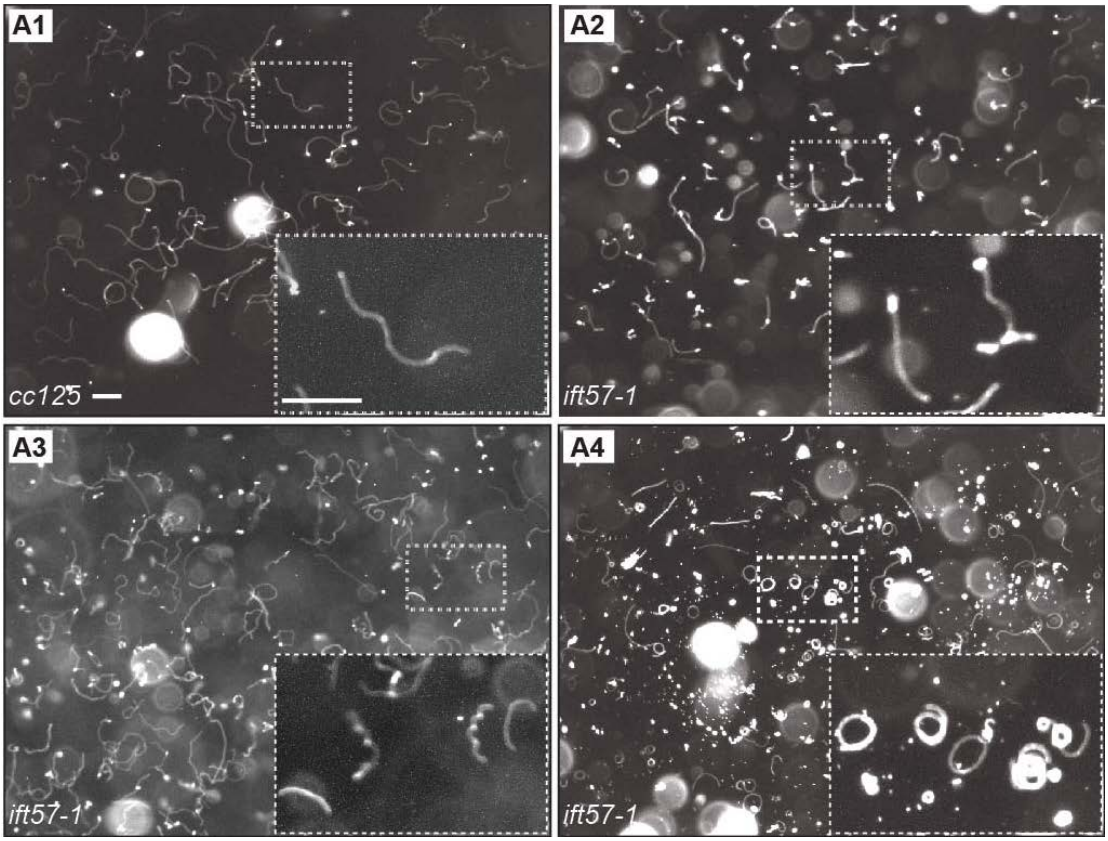

Figure 3-11. IFT57 is essential for normal flagellar motility.
A. Cell swimming paths were recorded by imaging cells with two-second exposures in dark field view. Panel A2, A3, and A4 were representative recordings of swimming paths of *ift57-1* from three batches of cells. Enlarged dotted regions are for detailed viewing of individual swimming paths. The scale bars equal 100μm. **B.** One beating cycle of wild-type cell flagella consists a recovery stroke (B1 frame 1-6) followed by a power stroke (B1 frame 7-12). The waveform of *ift57-1* was abnormal (B2) or uncoordinated (B3). These consecutive frames were taken from high-speed recordings (600 fps) of *cc125* and *ift57-1* under microscopes.

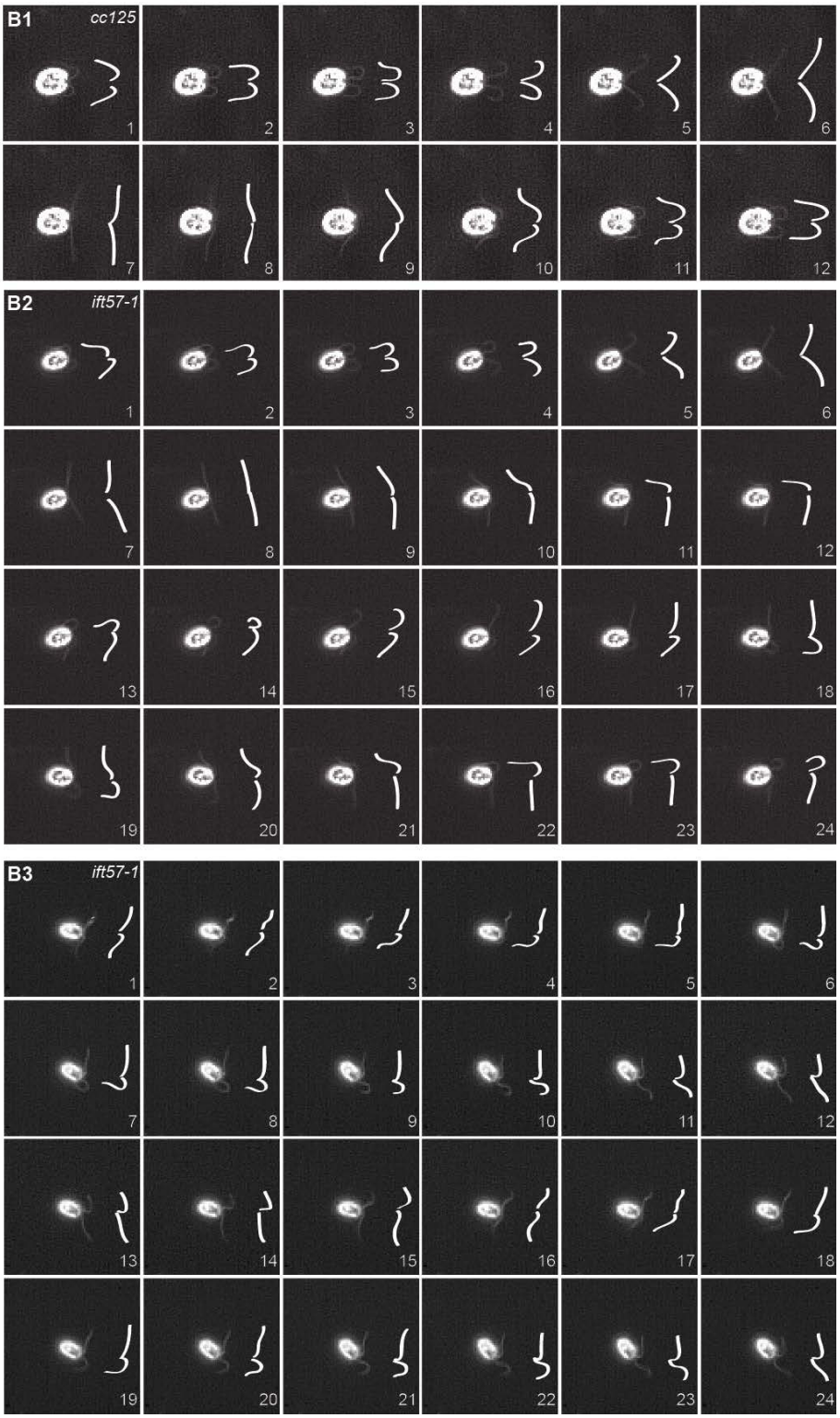

Figure 3-11. Continued

The Inner dynein arm I1 subunit IC97 is greatly reduced in ift57-1 mutant flagella

We checked levels of several motility-related axonemal proteins in whole flagellar samples by immunoblotting. While the levels of the inner dynein arm I1 subunits IC138 [144] and IC140 [145, 146], microtubule doublet inner junction protein FAP20 [137], outer dynein arm components LC1 and IC69 [147], radial spoke protein RSP3 [148], and axonemal protein MBO2 [149] were near wild-type levels, the amount of IC97 [150] was significantly reduced in *ift57-1* mutant flagella (Figure 3-12). The IC97 expression in *ift57-1* mutant at the whole cell level was normal (data were not shown). Thus, the deduction of IC97 in *ift57-1* flagella was not due to expression inhibition but caused by a low efficiency in flagellar entry, retention on the axoneme, or both.

To further access the effect of depletion of IFT57 on flagellar composition, we separated the flagellar proteins of *cc125* and *ift57-1* by electrophoresis (Figure 3-13). On Coomassie-Blue-stained gels, one specific band around 25kDa consistently appeared in *ift57-1* sample. In contrast, it was completely invisible or was just faintly visible in the wild-type sample. Furthermore, a few additional proteins showed altered amounts. The identities of these proteins were still unknown.

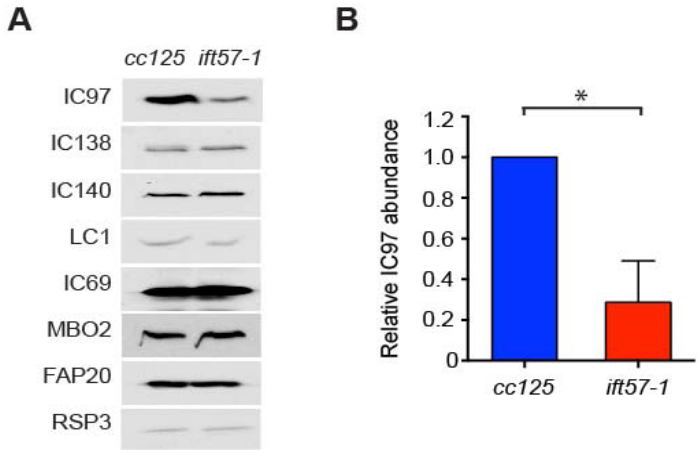

Figure 3-12. The axonemal protein IC97 is decreased in *ift57-1* flagella.
A. Immunoblots of isolated flagella were probed with indicated antibodies. Among all examined axonemal proteins, only the level of IC97 was decreased in *ift57-1* flagella. **B.** The relative IC97 protein abundances in the flagellar extracts of *cc125* and *ift57-1*. The graph shows the intensity of the bands on immunoblots from three independent results.

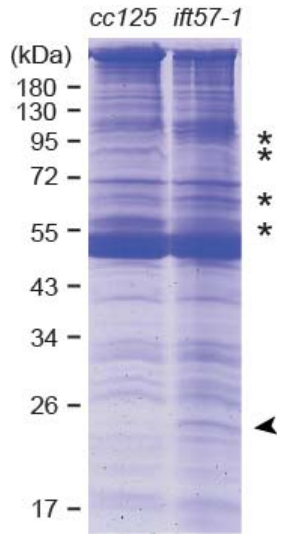

Figure 3-13. The axonemal protein composition is altered in *ift57-1* flagella.
A Coomassie-Blue stained 12% SDS-PAGE gel of flagellar extracts from *cc125* and *ift57-1*. The arrowhead highlighted a protein band that consistently increased in *ift57-1* flagella in three repeated experiments. Stars (*) labels a few bands showed different amounts between *cc125* and *ift57-1*.

Discussion

Here, we report how IFT57 functions in flagellar assembly and motility in *Chlamydomonas* (Figure 3-14). The hypomorphic mutant *ift57-1* expressed a greatly reduced amount of IFT57 and was poorly flagellated (Figure 3-1, 3-3). At the whole cell level, IFT57 along with other IFT-B proteins were highly reduced, indicating that IFT57 is important to maintain the stability of the IFT-B complex (Figure 3-1). Strikingly, although the flagellar level of IFT57 was reduced, the levels of other IFT proteins were not concomitantly affected by the depletion of IFT57 (Figure 3-10). In *ift57-1* flagella, the level of all tested IFT particle proteins, except IFT57, was not reduced. Additionally, the anterograde IFT motility in flagellated *ift57-1* cells was also comparable to that in wild-type cells (Figure 3-10 D, E). Therefore, although IFT57 is important for flagellation by maintaining the cellular amount of IFT particles, it is not essential for the IFT complex assembly or the flagellar entry of IFT particles. Another noted defect in *ift57-1* is that the cells have defective flagellar waveforms and/or beating coordination (Figure 3-11). Several flagellar proteins including the intermediate chain of I1 dynein IC97 were drastically altered in *ift57-1* flagella (Figure 3-12 and Figure 3-13), suggesting that IFT57 is involved in the transport of a specific set of motility-related cargoes.

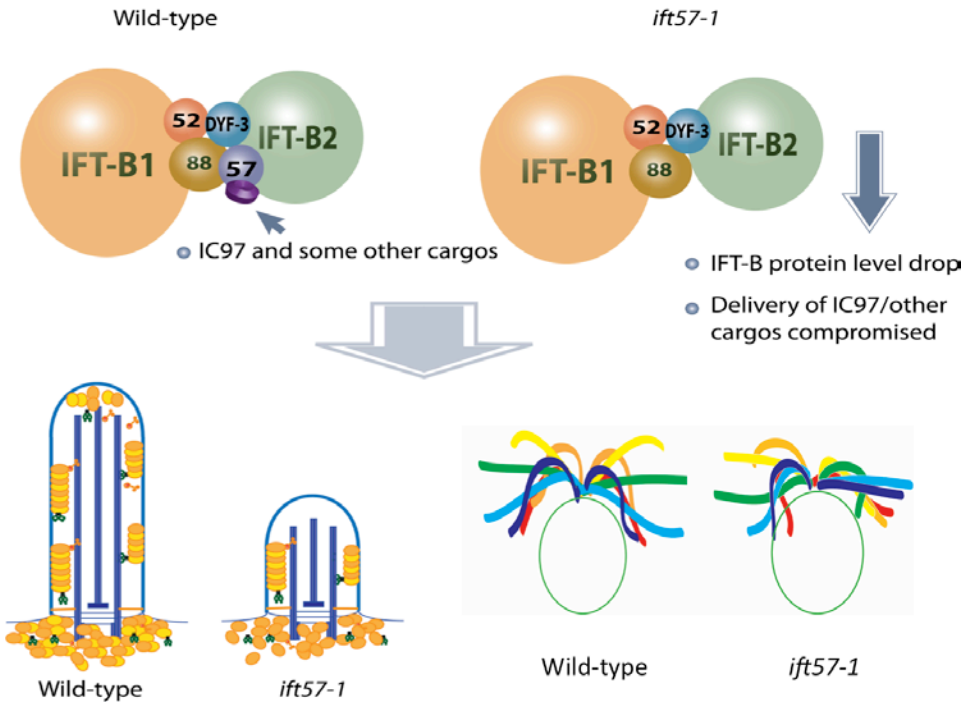

Figure 3-14. The functions of IFT57.
IFT57 sits at the interface of the two IFT-B subcomplexes, IFT-B1 and IFT-B2. Without IFT57, the IFT-B still assembles but has a compromised stability. Thus, the level of the IFT-B at the whole cell level decrease dramatically, which lead to ciliogenesis defects due to the shortage of IFT for cargo delivery. At the same time, IFT57 may be involved in delivering specific sets of motility-related cargo including IC97. Thus, the *arl3* mutant displays abnormal flagellar waveforms. In the right corner, flagella with different color represent the positions of the flagella at different time points.

Here, we show that the IFT57-depleted *Chlamydomonas* cells had severely reduced and unstable IFT-B1 proteins (Figure 3-1 E, G). Therefore, although being an IFT-B2 subunit, IFT57 is critical for the stability of IFT-B1. The previous report shows that IFT57 works as a linkage between IFT172 and IFT20 in IFT-B2 [125]. Interestingly, our work finds that the depletion of IFT57 does not affect the expression of IFT172 and IFT20 (Figure 3-1 E and Figure 3-8). These two proteins are likely biochemically stable.

In this study, two lines of evidence demonstrate that IFT57 is not essential for the IFT-B complex assembly. Firstly, the IFT-B from *ift57-1* whole cell extracts sedimented at about 16S, demonstrating that IFT-B is relatively intact (Figure 3-10 C). Secondly, the low cellular pool of IFT-B proteins did not lead to a low flagellar level of IFT-B proteins. Instead, although IFT57 was reduced significantly, all other IFT-B proteins were at wild-type levels or an even higher level in *ift57-1* flagella (Figure 3-10 A, B). Moreover, the IFT-B complex assembled in *ift57-1* mutant flagella was apparently functional since it underwent IFT movement at the wild-type velocity (Figure 3-10 D, E). These results strongly support that the IFT-B complex assembles and functions normally in the absence of IFT57. Taken together, we conclude that IFT57 is important for maintaining the stability of IFT-B, but is likely dispensable for the IFT-B complex formation and IFT motility.

The recent work from both the Lorentzen and the Nakayama laboratories conclude that IFT57/DYF-3 (IFT-B2) and IFT52/IFT88 (IFT-B1) are essential for linking IFT-B1 and IFT-B2 together [55, 125]. However, they disagree on how IFT57 functions. Using *E. coli* expressed and purified *Chlamydomonas* gene coded proteins, Lorentzen and colleagues show that IFT57 and DYF-3 directly interact to form a dimer, which is essential for binding to IFT52/IFT88 [55]. However, they cannot tell which one of the two proteins, or both, is sufficient for binding to IFT52/IFT88 since it is technically difficult to purify individual proteins. On the other hand, using overexpressed human/mouse IFT proteins in mammalian culture cells, the Nakayama group shows that IFT57 and DYF-3 do not interact directly. They rely on IFT20 to bridge them together

[125]. In this study, we have confirmed that recombinant *E. coli* expressed *Chlamydomonas* IFT57 and CrDYF-3 can be co-purified, supporting the idea that these two proteins form a dimer (Figure 3-9 D, E). Moreover, we have shown that, in *ift57-1* mutant flagella, IFT57 was significantly reduced, while CrDYF-3 and other IFT-B proteins remained at the wild-type level (Figure 3-10 A, B). Clearly, in *ift57-1* mutant flagella, IFT57 was at a much lower level relative to CrDYF-3. Because CrDYF-3 presented at a molar ratio relative to other IFT-B proteins when IFT57 was depleted (Figure 3-10 A, B), we propose that CrDYF-3 alone is sufficient to mediate the integration of IFT-B1 and IFT-B2. On the other hand, CrDYF-3 and IFT57 have similar predicted 3D structures [55]. It is possible that although both CrDYF-3 and IFT57 sit at the interface between IFT-B1 and IFT-B2, either one of them is sufficient to bridge IFT-B1 and IFT-B2 together. The binding of IFT57 onto the complex might also stabilize the structure of IFT-B since the IFT57-deficient-IFT-B complex was unstable, and prone to degradation in the cell body (Figure 3-1 G). This notion is supported by the fact that when the IFT57-deficient-IFT-B complex enters flagella, it could accumulate inside the flagellar compartment (Figure 3-10 A, B) since the flagellum contains few proteases [22].

In this study, we noticed that the flagellated *ift57-1* cells, even the ones with relatively long flagella, showed certain degrees of motility defects (Figure 3-4 C, D and Figure 3-11 A). Further flagellar waveform analysis revealed that in *ift57-1* mutant cells the beatings of the two flagella were uncoordinated (Figure 3-11 B). IFT57 and IFT20 are previously proposed to facilitate the dissociation between the anterograde motor kinesin-

II and IFT particles when they reached the flagellar tip [151]. However, by examining the motility of the anterograde motor subunit KAP-GFP in *ift57-1* mutant flagella (Figure 3-10 D, E), we observed no retrograde tracks, indicating that kinesin-II dissociates from IFT particles at the correct time normally. Moreover, the anterograde IFT speed was not affected at all. Therefore, the IFT movement is normal in *ift57-1* mutant flagella. However, the IFT57-deficeint-IFT-particles, although they undergo IFT movement, may have a reduced efficiency in transporting specific sets of flagellar motility components. In *ift57-1* flagella, the level of the intermediate chain of I1 dynein IC97 decreased dramatically (Figure 3-12). IC97 is a regulatory subunit of I1 and required for I1-dynein–mediated control of microtubule sliding *in vitro* [150]. The low level of IC97 in *ift57-1* flagella is likely responsible for the flagellar waveform defects.

IFT particles deliver different types of structural and functional cargos in and out of the flagellum. IFT proteins use their cargo binding sites to transport flagellar precursors for assembly and function [20, 44, 53, 56, 62, 63, 65-67, 143, 152]. The I1 dynein complex is pre-assembled in the cytoplasm as a 20S complex including IC140, IC138, IC97, and other subunits, and then delivered to flagella by IFT with the assistance of the adaptor IDA3 [153]. Although IC97 is a subunit of the I1 dynein complex, it is not a structural component of I1, nor is it required for I1 dynein axonemal assembly [150]. It could be that IFT57 directly binds to IC97. Alternatively, the structural change of IFT particles caused by IFT57 depletion might reduce its efficiency in transporting IC97 into flagella. Moreover, a few unknown proteins also changed their levels in the flagella (Figure 3-13). These changes may block IC97 binding onto the axoneme, causing it to be depleted

from flagella. Future research is needed to address which of the above hypothetic scenarios is correct.

Methods and Materials

Strains and cultures conditions

The mutant *ift57-1*, the rescue strain *ift57-1-rescue*, and *ift57-1 fla3-1b:: KAP-GFP* were made in this study. All other strains were obtained from the *Chlamydomonas* Center (http://chlamycollection.org/). Strains were maintained on Tris-acetate-phosphate (TAP) plates. Cells were cultured in either TAP or M1 liquid medium with constant aeration in a plant growth chamber (Conviron, Manitoba, Canada) at 21°C with continuous light. The M1 medium was used to culture cells in experiments for Figures 3-4 C-E, Figure 3-10 D, E, and Figure 3-11 A. TAP medium was used for experiments shown in Figures 3-1, 3-2, 3-3, 3-6, 3-7, 3-8, 3-9, Figure 3-10 A-C, Figure 3-11 B, Figure 3-12, and Figure 3-13. The medium used for experiments shown in Figure 3-4 A, B, and Figure 3-5 were labeled on the figures.

ift57-1 mutant isolation and mutation mapping

The mutant *2P40* was selected from a set of flagellar assembly mutants containing hygromycin-resistant *pHyg3*. The insertion site was mapped using an LA PCR *in vitro* Cloning Kit from Takara (Japan) with modifications. Briefly, enzymes (*Pst*I, *Hin*dIII, *Sac*II, *Nco*I, and *Apa*L1), whose cutting sequences were frequently found in *C. reinhardtii* genome, were used to digest genomic DNAs. Digestion products were ligated to short linkers and then used as a template for nested PCRs. The primers were based on

tagged sequences on both ends of the insertion site. Specifically amplified fragments were then sequenced to identify the insertion site. The *2P40* strain was backcrossed and was called *ift57-1*.

Rescue of ift57-1

We used the *Chlamydomonas* Bacterial Artificial Chromosome (BAC) clone 13E3 (http://www.genome.clemson.edu/), which contains the *IFT57* gene, to rescue *ift57-1*. The linearized 13E3 was co-transformed with the paromomycin-resistant *pSI103* plasmid for selection. Before transformation, we treated cells with gametic autolysin for 15-20 minutes to dissociate cell clumps. The transformation was carried out by electroporation as described with modifications [154]. Cells were re-suspended in TAP liquid media containing 60mM sorbitol and then transferred to a 4mm electroporation cuvette. After adding ~ 300 ng of linearized *pSI103* and 900ng of linearized 13E3, cells were chilled on ice for 5 minutes and then electroporated in an ECM630 electroporator (BTX, USA) with following parameters: capacitance 50μF, resistance 650Ω, and voltage 825V. Transformants were obtained from TAP plates containing 10ng μL^{-1} paromomycin and screened for recovered swimming. Integration of *IFT57* gene was confirmed by PCR using *IFT57* gene specific primers, *IFT57*-51-69-F and *IFT57*-515-535-R (Table S1). Expressions of *IFT57* were confirmed by Western Blots. We chose one of rescue colonies for detailed analysis and named it *ift57-1-rescue*.

Comparison of effects of different types of media on flagellar assembly

ift57-1 and *cc125* cells from fresh TAP plates were transferred to TAP and M1 liquid medium respectively and were shook under light at 110 rpm for three days. Supernatants without visible cell clumps were then transferred to fresh TAP and M1. After cultured for three days, three hundred randomly picked cells/cell clusters from each flask (TAP *cc125*, TAP *2P40*, M1 *cc125*, and M1 *2P40*) were analyzed. Cells were divided into four categories: 1) aggregate: four or more than four cells formed clumps; 2) bald: single cells with no flagella; 3) short flagella: single cells with flagella shorter than half-length (≤ 6 μm); 4) long flagella: single cells with flagella longer than half-length (>6μm).

Antibodies and immunoblotting assay

The polyclonal rabbit anti-CrDYF-3 antibody was produced by Bethyl Laboratories, Inc in Montgomery, TX. The immunogen is an internal peptide (N-terminus - CLYDALGQEPELREHR- C-terminus) of CrDYF-3 protein. The peptide was synthesized, purified by HPLC, and verified by mass spectrometry. The peptide was conjugated to KLH before used for immunization. The antisera were affinity purified before used in immunoblotting.

Other antibodies used in this study include antibodies against IFT proteins: FLA10, IFT57, IFT81, IFT139, IFT172 [18], IFT20, IFT46 [20], IFT70 [155], IFT56 [53], IFT74 [156], and IFT122 [124]; antibodies against motility-related proteins: FAP20 [137], MBO2 [149], RSP3 [157] and IC97 [150], IC138 [158], IC140 [146], LC1[159] ; and antibody against IFT cargo BBS4 [143]. Anti–β-F_1-ATPase (AtpB) was purchased from

Agrisera (Sweden). Anti-IC69 was from Sigma-Aldrich (USA). The dilution of each antibody can be found in Appendix table.

The SDS-PAGE and immunoblotting assays were performed as described [160]. Chemiluminescence was used to detect the primary antibodies. The intensities of the immunoblot bands were quantified by the Image LabTM Software (Bio-Rad, California, USA).

qPCR assay

The quantitative PCR was performed using Sybr Green PCR Dye as described previously [138]. Following pairs of qPCR primers were used: q*IFT57*F/q*IFT57*R, q*IFT74*F/q*IFT74*R, q*IFT140*F/q*IFT140*R, q*IFT88*F/q*IFT88*R, and q*GBLP*F/q*GBLP*R (Table S1). Primers for *IFT57* gene were designed for this study. The remaining primers were described in a previous publication [138]. The guanine nucleotide-binding protein subunit beta-like protein (GBLP) was used as an internal control. The program used for amplification is 94°C for 2 minutes, 40 cycles of 94°C for 10 seconds and 60°C for 30 seconds, then 60°C for 2 minutes, finish with a melting curve.

Photoaccumulation assay

Since most cells in *ift57-1* liquid culture were in clumps, we used the following procedure to get rid of bald cells or cell clumps before performing photoaccumulation assays [161]. The *cc125* and *ift57-1* cells from fresh TAP plates were transferred to M1 [162] liquid medium and cultured with aeration for three days. Then flasks were left

stand still for 10 minutes to allow bald cells or clumps to sediment to the bottom of the flask. The upper layers were transferred to new flasks with fresh M1 media. After cultured for two more days, 20 mL of *cc125* and *ift57-1* cells were transferred to Petri dishes for photoaccumulation assays. Half of the Petri dishes were covered by foils. The light was then shed from open sides of the dishes for 20 minutes. One sample was taken from the side close to the light from each dish (site 1 from *cc125*, site 3 from *ift57-1*), and one sample was taken from the side away from the light (site 2 from *cc125*, site 4 from *ift57-1*). Three hundred randomly picked cells were analyzed for flagellar assembly from sample 1, 3, and 4; however, there were almost no cells recovered in sample 2 since almost all cells went to site 1.

Flagella isolation

Flagella were isolated as previously described [18]. Briefly, cells cultured in TAP medium were deflagellated by pH shock, and then cell bodies were removed by centrifugation through a 25% sucrose cushion at 1800rpm. Isolated flagella were collected at 10000rpm in an SW 32 Ti motor (Beckman Coulter, USA). Due to the presence of cell clumps in *ift57-1*, cells were treated with gametic autolysin for 15-20 minutes to dissociate clumps followed by 4 hours' incubation in 10mM HEPES to encourage flagellation before flagella isolation.

Cycloheximide treatment

Chlamydomonas cells were cultured to dark green before cycloheximide (12.5μg mL^{-1}) treatments. Protein samples were prepared at 0h, 6h, and 12h after adding cycloheximide.

Whole cell sucrose density gradient

The sucrose density gradient centrifugation of whole cell extracts was prepared the same way as described previously [52]. The Optima XE-90 Ultracentrifuge (Beckman Coulter, USA) with a sw41 rotor was used. *Cw92*, a cell-wall deficient mutant in *the cc125* background, was used as a wild-type control. Fractions at 19S, 12S, and 10S were estimated by sedimentation positions of Rubisco, RSP3, and FLA10, respectively.

Imaging

Flagellar assembly status analysis and length measurements

C. reinhardtii cells were fixed with 2% glutaraldehyde. Images were collected on an Axioplan phase contrast microscope (Carl Zeiss, Oberkochen, Germany) using a 63×/1.40 oil Plan-Apochromat objective (Olympus, Tokyo, Japan). Measurement of flagellar length was done using ImageJ (NIH).

Assessment of flagellar waveform pattern

C. reinhardtii cells were placed in a hand-made swimming chamber with about 100μm thickness and observed under an Axioplan phase contrast microscope with a 63×/1.40 oil Plan-Apochromat lens. Movies were taken with a Phantom High-Speed Mico-eX2

camera (Vision Research) at 600 frames per second (fps) and processed using the Cine Viewer software (version 2.6, Vision Research Inc, Prince Edward Island (P.E.I.), Canada). Movies were imported to ImageJ for analysis.

Recording of cell-swimming tracks

Cells were cultured in M1 medium with aeration. After removing bald and cell clumps, flagellated cells were placed in chambers as described above and observed through a dark-field microscope. Tracks of swimming cells were taken with two seconds exposures and processed in ImageJ.

TIRF microscopy and analytical methods

The strain *ift57-1 fla3-1b:: KAP-GFP* was generated by crossing *ift57-1* with the strain *fla3-1b:: KAP-GFP* [163]. The cross progenies were selected by phenotypes, PCR, and fluorescent microscopy. The PCRs were performed using an *IFT57* specific primer *IFT57*-51-69-F and a primer named pHyg3-624-643-R (Table S1) according to the sequence of *pHyg3*. The *fla3-1b*:: KAP-GFP and *fla3-1bift57-1*:: KAP-GFP cells were started in TAP and then transferred to M1 liquid medium with aeration to encourage flagellar assembly. Only the cells with near full-length flagella were used for microscopic observation. The cells were immobilized in M1 medium supplemented with 10 mM Hepes (pH 7) and 6.25mM EGTA [62]. To record the motility of KAP-GFP, an inverted Nikon eclipse-Ti microscope (Tokyo, Japan) with a 100X 1.49 NA TIRF objective was used for imaging. Microscopic images and time-lapses were captured using a Hamamatsu ImagEM X2™ EM-CCD camera C9100-23B (Shizuoka Prefecture,

Japan). The motility of KAP-GFP was imaged with a 488nm laser under a 100X objective with a 1.5X amplifier at 30 fps. The kymograph was then made using the Reslice function in ImageJ (http://rsb.info.nih.gov/ij/).

Immunofluorescence microscopy

The cell staining was carried out as previously described [52] with slight modifications. Briefly, cells were fixed with 100% cold methanol and then blocked in PBS containing 10% goat serum, 5% BSA, and 1% Cold Water Fish Gelatin. Then slides were incubated with primary antibodies for 4 hours at room temperature, followed by three washes with PBS. Slides were then incubated with secondary antibodies for 1 hour at room temperature. Images were taken on an Olympus IX81 microscope (Olympus, Tokyo, Japan) with a Yokogawa CSU-X1 Spinning Disk Unit (Andor Technology, CT, USA).

Statistical analysis

Statistical analyses were performed using the software GraphPad Prism (GraphPad Software, San Diego, California, USA). Quantitative data was presented as average ± s.d.. Statistical analysis between two groups was performed by t-student test (* represents <0.05; ** represents <0.01, *** represents <0.001, ns represents no significant difference).

CHAPTER IV

IFT-B SUBUNIT IFT56 (DYF-13) IS NOT ESSENTIAL FOR THE IFT-B ASSEMBLY AND STABILITY BUT IS CRITICAL FOR NORMAL CILIOGENESIS

Introduction

Flagellar/Ciliary length is critical for flagellar/ciliary function. Motile cilia rely on the "just right" length to generate effective beat force, which is critical to propel the movement of the cell itself or generate a fluid flow. Consequently, both long and short flagella are motility defective, which is best characterized in mutants of *Chlamydomonas* [164, 165]. In humans, motile cilia with abnormal length cause symptoms such as infertility and chronic respiratory diseases [166]. The right length is also important for primary cilia to function as sensory hubs [76, 77]. The abnormal length of primary cilia is always correlated with human diseases or injuries of tissue [78-80]. For example, altered dynamic of cilia assembly in *bbs-4* is associated with renal cystic diseases [81]

Mutations of subunits from the IFT complex, especially from IFT-B (generally responsible for anterograde transport), are common reasons for ciliogenesis defects. Although a few subunits in IFT-B (such as IFT22, IFT25, and IFT27) do not affect cilia assembly [167-169], most IFT-B subunits are involved in ciliogenesis. Many IFT-B mutants do not assemble flagella/cilia or assemble short flagella/cilia [36]. These subunits that are involved in ciliogenesis can be divided into two major types. In the first type, the subunit only plays a critical role in the IFT complex assembly or IFT complex stability. The typical examples of this type include IFT52, IFT88, and IFT46 [20, 51, 52,

170]. In the previous chapter, we also showed that the IFT complex stability is severely affected in *ift57-1*, which either fails to assemble flagella or assemble short flagella. In the second type, the subunits play critical roles in both IFT complex assembly/stability and the tubulin delivery. This type includes IFT74 and IFT81 [56, 64, 171].

DYF-13 has originally identified in *Caenorhabditis elegans* "dye-filling" chemosensory mutants and found to be involved in ciliogenesis [107]. *C. elegans* chemosensory amphid and phasmid cilia have two segments, the middle and distal segments. The middle segment is composed of microtubule doublets, while the distal segment has singlet microtubules. GFP-tagged DYF-13 undergoes IFT-like movement, which is the earliest evidence that DYF-13 functions in IFT [172]. Moreover, DYF-13 and its homologs are highly conserved throughout all ciliated organisms, but not in non-ciliated organisms [108]. Its homolog in Trypanosomes is called PIFTC3 [173], and in mice is called TTC26. Purification of PIFTC3 and a tightly associated complex, which include most IFT proteins, indicate that PIFTC3 is associated with the IFT complex [109]. A published work from Pazour's lab showed that TTC26 co-precipitated with the IFT-B protein IFT88 but not with IFT-A protein IFT140, indicating that TTC26 is associated with IFT-B [110]. In conclusion, it shows that DYF-13 and its homologs are involved in ciliogenesis, and they are putative IFT proteins. However, the exact role of this potential IFT-B subunit DYF-13, especially its role in ciliogenesis, is unknown.

Here, we confirmed that CrDYF-13 is a bona fide IFT-B subunit by using sucrose density gradients. Also, we isolated a CrDYF-13 null mutant *crdyf-13* in

Chlamydomonas, which assembles short flagella with motility defect*s*. We showed that unlike the other IFT-B subunits whose absence results in ciliogenesis defects, CrDYF-13 is not required for the IFT-B assembly and stability. We also showed that the flagellar regeneration rate of the *crdyf-13* mutant is compromised. The slower regeneration rate is neither due to the smaller precursor pool nor the accelerated disassembly rate. Also, a few tested flagella length regulators function normally in the *crdyf-13* mutant. Moreover, further motility analyses showed that the *crdyf-13* mutant has defects in the flagellar waveform, and we noticed that the severity of the motility defects is variable in different preparations. These data shed light on the specific functions of CrDYF-13 in flagella assembly and function. It also may help in deciphering the mechanism of how ciliated organisms tightly control their cilia length, and how IFT system is regulated to deliver their cargos.

Results

CrDYF-13 expression is abolished in the isolated crdyf-13 mutant due to an insertion at third intron of the CrDYF-13 gene

Mutations of IFT subunits, especially the IFT-B subunits, usually cause defects in ciliogenesis. To isolate IFT-B mutants, we screened the mutants with ciliogenesis defects from our flagellar defective mutant library. One strain numbered *3P3*, which forms palmelloid or assembles short flagella, was isolated. Further analysis showed that it contains a hygromycin insertion in the 3rd intron of *CrDYF-13* (Figure 4-1 A). Using an antibody against CrDYF-13, we failed to identify any specific band in the mutant *3P3*, while a single band at around 56kDa was recognized from both the whole cell and

the isolated flagella extracts of wild-type cell *cc125* (Figure 4-1 B). Therefore, the insertion at the 3rd intron completely abolishes the expression of *CrDYF-13* in the mutant. The strain *3P3* was used for further analyses after backcrossing three times [53].

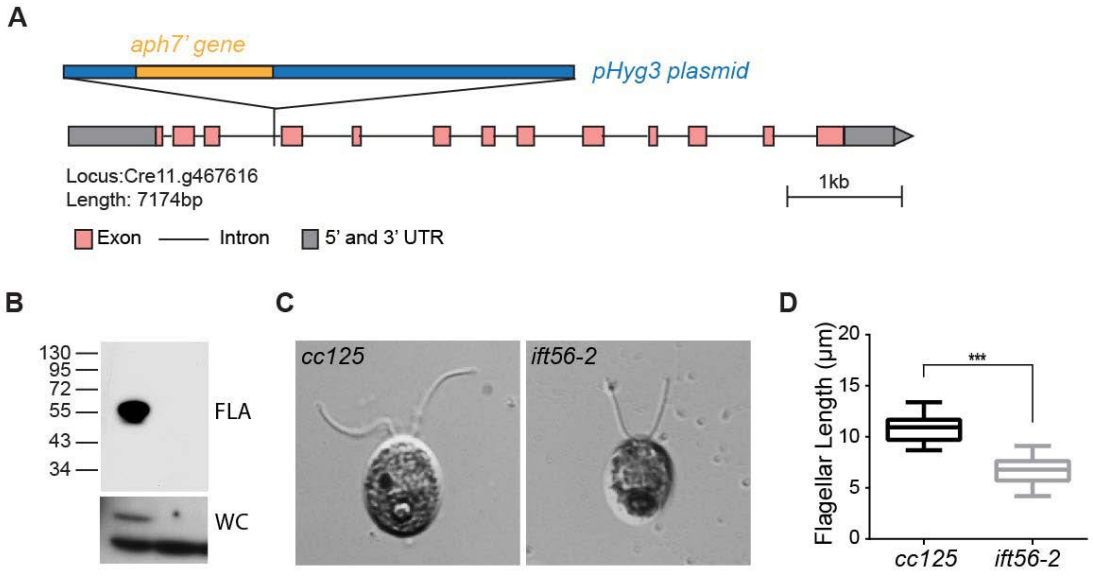

Figure 4-1. *C. reinhardtii* mutant *3P3* has ciliogenesis defects.
A. Schematic representation of *C. reinhardtii* mutant *3P3*. The blue bar indicates the inserted linearized plasmid *phyg3* that containing hygromycin gene *aph7* (indicated by the orange box). **B.** Immunoblots of the wild type control *cc125* and the mutant *3P3*. The CrDYF-13 antibody specifically recognizes a ~56 kDa band in *cc125*, while noting is detected in *3P3*. The upper panel represents the result from isolated flagella (FLA) while the lower panel represents the result from the whole cell lysates (WC). **C.** Images of the wild-type *cc125* and the *3P3* mutant cells. **D.** Comparison of flagellar length between wild-type cells (n = 100) and *3P3* mutant cells (n = 100), (5%-95% ; p <0.001, Student t-test). Cells forms palmelloid or bad were excluded from the analysis.

Absence of CrDYF-13 results in ciliary defects

All the mutants in the established flagellar defective mutant library were screened out due to their bad performances in the phototaxis assay. As the other mutants, *3P3* cannot swim to light as quickly as wild-type *cc125*. Close microscopic analyses revealed that

3P3 assembles short flagella, which are 1/2 or 2/3 of the length of flagella from *cc125* (Figure 4-1 C, D). We also noticed that the phototaxis defect is mainly due to the significantly reduced swimming speed of *3P3* (Figure 4-2 A, Video 4-1, and Video 4-2). These phenotypes are consistent with the phenotypes of another null mutant, which has point mutations in *CrDYF-13*, generated in Dr. Marshall's lab [53]. Using a high-speed camera, we were able to watch and record the flagellar waveforms of individual cells closely. Videos showed that the *3P3* mutant cells have a weak stroke due to the length of its flagella (Video 4-4 and Video 4-5). Moreover, the mutant cells have a slower beating frequency (Figure 4-2 B-E, Video 4-4 and Video 4-5). The cells frequently showed the incoordination of the two flagella (Figure 4-2 D and Video 4-4), which might be due to the imbalanced force generated by two flagella. Thus, the beating frequency is also not consistent in *3P3*, while it is consistent in *cc125* (Figure 4-2 B, Video 4-3 and Video 4-4). To summarize, the shorter flagellar length, slower beating frequency, and frequently uncoordinated flagellar beating cause the slowly and jerky movement of the mutant cells.

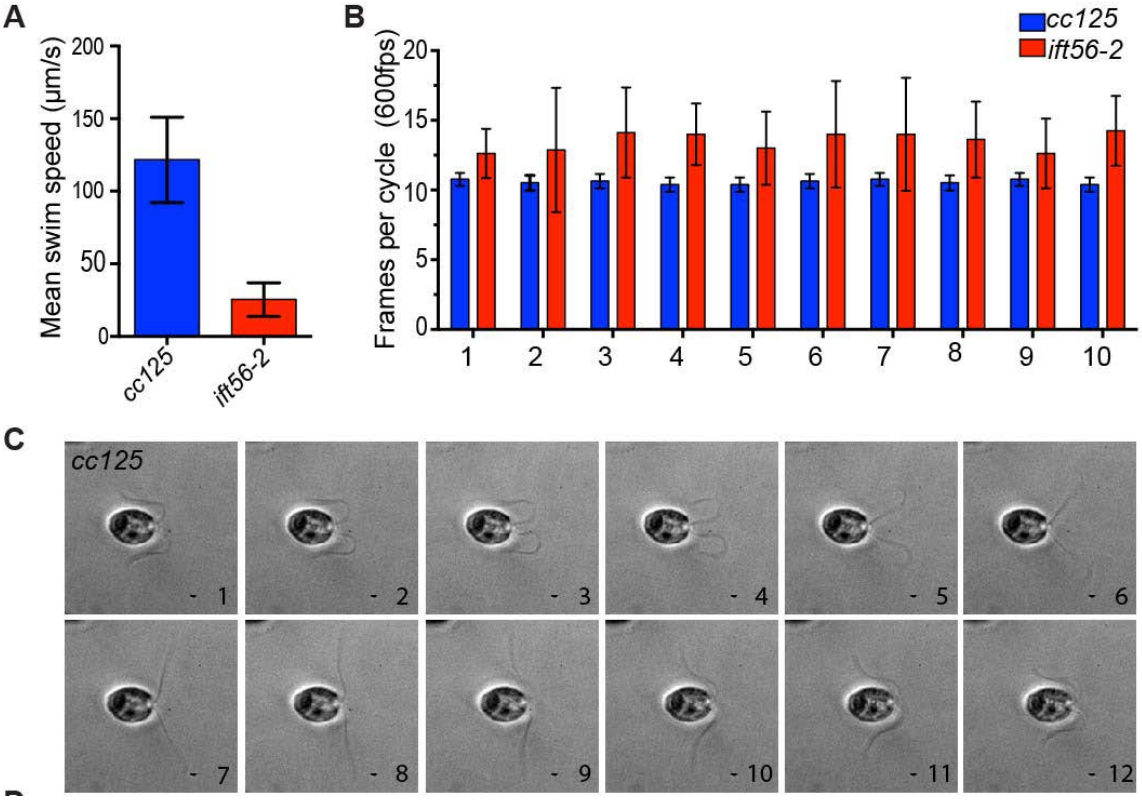

Figure 4-2. *C.reinhardtii* mutant *3P3* has motility defects.
A. The mutant *3P3* has a significantly slower swimming speed than the wild-type *cc125*. Ten randomly recorded cells from each strain were analyzed. Error bars represent s.d.. Due to the inconsistency of 3P3's phenotype, videos taken from the same preparation were used for analysis. A similar trend was shown in repeats. **B.** The frequency and consistency of flagellar beating are affected in the mutant *3P3*. Ten cells from each strain were recorded. Ten beating cycles in each cell were analyzed by counting how many frames it took to finish a cycle. For the cells with uncoordinated flagella, the analysis was done based on one of its flagella. Error bars represent s.d.. Due to the inconsistency of 3P3's phenotype, videos taken from the same preparation were used for analysis. A similar trend was shown in repeats. **C.** One beating cycle of the wild-type flagella is presented. The two flagella from wild-type cells coordinate well with each other and propel cell move forward efficiently. These consecutive frames were taken from the high-speed recording (600fps) of the *cc125*. **D-E.** Twenty-four consecutive frames from *3P3* recording are presented (600fps). The beating frequency is slower in *3P3* (Panel **D** and Panel **E**). Also, the two flagella of the mutant *3P3* are frequently uncoordinated (Panel **D**).

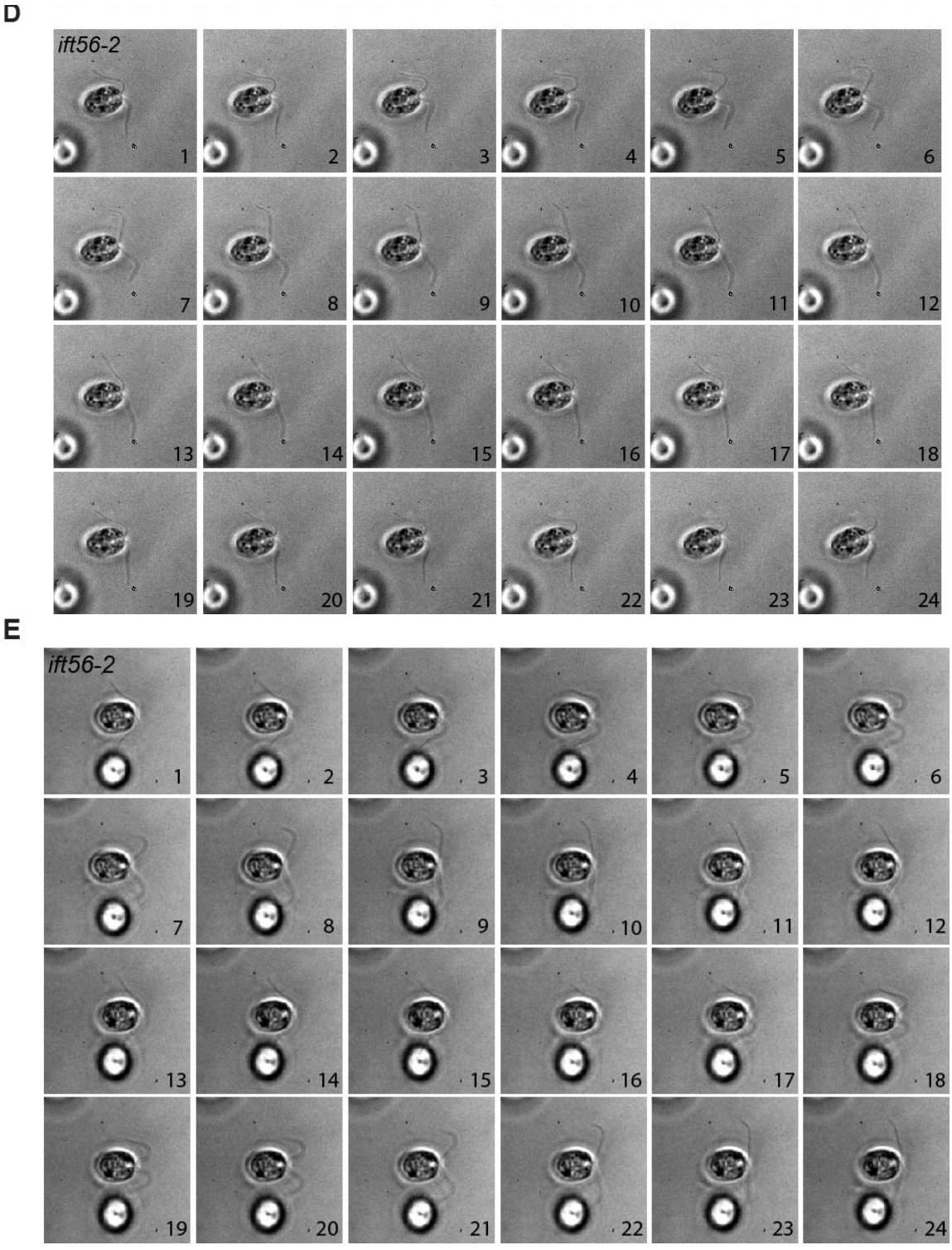

Figure 4-2. Continued.

CrDYF-13 is a bona fide IFT-B subunit

We have already known that IFT system is critical for flagella assembly, maintenance, and function. The defects of the isolated *3P3* mutant are likely due to the inadequate IFT system. Multiple pieces of evidence show that DYF-13 is a putative IFT protein [109, 110, 172]. To verify CrDYF-13 is a *bona fide* IFT subunit, we used a temperature-sensitive mutant *fla10-1*, which contains a point mutation in the kinesin-II motor subunit. In *fla10-1*, the anterograde IFT can be controlled by the temperature change. The anterograde IFT normally works at the permissive temperature (18°C) and can be completely shut down in the non-permissive temperature (32°C). Immunoblots showed that like the other two IFT subunits IFT46 and IFT74, CrDYF-13 disappear after one-hour treatment at 32°C, indicating that the entry of CrDYF-13 to flagella depends on FLA10 (Figure 4-3 B). We also fractioned the wild-type-flagellar extracts using sucrose density gradients. Using the CrDYF-13 antibody mentioned above, CrDYF-13 was found co-migrated with IFT-B proteins IFT46 and IFT74, but not with the IFT-A protein IFT139 (Fig 4-3-A). Based on the size of the immunoblotting band (Figure 4-1 B and Figure 4-3 A, B), we cut the corresponding bands at IFT-B concentrated lanes on a Coomassie-blue stained gel (loaded by sucrose density gradient fractions) and sent them for mass spectrometry sequencing. It turned out to be the CrDYF-13 protein (Figure 4-3 C, D). These results reveal that CrDYF-13 is a bona fide IFT-B subunit. According to the widely accepted nomenclature of IFT proteins [47], we named the protein CrDYF-13 IFT56 [53]. Then we renamed the backcrossed *3P3* as *ift56-2* to differentiate it with the strain in the previous publication (referred as *ift56-1* here) [53].

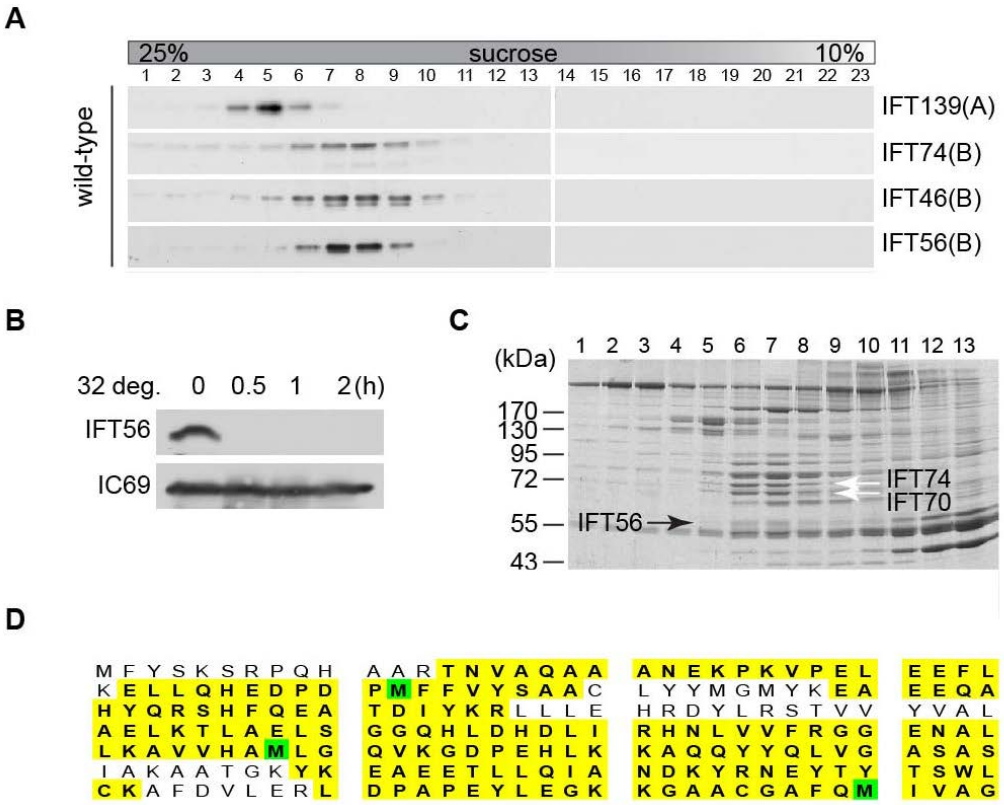

Figure 4-3. CrDYF-13 (IFT56) is a bona fide IFT-B subunit.
A. CrDYF-13 co-migrates with IFT-B subunits IFT74 and IFT46 on the wild-type flagellar sucrose density gradients (10–25%). **B.** The temperature sensitive mutant *fla10-1* was cultured at a permissive temperature (20°C) and then shifted to a non-permissive temperature (32°C). Flagellar samples were isolated at 0h, 0.5h, 1h, and 2h, respectively. Immunoblots showed that CrDYF-13 disappears when IFT system is shut down. Axonemal protein IC69 was used as loading control. **C.** A Coomassie-Blue stained gel of gradient fractions (only fractions 1-13 out of 23 fractions are shown) shows the position of CrDYF-13. The black arrow indicates the CrDYF-13 band. White arrows indicate the reference bands IFT74 and IFT70. **D.** The corresponding bands on Coomassie-Blue stained gel are confirmed by mass spectrometry. Fragments labeled with yellow color were detected in sequencing (356/555 amino acids, 64% coverage).

The absence of IFT56 does not affect the assembly of the IFT-B complex

Because *ift56-2* is still capable of assembling short flagella, we reasoned that the IFT complexes in *ift56-2* should still retain some functions. Indeed, immunoblots of *ift56-2* flagellar sucrose density gradients revealed that the tested IFT-B proteins (IFT81, IFT74,

and IFT46) still migrate together as in the wild-type, indicating that the absence of IFT56 did not completely disrupt the assembly of IFT-B (Figure 4-4 A, B). However, the size of IFT-B from the *ift56-2* flagella is a little bit smaller (Fig 4-4-A, B). The smaller size could be due to the absence of either IFT56 alone or IFT56 together with other IFT proteins. To figure out whether the IFT56 is necessary for the assembly of other IFT subunits onto IFT-B, we compared the band patterns of IFT-B concentrated fractions from the sucrose density gradients of *ift56-2* and *cc125*. Results revealed that only one major band was missing from the *ift56-2* flagella extract, and the size of the band matched IFT56 (Figure 4-4 C). Using available IFT antibodies, we examined the level of specific subunits in flagella by immunoblotting. The levels of all tested subunits in the flagella were comparable to wild-type cells as previously published [53] (data not shown). These results revealed that IFT56 is likely to be the only missing subunit in IFT-B from *ift56-2*. Therefore, IFT56 is not necessary for the IFT-B assembly. It is consistent with the recently published data that without IFT56, the other IFT subunits can normally assemble [54, 55]. Also, IFT56 only interacts with one IFT subunit, IFT46 [54]. It explains the fact that the *ift56* mutants have less severe phenotypes than most of the other IFT-B mutants.

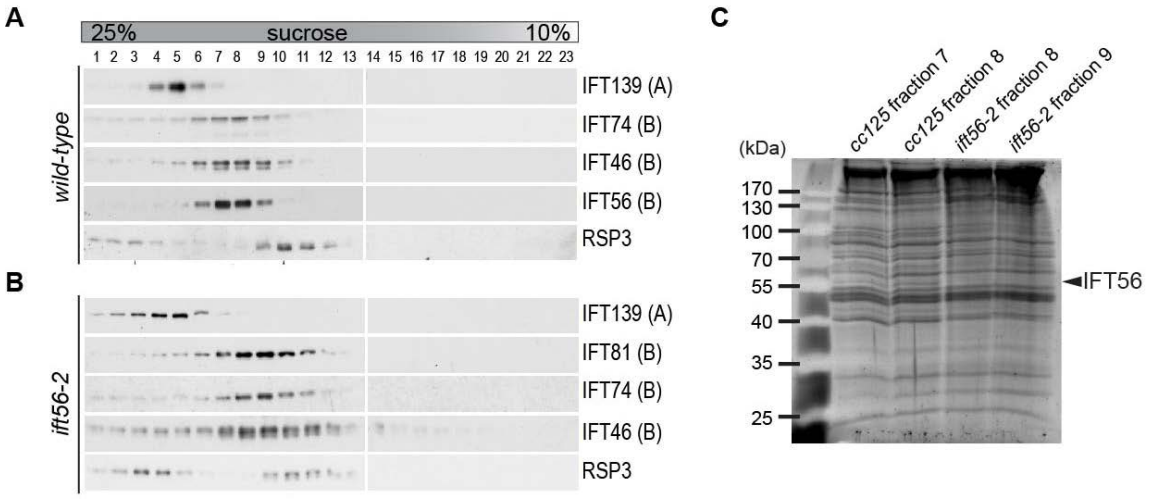

Figure 4-4. IFT56 is not essential for the IFT complex B assembly.
A. The same panel as Figure 4-3 A. (Used for comparison with panel B). **B.** IFT-B subunits IFT46, IFT74, and IFT81 still co-migrate together on the *ift56-2* flagellar sucrose density gradients (10–25%). RSP3, a component of the radial spoke, is used as a gradient marker. White arrowheads indicate its peaks at the 20S and 12S on the gradients. Black arrows show peaks of IFT-A and IFT-B. **C.** Comparison of IFT-B concentrated gradient fractions from *cc125*(fraction 7, 8)and *ift56-2*(fraction 8,9). One band is missing from *ift56-2* at around 56kDa, while the other bands do not show obvious differences. The fractions were separated on SDS-PAGE gel and stained.

Absence of IFT56 does not affect the stability of IFT-B

The mutant *ift56*-2 still assembles flagella, even though they are shorter than wild-type flagella (Figure 4-1 C, D). This phenotype is similar to the mutant *ift46, ift57-1*, and *ift74-2* [20, 64] (*ift57-1* is described in Chapter III). Because all three mutants mentioned above have defects in the stability of IFT-B, we wanted to examine whether IFT56 plays a similar role in stabilizing the IFT complexes. Although we have already done immunoblots in flagella partition, flagella are not ideal materials for the stability test due to the lack of proteases in flagella [22]. Thus, immunoblots of whole cell extracts were used to examine the effects of IFT56 absence on the other IFT proteins. Some previously

characterized IFT-B mutants including *ift46-suppressor*, *ift46*, *ift88*, and *ift57-1* were also included for comparison. Surprisingly, *ift56-2* had a normal or an elevated cellular level of both tested IFT-B subunits IFT81 and IFT46, while the other IFT-B mutants showed various degrees of reduction in these two subunits (Figure 4-5 A). We also conducted a time-course cycloheximide treatment experiment to measure the turnover rates of IFT proteins in both *cc125* and *ift56-2* as previously described in Chapter III. Western blots showed that the IFT proteins stability in *ift56-2* is comparable to wild-type *cc125* (Figure 4-5 B). These results revealed that IFT56 does not play a role in the stability of IFT-B.

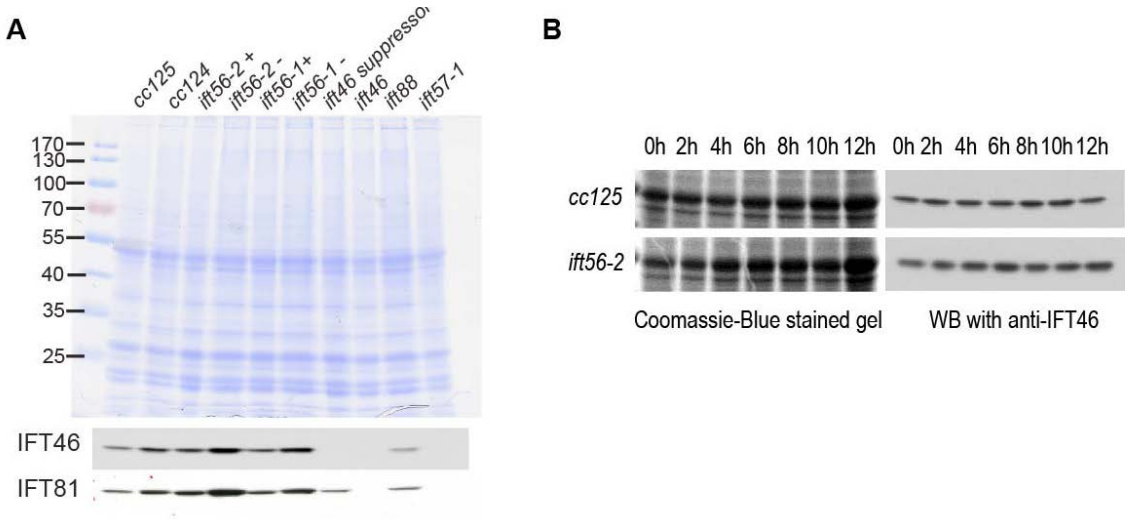

Figure 4-5. IFT56 is not essential for the IFT-B stability.
A. Immunoblots of the whole cell lysates revealed that the levels of two IFT-B subunits (IFT81 and IFT46) are not reduced in *ift56-2*. Wild type control (*cc125* and *cc124*), the *ift56* mutants (*ift56-1* and *ift56-2*), and four other IFT-B mutants (*ift46*, *ift46-sup*, *ift88*, and *ift57*-1) were probed with antibodies against IFT81 and IFT46, respectively. (+) represents mating type plus strain, while (-) represents mating type minus strain. **B.** The stability of IFT-B protein IFT46 is not affected in *ift56-2*. Cells were treated with cycloheximide for 12 hours. The degradation rate of the existing IFT-B subunit IFT46 was measured at 2h intervals. The Coomassie-blue stained SDS-PAGE gel was used as loading control.

IFT proteins still localize and concentrate normally at basal bodies in ift56-2

It has been reported that the recruitment of IFT complexes can affect the cilia assembly [92, 174]. Due to the short flagella assembled, we expected at least some IFT complexes still localize to basal bodies in *ift56-2*. However, whether enough IFT complexes are accumulated at the basal bodies in *ift56-2* is not known. We have already shown that the whole cell level of IFT proteins in *ift56-2* is comparable to *cc125* (Figure 4-5 A). Thus, the distributions of IFT proteins can indirectly show the amount of IFT proteins that were recruited. We did indirect immunofluorescence as described in Chapter III to examine the cellular distribution of two IFT-B subunits, an IFT-B1 subunit IFT46, and an IFT-B2 subunit IFT172. Results showed that the cellular distributions of both subunits are normal in *ift56-2*. They concentrated at the basal bodies and flagella as wild-type *cc125* (Figure 4-6 A-D). However, we did detect a little bit IFT172 localized at the peripheral regions of the basal body (Figure 4-6 D). We did not know whether this mislocalization is functionally significant.

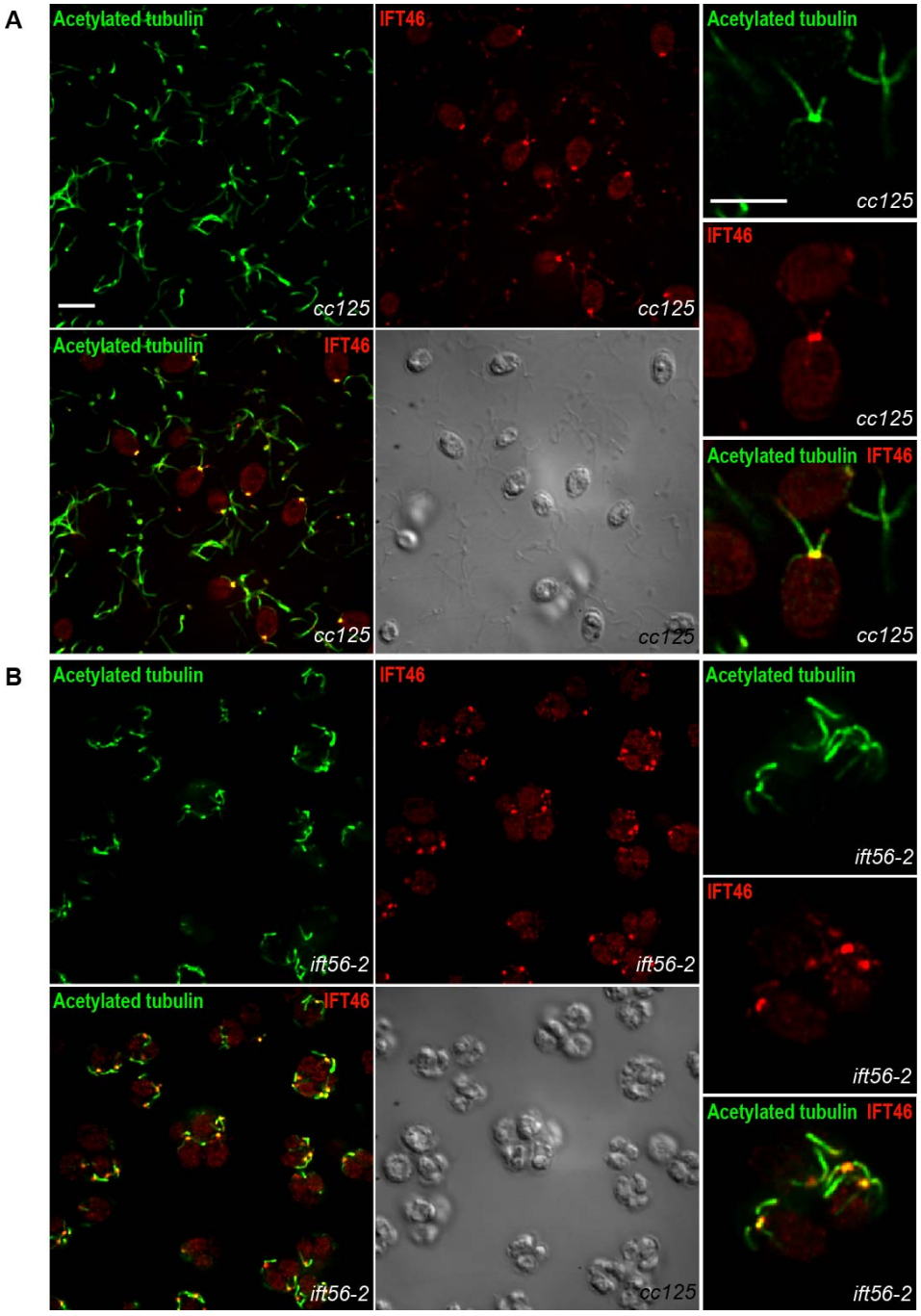

Figure 4-6. The absence of IFT56 does not affect IFT recruitment to basal bodies.
A. Immunofluorescent staining of the wild-type *cc125* against anti-IFT46. **B.** Immunofluorescent staining of the mutant *ift56-2* against anti-IFT46. In panel (A) and (B), acetylated tubulin was used as a marker for basal body and flagella. Scale bars represent 10μm. **C.** Immunofluorescent staining of the wild-type *cc125* against anti-IFT46 and anti-IFT172. **D.** Immunofluorescent staining of the mutant *ift56-2* against anti-IFT46 and anti-IFT172. Scale bars represent 10μm.

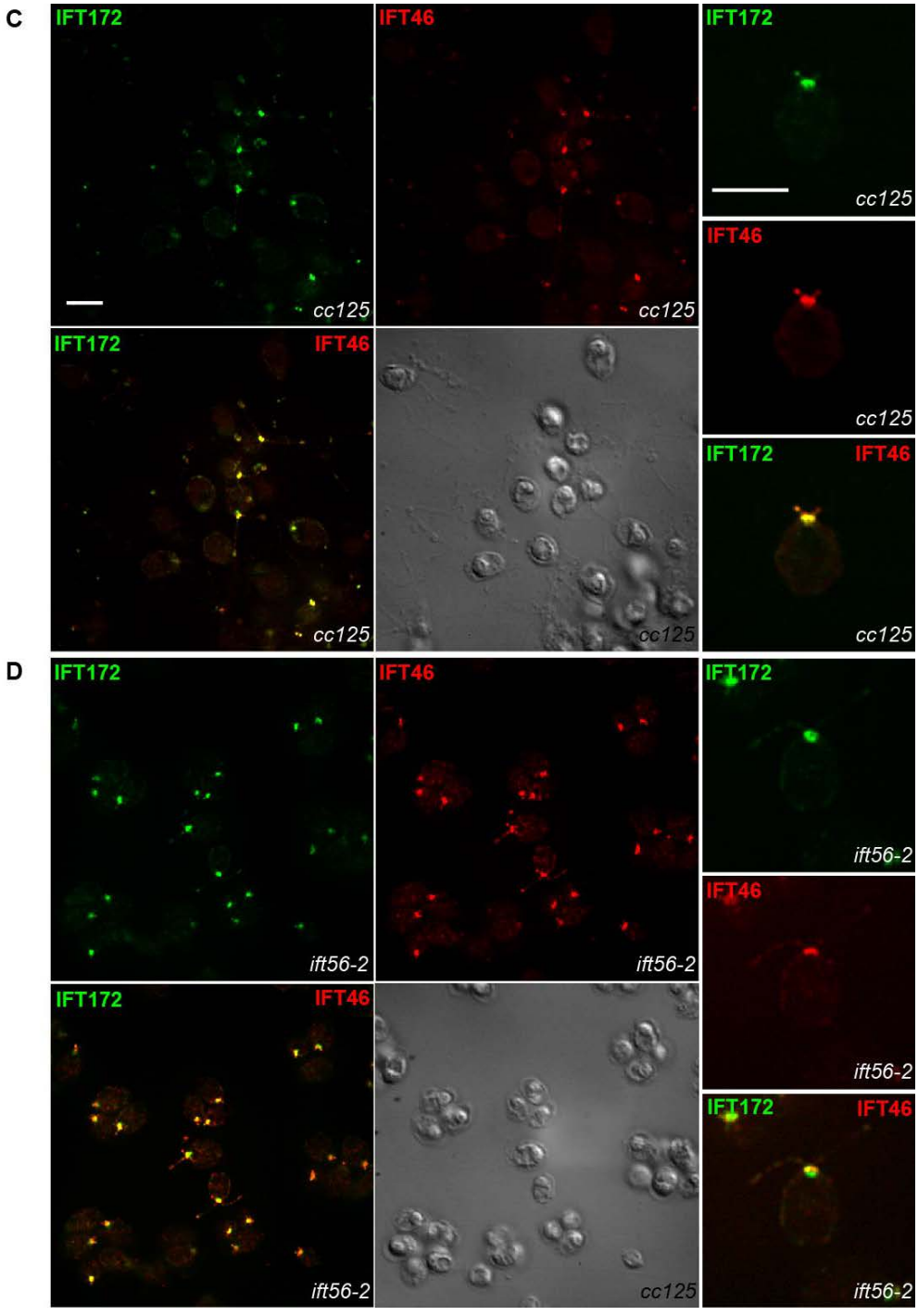

Figure 4-6. Continued.

ift56-2 has a compromised flagella regeneration rate

We showed that IFT56 is not necessary for the assembly and stability of IFT-B. Also, using TIRF microscope, Dr. Marshall's lab showed that the absence of the IFT56 does not affect the motility, either speed nor frequency, of the IFT particles [53]. Therefore, we are curious about why *ift56-2* cannot assemble full-length flagella (Figure 4-1 C, D). To address this question, we started with examining the flagella regeneration rate in *ift56-2*. In *Chlamydomonas*, removing existing flagella readily induces the flagella regeneration [21]. Taking advantage of this character of *Chlamydomonas*, we were able to generate the flagella regeneration curve of *ift56-2* and compared it to the curve of the wild-type *cc125*. Results showed that the flagella regeneration rate is significantly affected in *ift56-2* (Figure 4-7). Although both *cc125* and *ift56*-2 started to assemble flagella at the same time (10 minutes) after deflagellation, the flagella regeneration rates were different. The *cc125* assembled 4μm long flagella in less than 40 minutes, while *ift56-2* took around 40 minutes.

Many reasons can cause the lower flagella regeneration rate, including an insufficient number of active precursors in the cell body, increased flagellar disassembly rate, the compromised cargo transport efficiency or affected length indicator or regulators.

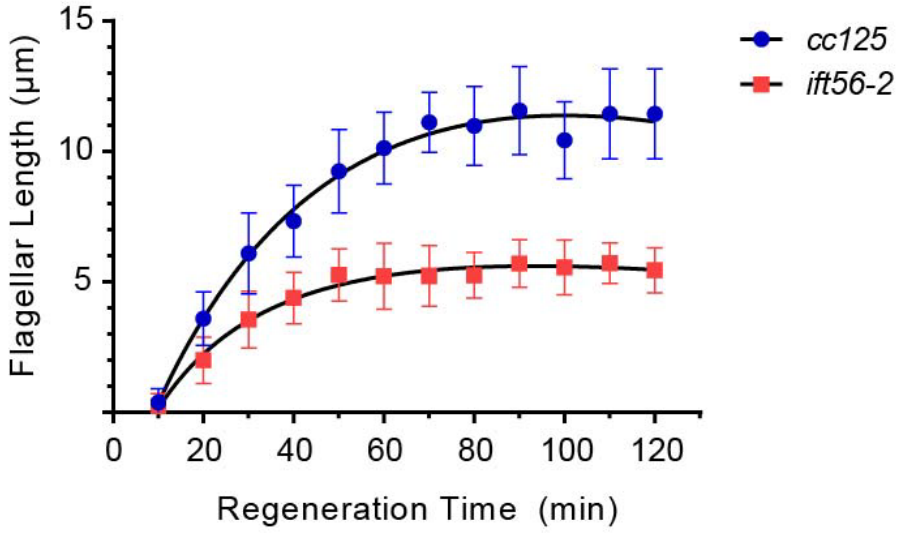

Figure 4-7. The absence of IFT56 leads to a compromised flagellar regeneration rate.
Flagellar regeneration was induced in both the wild-type *cc125* and the mutant *ift56-2* by deflagellation. Cells were collected at 20 minutes interval within 2 hours of time frame. The length of regenerated flagella was determined using phase contrast microscopy. At each time point, forty randomly picked cells from each strain were analyzed. Error bars represent s.d.. The result from one experiment was represented. A similar trend was shown in repeats.

The absence of IFT56 does not affect the size of precursor pool

Previous studies reveal that an excessive amount of axonemal precursors are stored in the cytosol. When cells are deflagellated after being treated with the protein synthesis inhibitor cycloheximide, the flagella of these cells can still be assembled and reach about one-half to two-thirds of their full length [21]. It indicates that the size of pre-exist precursor pool is enough to support the cell to generate longer flagella. If other factors are excluded, wild-type cells have enough precursors to assemble at least one and a half long flagella. If the newly regenerated flagella detach again in the presence of cycloheximide, cells can no longer regenerate any flagella, indicating the first regeneration has depleted the precursor pool [21]. Some short flagella mutants, such as

shf-1, *shf-2*, and *shf-3*, have a smaller precursor pool [175], which may correlate with their short length flagella. To examine whether *ift56-2* has a normal-size precursor pool, the cycloheximide treatment was utilized to block new protein synthesis. Then cells were deflagellated by pH shock. Samples were taken and measured at different time points to determine whether flagella can regenerate and how long their final length can be reached. Results showed that, after treatment, i*ft56-2* regenerated flagella with a similar length as *cc125*, indicating the size of precursor pool was normal in *ift56-2* (Figure 4-8 A). As we know, *ift56-2* assembles short flagella. It is possible that the "ruler" inside of flagella, which is capable of controlling the flagellar length, is reset to a shorter length in the *ift56-2*. In this case, even if there are more precursors left in the pool due to shorter original flagella length, it still cannot assemble longer flagella. To exclude this possibility, we deflagellated treated cells again to test whether the precursor pool had been depleted. Results showed that neither *cc125* nor *ift56-2* assembled flagella after second deflagellation (Figure 4-8 B), indicating that in both strains, the precursor pools were depleted in the first-time regeneration. Together, we concluded that the precursor pool size is not the reason that causes *ift56-2* to assemble shortened flagella.

Absence of IFT56 does not affect the flagellar disassembly rate

Although disassembly rate has long been ignored in cilia length control, it plays a similarly important role in flagellar length regulation. Laura et al. showed that disassembly rate could be actively regulated to help cell maintain their cilia length [93]. Moreover, we know that some MAPs are critical in stabilizing tubulin-related structures. Some IFT subunits, including IFT56 itself, are involved in carrying specific sets of

cargos [20, 53, 56, 66, 171]. Thus, it is also possible that IFT56 indirectly help maintain the flagellar length by carrying specific cargos. To test flagella disassembly rate, we treated cells with sodium pyrophosphate (NaPPi) to induce the flagellar resorption [27]. Experimental data revealed the parallel resorption curves between *ift56-2* and *cc125*, suggesting that the disassembly rate is not affected in *ift56-2* (Figure 4-9 A, B).

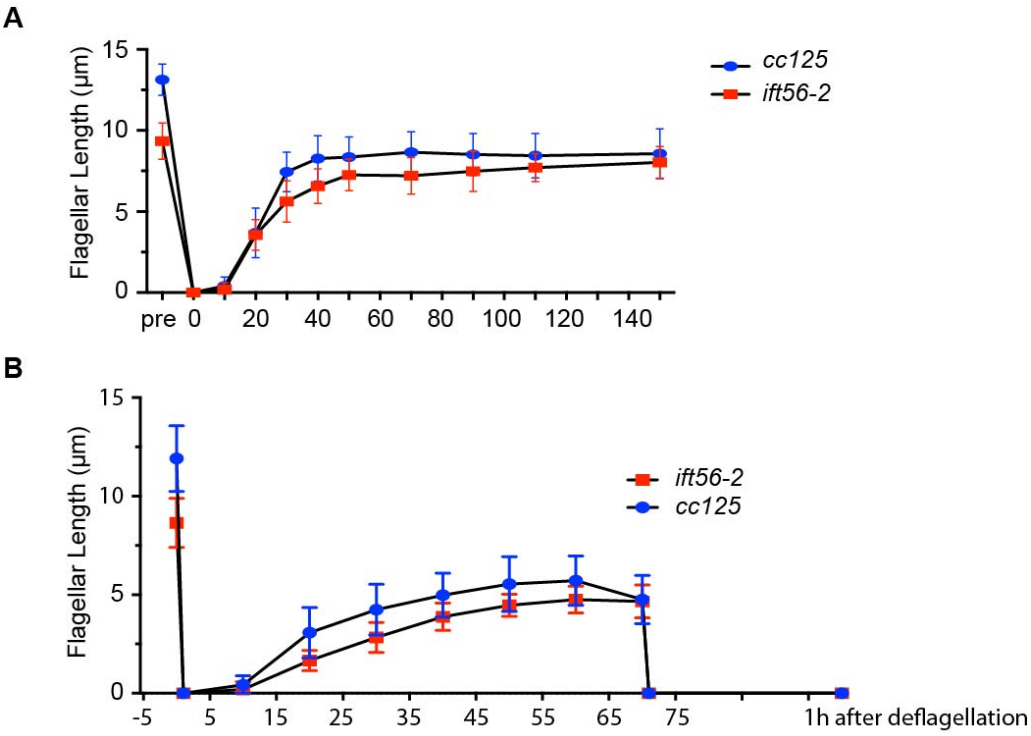

Figure 4-8. The size of precursor pool is not affected in *ift56-2*.
A. The wild- type *cc125* and *ift56-2* were deflagellated by pH shock and treated with protein synthesis inhibitor cycloheximide. Cells were collected at different time points. At each time point, fifty randomly picked cells were analyzed. TAP medium was used in this experiment. The result from one experiment was represented. A similar trend was shown in repeats. **B.** Cells are deflagellated twice during cycloheximide treatment. When flagella reach their steady-length during first regeneration, cells were deflagellated again. Samples were collected at different time points before and after first and second-time deflagellation. The length of flagella at different times was determined by using phase contrast microscope. Thirty cells from each strain were analyzed at each time point. Error bars represent s.d.. Cells were cultured in M1 medium in this experiment. The result from one experiment was represented. A similar trend was shown in repeats.

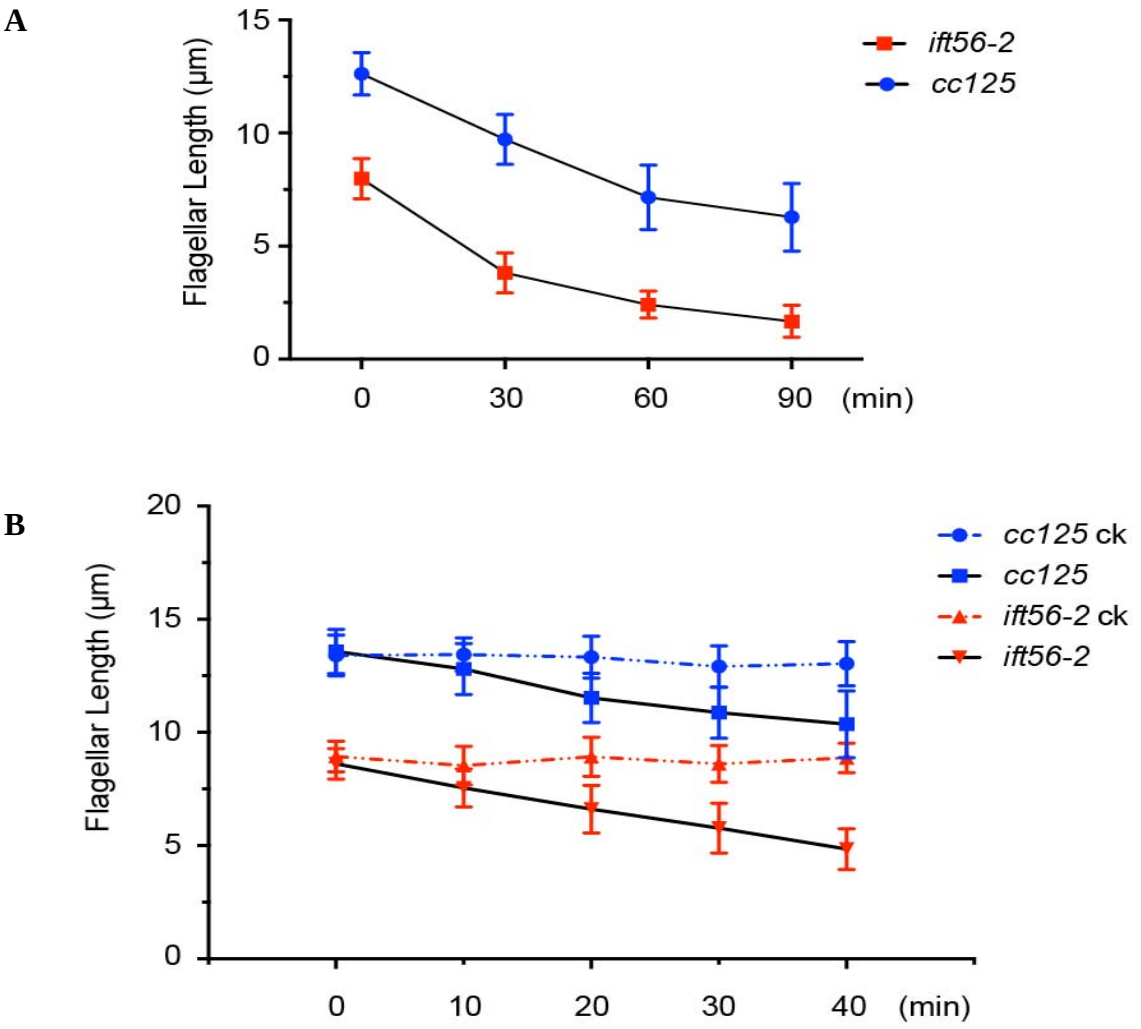

Figure 4-9. The absence of IFT56 does not affect the flagellar disassembly rate.
A. Flagellar resorption was induced by 15mM Nappi treatment. Samples were collected from the wild type *cc125* and the mutant *ift56-2* at 30 minutes intervals. The length of flagella was determined by using phase contrast microscope. Thirty randomly picked cells from each strain were analyzed at each time point. Error bars represent s.d.. The result from one experiment was represented. A similar trend was shown in repeats. **B.** Flagellar resorption rate in the beginning. Cells were collected at 10 minutes' interval within 40 minutes. Thirty cells from each strain were analyzed at each time point. Dotted lines represent the controls (cells without treatment). Error bars represent s.d.. The result from one experiment was represented. A similar trend was shown in repeats.

A couple of tested regulation systems are not compromised in ift56-2

Flagella length is tightly regulated. Several flagella-length regulators or indicators, such as LF1-LF5, CNK2, and GSK3, haven been identified and characterized. It is possible that the ciliogenesis defect seen in *ift56*-2 is a collective output of the altered activities of these regulators. We tested whether IFT56 functions together with these known indicators and regulators by analyzing double mutants and treating cells with chemicals.

For the regulator GSK3, which is essential for survival in *Chlamydomonas,* lithium was used to block its enzymatic activity. When treated with 50mM lithium acetate, wild type cells will elongate their flagella to about 1.4 times of the original length [176]. It also has been shown that actin is required for IFT regulation [174]. The inner dynein arm complexes within the flagella contain actin. Moreover, the absence of IFT56 affects the delivery of certain types of inner dynein arms [53]. Dr. Marshall's lab showed that an inner dynein arm mutant *ida5,* which lacks actin, displayed a compromised flagellar regeneration rate [174]. Thus, it is possible that the compromised flagellar regeneration rate is due to the severely reduced amount of actin in *ift56-2* flagella. It worth noticing that the lithium treatment does not affect the flagellar length of *ida5* [174]. Therefore, we used the same treatment to examine whether *ift56-2* has the same phenotype. Results showed that the wild-type *cc125* elongate its flagella to about 1.4 times of its original length as expect (1.40 times, from 12.65μm to 17.33μm), while the *ift56-2* also elongated its flagella with a similar ratio (1.34 times, from 7.98μm to 10.70μm). It indicates that the regulation through GSK3 is not affected in the *ift56*-2 (Figure 4-10 A).

For some other regulators, whose mutants are available, we tested them by crossing them with *ift56-2*. We generated a few double mutants including *lf4 ift56-2*, *lf5 ift56-2*, and *cnk2 ift56-2*. The flagellar length of double mutants was measured and compared with both parent strains (Figure 4-10 C, D). The double mutant *lf4 ift56-2* assembled longer flagella than *ift56-2*, however, the elongate ratio between *lf4 ift56-2* and *ift56-2* (1.36 and 1.27) is much lower than the ratio between *lf4* and *cc125* (1.71) (Figure 4-10 B). Experiment results from *lf5 ift56-2* and *cnk2 ift56-2* are not convincing due to the small differences caused by the mutations and the variance between different double mutant strains. Results showed that the mutant *lf5-2* elongated to 1.16 times of the wild-type strain, while the mutant cnk2 only elongate to 1.07 times of the wild-type strain. In randomly selected multiple double strains, some of them are longer than *ift56-2*, while some of them are shorter than *ift56-2* (Figure 4-10 C, D). Thus, we cannot draw a confirm conclusion about the last two double mutants.

Motility of ift56 mutants is not consistent in different preparations

We noticed that the *ift56-2*'s defects, especially the motility defects, show slight to obvious differences among different culture preparations (Video 4-4 and Video 4-5) while the wild-type *cc125* is always consistent (Video 4-3). Although after tightly controlling the culture conditions and other parameters we got a pretty consistent result at the end, however, it worth noticing that *ift56-2* is sensitive to conditions. To exclude the possibility that the phenotype inconsistency is due to the insertions, we include the *ift56-1*, which is a UV generated a null mutant with point mutations, in our study. This mutant also has a huge difference in motility between different preparations (Video 4-6).

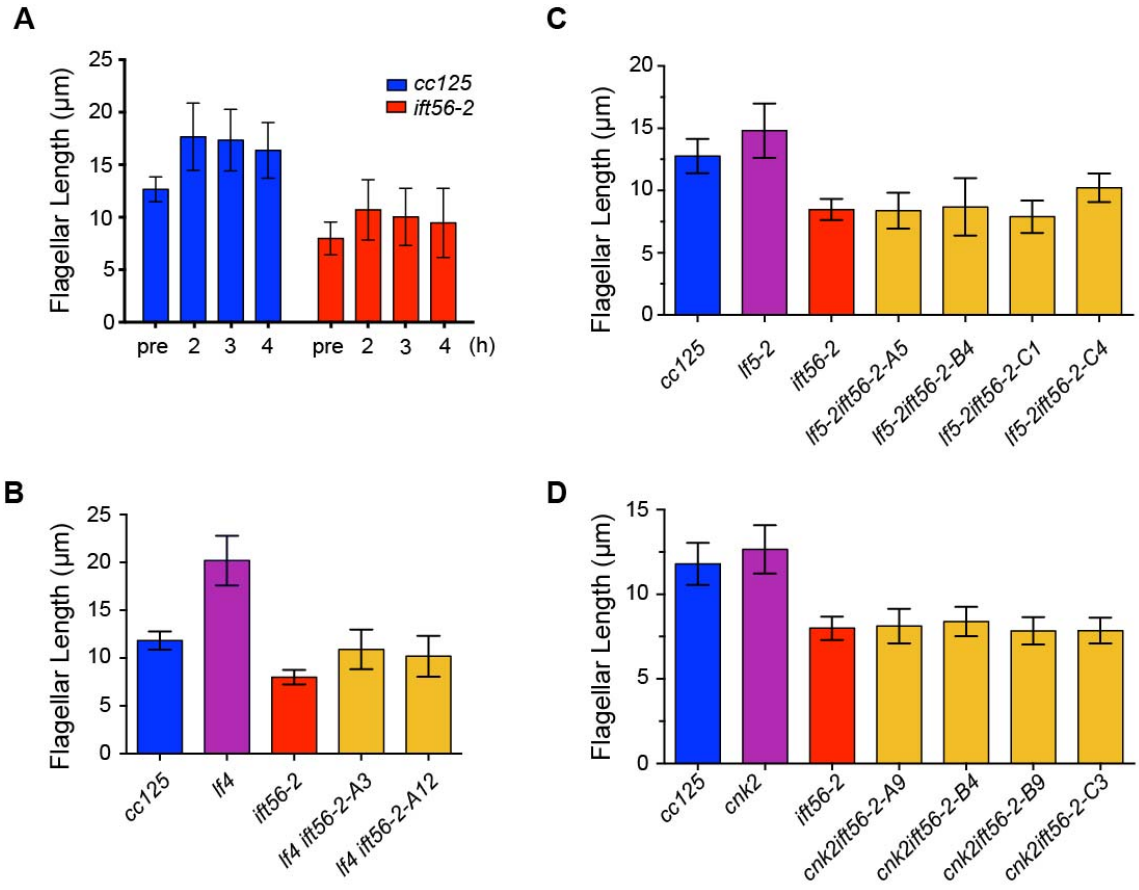

Figure 4-10. The tested regulators are not severely affected in *ift56-2*.
A. Both the wild-type *cc125* and the mutant *ift56-2* elongate their flagella during the 50mM lithium acetate treatment. Samples were collected before treatment and at 2h, 3h, and 4h after treatment. Fifty randomly picked cells were analyzed in each sample. Error bars represent s.d.. **B.** Flagellar length comparison among the wild-type *cc125*, the mutant *lf4* and *ift56-2*, and two randomly selected double mutants. One hundred and ten randomly picked cells were analyzed from each strain. Error bars represent s.d.. **C.** Flagellar length comparison among the wild-type *cc125*, the mutant *lf5,* and *ift56-2*, and four randomly selected double mutants. One hundred randomly picked cells were analyzed from each strain. Error bars represent s.d.. **D.** Flagellar length comparison among the wild-type *cc125*, the mutant *cnk2* and *ift56-2*, and four randomly selected double mutants. Randomly picked cells (n=110) were analyzed from each strain. Error bars represent s.d..

Methods and Materials

Most part of methods has already been described in Chapter III. Here, we only show the methods that are not included in the previous chapter.

Strains and cultures conditions

The mutant *ift56-2*, *lf4-7 ift56-2*, *lf5 ift56-2*, and *cnk2 ift56-2* were generated in this study. The mutant *ift56-2* was screened out from a set of flagellar-defective mutants. The insertion site was identified by the method described in Chapter II. Double mutants were generated as previously described [177]. The mutant *lf4-6* was generated in the lab. Dr. Marshall Wallace kindly provided the *ift56-1*. All other strains were obtained from the *Chlamydomonas* Center. Strains were maintained on Tris-acetate-phosphate (TAP) plates. Unless otherwise specified, liquid cultures are in TAP with constant aeration at 21°C with continuous light.

Measure flagellar precursor pool size

Chlamydomonas cells were prepared as described [21]. Briefly, cells were cultured in 75mL TAP medium or M1 medium (250mL flask) at 25°C with aeration to a density f 1-4×10^6 cell/mL. During culture procedure, a cycle of 14 hours light and 10 hours dark was used to induce synchronous growth. The cells were used between 2^{nd} and 4^{th} hours of the light cycle. The cells were deflagellated using pH shock and then treated with 10μg/mL cycloheximide. Samples were collected before deflagellation and at different time points after deflagellation. For the experiment with the second deflagellation, the treated cells were deflagellated again using pH shock.

Lithium acetate treatment

Chlamydomonas cells were prepared as described [21]. Then the cells were treated with 50mM lithium acetate for four hours. Samples were taken before and after treatment at specific time points (0-pre-treatment; 2h; 3h; 4h) and fixed in 2% glutaraldehyde. Fifty randomly picked cells were analyzed in each sample, and one flagellum from each cell was measured.

Sodium pyrophosphate treatment (chemical induced flagellar resorption)

Chlamydomonas cells were prepared as described [21]. M1 was used instead of TAP medium. Then the cells were concentrated and treated with 15mM sodium pyrophosphate (NaPPi) to induce the flagellar resorption. Samples were taken before and after treatment (0-pre-treatment; 30 minutes; 60 minutes; 90 minutes) and fixed in 2% glutaraldehyde. Thirty randomly picked cells were analyzed in each sample, and one flagellum from each cell was measured.

Discussion

Here, we report that IFT56, a *bona fide* IFT-B subunit, functions in the flagellar assembly and motility in *Chlamydomonas*. Strikingly, although the isolated null mutant *ift56-2* assembles short flagella, the assembly and stability of IFT-B are not affected, indicating that IFT56 does not function as a structural subunit in IFT-B. Moreover, we showed that *ift56-2* has a compromised flagellar regeneration rate. Further analyses revealed that the reduced flagellar regeneration rate is neither due to a limited precursor pool nor the accelerated disassembly rate. According to a previous paper, the motility of

the IFT particles is not affected [53]. In conclusion, our findings indicate that the defect in *ift56-2* ciliogenesis is likely due to the compromised IFT delivery efficiency.

IFT56, as a bona find IFT-B subunit, does not play a structural role in IFT-B

The IFT56/ DYF-13/TTC26/PIFTC3 has been shown undergo IFT-like movement and associate with the IFT complexes [110, 172]. The IFT complex comprises two sub-complexes, IFT-A and IFT-B. In this study, we show that, in sucrose density gradients of *Chlamydomonas* flagella extracts, IFT56 co-migrates with IFT-B subunits IFT74 and IFT46 instead of IFT-A subunit IFT139, indicating that IFT56 is an IFT-B subunit (Figure 4-3 A). Surprisingly, as an IFT-B subunit, IFT56 is not essential for the assembly of IFT-B. Our result shows that the IFT-B complex from *ift56-2* flagella extracts still sediment at the similar position as the wild-type IFT-B complex on the sucrose density gradients, suggesting that the IFT-B assembly is not affected in *ift56-2* (Figure 4-4 A, B). It is consistent with a recent published overall structure of the IFT-B complex (a complex could be further divided into two sub-complexes, IFT-B1 and IFT-B2), in which IFT56 is not necessary for IFT-B assembly [51, 54, 55]. The IFT-B model from the Nakayama's lab suggested that IFT56 is dispensable for the IFT-B1 assembly. It only interacts with one of the IFT-B1 subunits, IFT46. Thus, it stays in IFT-B1 [54]. The similar IFT-B model from Lorentzen's lab does not contain IFT56. Without IFT56, they are still able to reconstitute 9-subunit IFT-B1 and the 15-subunit IFT-B using recombinant *Chlamydomonas* proteins. Both groups showed that without IFT56, IFT-B assembly is ok. In our study, we also showed that the absence of IFT56 does not affect the stability of assembled IFT-B. Western blots of the whole-cell extracts showed that

the levels of all the other IFT-B subunits are not affected in the mutant *ift56-2* (Figure 4-5 A). Moreover, data from the 12-hour cycloheximide treatment revealed that the turnover rate of IFT46, a marker for IFT complex stability [52], in *ift56-2* is comparable to the wild-type *cc125*, suggesting that the stability of IFT-B is not affected in the absence of IFT56 (Figure 4-5 B). To summarize, these results reveal that IFT56 does not function as a structural subunit in IFT-B.

Thus, IFT56 is unique among the well-studied IFT-B subunits. The isolated *ift56-2* mutant assembles short flagella, which is consistent with other ciliated organisms [107], indicating that IFT56 does play a role in ciliogenesis. However, the IFT56 does not play a structural role in IFT-B. Also, IFT56 is not likely involved in tubulin delivery since protein sequence analysis showed that the IFT56 does not contain CH domains, which was reported to be responsible for tubulin binding [56, 64, 171, 178].

IFT56 plays a role in delivering a specific set of motility-related cargos

Although IFT56 is not essential for IFT-B structurally, it plays a functional role in IFT system. Our results show that *ift56-2* is defective in cell motility. Further motility analyses showed that *ift56-2* has abnormal waveforms, in which the angle of the flagellar beating is significantly smaller than the wild-type *cc125* (Figure 4-2 D, E and Video 4-3, Video 4-4). Also, the beating frequency of *ift56-2* is affected as well partially due to the incoordination of the two flagella (Figure 4-2 B, D, E and Video 4-4). A recent study from Marshall's lab can explain the motility defects. Using proteomic and biochemical analyses, they showed that the IFT56 plays a role in delivering a particular set of

proteins involved in motility [53]. Thus, IFT56 performs a functional role in IFT-B as an adaptor for motility-related cargo binding. The structure of IFT56 also supports its role as a potential adapter. IFT56 contains TPR motifs, a feature which it shares with IFT88 and IFT139 [179]. The TPR motif is present in some proteins that are functionally unrelated and can mediate different protein-protein interactions [180]. The TPR motif has been determined by crystal structure studies of multiple TPR-containing proteins [181, 182]. It is a motif containing two antiparallel α-helices. When packed in tandem arrays, they form specific structures and play roles in protein-protein interactions that lead to the formation of multi-protein complexes [183]. In IFT-B, IFT56 has only one interaction partner IFT46. The enriched TPR domain may interact with other cargos.

A fact worth noticing is that the motility defects of both *ift56* mutants varied in different preparations. Both mutants show motility defects varies from completely immobile to almost the wild type like motions in different preparations. Since IFT56 is a subunit of IFT-B, and the absence of IFT56 caused a significantly reduced level of many motility-related cargos, it is possible that IFT56 functions together with other IFT subunit(s) for cargo delivery. The similar cooperation has already been shown in the case of tubulin delivery. It has been shown that both *ift74Δ130* (produce IFT74 without N-terminal) and *ift81-1* IFT81 (5E) (produce IFT81 with mutated tubulin-binding module) assemble full-length or nearly full-length flagella. However, the double mutant only assembles tiny flagella [56], which indicates that neither IFT81 nor IFT74 tubulin-binding module alone is essential for the transport of tubulin [56].

The ift56-2 mutant is a valuable tool to study flagellar length control

Although the motility defects are well explained by the depletion of the motility- related cargo, there is no clue about the observation that *ift56-2* has defects in ciliogenesis. Consistent with previous studies of IFT56's homologs in ciliated organisms [53, 172, 184], *ift56-2* assembles short flagella. Its flagellar length is 1/2 -2/3 of the wild-type length (Figure 4-1 C, D). It worth noticing that IFT56 and its homologs were identified in multiple proteomic analyses [185, 186] and other systematic studies of the primary cilia [172, 187]. It indicates that IFT56 plays a conserved role other than just delivering motility-related cargos. In this report, we showed that *ift56-2* has a compromised flagella regeneration rate (Figure 4-7). Moreover, we demonstrated that the compromised regeneration rate is neither due to a limited precursor pool nor the accelerated disassembly rate, suggesting that the absence of IFT56 affect flagella assembly efficiency (Figure 4-8 and Figure 4-9). Because without IFT56 the motility of IFT particles is comparable to the wild-type [53], we suggest that either the IFT general transport efficiency is compromised (the structural subunit cannot be delivered efficiently) or the delivery of some length regulators was affected in *ift56-2*. Further research is needed to address which of the above hypothesis is correct. Recently, the single-particle imaging of fluorescence-tagged IFT cargos has been successfully applied in *Chlamydomonas* IFT related research and provide some clues about flagella assembly [23, 56, 62]. Using the GFP-tagged tubulin, the work from Dr. Witman's lab showed that the *Chlamydomonas* strain with modification at the tubulin-binding residues of IFT81 has a greatly reduced tubulin transport frequency and shows a slowed down flagella

regeneration. Moreover, the *ift74Δ130* and *ift81-1* IFT81 (5E) double mutant only assemble tiny flagella [56]. To summarize, with a severely compromised delivery of axonemal structural subunits can lead to ciliogenesis defects. Using GFP-tagged tubulin and DRC4 Lechtreck's lab showed that the cargo transport by IFT is regulated. The Tubulin and DRC4 transport by anterograde IFT was dramatically increased in growing flagella than in steady-state flagella [23, 62]. They also showed that mutants with abnormal ciliary length perform abnormal kinetics of tubulin transport. In the short flagella mutant *shf2*, the tubulin transport slowed down earlier than the wild-type [23]. Our mutant *ift56-2* also assembles short flagella as *shf2* though it has a normal-sized precursor pool (Figure 4-8). The same method can be used to analyze whether the tubulin transport is abnormally regulated in *ift56-2*. Although the tested length regulators are not functions together with IFT56 to collectively determine the flagella length (Figure 4-10), we cannot exclude the possibility that the other length regulator/indicator is involved in, such as aurora-like kinase CALK [96, 97]. In conclusion, because the IFT cargo transport is regulated and our mutant is an IFT-B subunit with abnormal flagella length (the short flagella is not due the assembly, stability or the motility of the IFT particles), it is a valuable tool to deciphering the regulation mechanisms.

CHAPTER V

CHARACTERIZING THE ROLE OF SMALL GTPASE ARL3 IN THE FORMATION AND FUNCTION OF THE *CHLAMYDOMONAS* FLAGELLA

Introduction

The cilium is a widespread organelle that projects from the surface of many eukaryotic cells. Besides its roles in cell locomotion and force generation (in motile cilia), the cilium is vital for sensory perception and cell signaling. Each cilium serves as a sensing/signaling hub to collect information from the outside environment and/or coordinate with other cells. These sensory functions mainly depend on their ciliary membrane composition. Although the ciliary membrane is continuous with the plasma membrane, the composition of the ciliary membrane is unique [1-3]. A subset of sensing/signaling-related proteins is enriched in cilia. In addition, some developmental signaling pathway components, such as component Ptch1, Smoothened, and Gpr162 in Shh, can dynamically localize to cilia [188]. So far, the processes of establishing the unique composition of the the ciliary membrane, such as delivery, retention, and removal, are not well understood.

ARL3 is a cilia-related protein expanding from single-cell protozoans to mammalians. It was identified in a few screens for ciliary proteins. One study involving comparative genomes analysis shows that *ARL3* exclusively exists in ciliated organisms [189, 190]. Another study shows that *ARL3* is in the list of X-box promoter motif (involved in ciliary gene regulation)-containing genes [187]. Furthermore, ARL3 was identified in

the purified flagella from the green algae *Chlamydomonas reinhardtii* [22]. Moreover, ARL3 was found to localize predominantly in the photoreceptor connecting cilium in rod and cone photoreceptors in human retina [191]. The evidence supports that ARL3 plays a role in the cilia.

ARL3 is a highly conserved small GTPase. It is one of the Arf-like (Arl) proteins in the Arf subfamily, which belongs to the Ras superfamily. Like other G-proteins, ARL3 contains a G-protein domain, which can be switched on and off by cycling between the active GTP-bound and inactive GDP-bound forms. The switch can be tightly regulated through interactions with specific guanine nucleotide exchange factors (GEFs) and GTPase-activating proteins (GAP) and affect the GTP-binding effectors. It has been shown that Retinitis Pigmentosa 2 (RP2), which causes retinitis pigmentosa disease when mutated, functions as an ARL3-specific GAP [192], while another small GTPase ARL13 is a GEF for ARL3 [193, 194]. Three GTP-specific effectors, UNC119, PDE6 delta and CCDC104/BARTL1, have been reported for ARL3 [195-197].

ARL3 has been shown to be involved in the ciliogenesis [198, 199] and serve as a displacement factor for the lipid-modified proteins [195, 200]. Also, it is proposed to play a role in the vesicle secretion and membrane fusion [198, 201, 202]. The first study that shed light on the physiological function of ARL3 is in a type of flagellated protozoan parasite *Leishmania*. It has been shown that the overexpression of the GTP-dominant form (constitutively active form) LdARL-3A (a homolog of the human *ARL3*) caused severely shortened flagella and released significantly less secreted acid

phosphatase, indicating that ARL3 plays a role in ciliogenesis and secretion. A later study in *C. elegans* also showed that the dominant form of ARL3 cause defects in ciliogenesis [203]. A study in mice showed that the *Arl3* (-/-) mice exhibits a pleiotropic phenotype and cannot survive longer than three weeks [204]. Typical phenotypes of cilia dysfunction, such as cyst formation and abnormal photoreceptor development, were detected. Although the cilia-related defects are prominent, apparently normal cilia are present in *Arl3* (-/-), indicating that ARL3 also plays a role in the ciliary function other than ciliogenesis [204].

Functions of ARL3 other than ciliogenesis may be caused by the misdistribution of a subset of lipid-modified peripheral membrane proteins. These proteins depend on ARL3 in order to be properly released to the cilia [199, 205]. A recent study shows that in the rod-specific *Arl3* knockout mice, the trafficking of lipid-modified peripheral membrane proteins is severely impaired while the transmembrane proteins are not affected [199]. It has been reported that ARL3 is essential for the ciliary targeting of a myristoylated ciliopathy protein NPHP3 by releasing it from UNC-119. In the proposed model, NPHP3 and other myristoylated cargoes bind to UNC119 in a myristoyl-dependent manner and are carried into cilia, then the active ARL3 (GTP-binding form) will interact with UNC119 and release binding cargoes. Then GTP-form ARL3 is switched to its GDP-form by RP2 (a specific GAP of ARL3) and detaches from UNC119 [206]. Biochemical experiments and structural considerations show that an active form of ARL3 is also capable of releasing the prenylated cargoes from PDEdelta by allosteric interaction *in vitro* [207, 208]. However, controversial results exist *in vivo*. It has been

shown that the ARL3 is not required for the ciliary localization of a PDEdelta dependent ciliary protein INPP5E [209, 210]. This result is challenged by a recently published study which shows a contradicting result. In this study, ARL3 indeed plays a vital role in releasing INPP5E from PDEdelta in ciliary part [211].

In contrast to its function as a cargo displacement factor, the role of ARL3 in ciliogenesis is more controversial and less understood. Although the apparently normal cilia are observed in germ-line *arl3*-/- [204], significant defects in ciliogenesis were found in the rod-specific *Arl3* knockout mice [199]. It is possible that ARL3 is only required for ciliogenesis in certain cell types. Moreover, it has been shown that the overexpression of GTP-form ARL3 leads to severely shortened cilia/flagella in a few model organisms [198, 203].

Although the knowledge about the function of ARL3 in cilia has expanded dramatically in recent years, many questions remain unclear, such as the role of ARL3 in ciliogenesis, and the relative extent that this *arl3*-dependent displacement pathway contributes. It is partly due to the difficulties in handling and separating such a tiny organelle. Due to the small size of the organelle, the changes are easily covered by large quantities of proteins in the cell body. *Chlamydomonas* is a perfect tool for studying this specific delivery pathway. ARL3 is highly conserved in *Chlamydomonas*. Also, a pure flagella sample can be easily isolated from a large volume of *Chlamydomonas*. It can significantly reduce the background noise from the cell body.

In this study, we characterized a *Chlamydomonas arl3* mutant, which presents various subtle flagellar defects. Also, using a mating assay, we showed that a myristoylated peripheral membrane protein CrPKG is likely affected in *arl3*. In addition, we rescued the *arl3* with the wild-type, constitutive active form (GTP-form), and constitutive-inactive form (GDP-form) of ARL3, respectively. We found that cells rescued with ARL3-GTP assemble significantly shortened flagella than others, confirming that overexpression of ARL3-GTP leads to ciliogenesis defects. Moreover, we compared the protein composition of isolated flagella between the mutant *arl3* and the wild-type *cc125*. As we expected, the axonemal composition did not show significant change whereas the protein bands with altered intensity were detected in the detergent-rich partition, which contains membrane proteins. This study provides insights into possible mechanisms of ciliary dysfunction caused by the depletion of ARL3. Moreover, the isolated *arl3* mutant can be a valuable tool in further function analysis of ARL3.

Results

Isolated arl3 mutant has an insertion in the second intron and is a null allele

In the screening for the IFT mutants, we accidently isolated a strain *10P10* that carries an insertion in *ARL3*, a gene encoding a small GTPase. Analyses of the insertion site showed that the insertion occurred in the second intron of *ARL3* (Figure 5-1 A). Since the insertion site exists in the intron, we performed an RT-PCR analysis to test whether the transcriptional level of *ARL3* was affected. We failed to detect any full-length *ARL3* in *arl3* while the specific band for ARL3 was prominent and clear in the wild-type *cc125* (Figure 5-1 B). Therefore, the transcription of the intact *ARL3* was completely abolished

in *10P10*. Although an incomplete *ARL3* (lacking an N-terminal) can be detected at an extremely low level (0.26%) (Figure 5-1 C), it should remain functionless, at least in cilia, because the N-terminal is critical for the ciliary localization of ARL3 [196].

The insertion co-segregates with the phenotypes mentioned above, suggesting that the allele is responsible for the mutant phenotypes. We named the mutant *arl3* after backcrossing it three times.

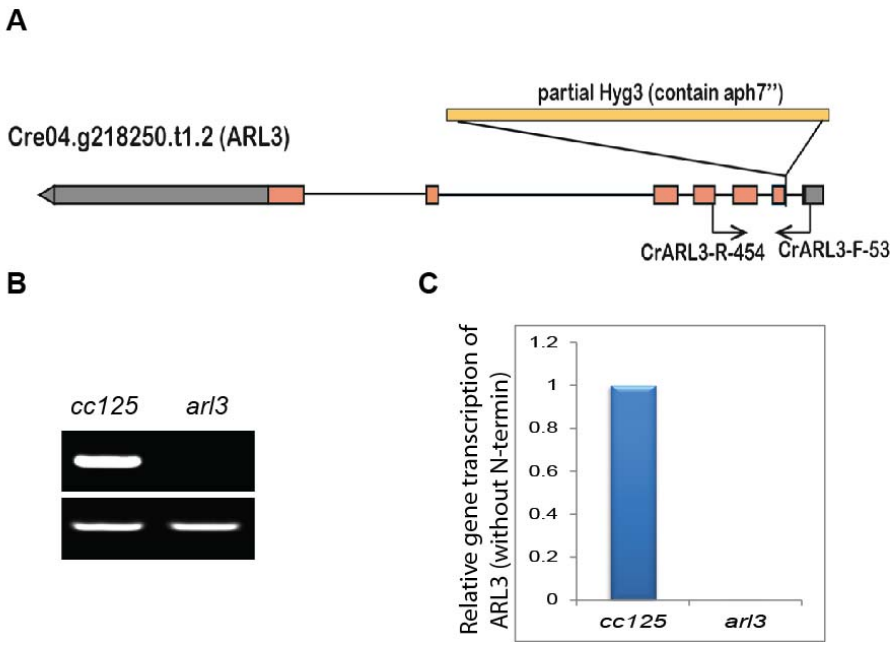

Figure 5-1. Characterization of the *arl3* mutant.
A. A hygromycin resistant gene *aph7'* cassette was inserted into the second intron of *ARL3*. **B.** RT-PCR reveals that the transcription of the intact *ARL3* is completely abolished in the *arl3* mutant. Another gene encoding a flagellar protein CrBug22 (FAP20) was used as a control. **C.** qPCR results reveal that incomplete *ARL3* can be transcribed at a substantially reduced level (0.26%).

ARL3 is not essential for the assembly of full-length flagella

ARL3 was implicated in ciliogenesis. However, whether the absence of ARL3 leads to ciliogenesis defect is still controversial [199, 204]. Thus, we examined the flagellar length of the *arl3* mutant. Our results showed that, under the standard culture conditions described in methods part, the flagellar length of *arl3* is not significantly affected, indicating that the ARL3 is not essential for the assembly of full-length flagella in *Chlamydomonas* (Figure 5-2).

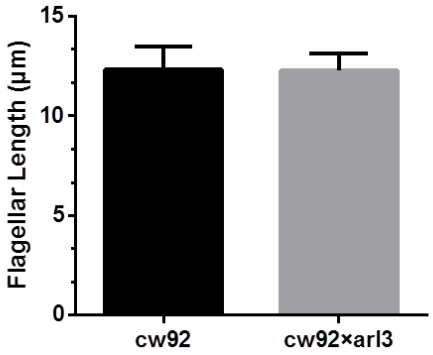

Figure 5-2. ARL3 is not essential for the assembly of full-length flagella.
There is no significant difference in flagellar length between *cw92* and *cw92× arl3*. *Cw92* is a wall-less mutant in the *cc125* background. It has a normal flagellar length. *cw92 × arl3* represents the strain that has the *arl3* mutation in the *cw92* background.

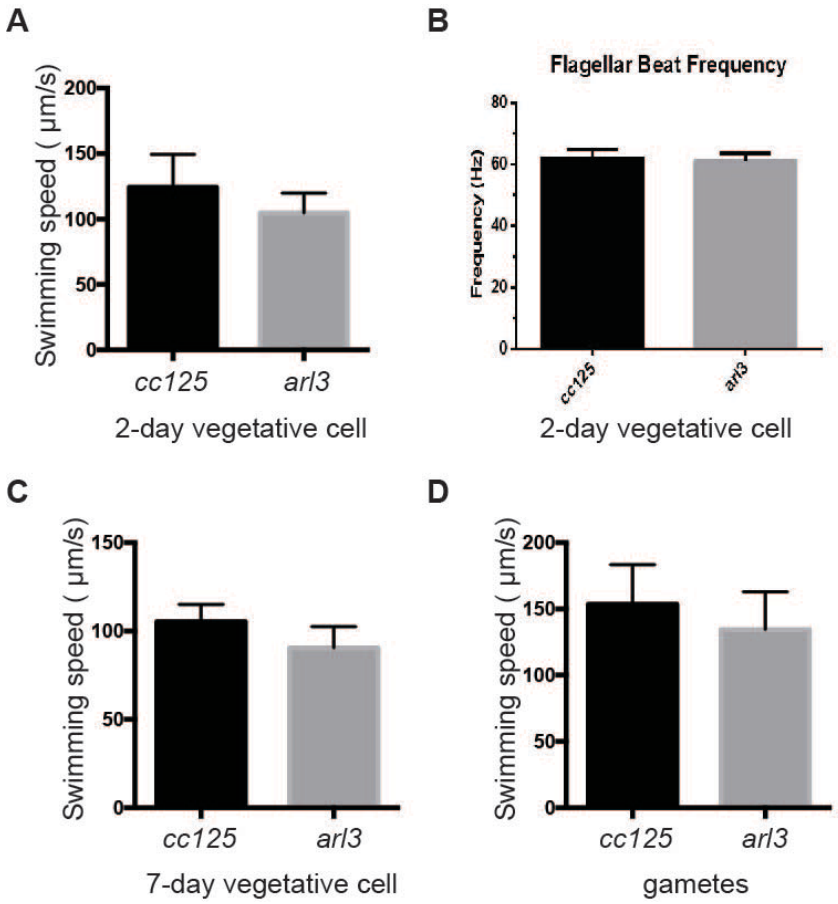

Figure 5-3. The *arl3* mutant displays motility defects.
The average swimming speed of the *arl3* mutant cells dramatically reduced when compared to the wild-type *cc125* in 2-day vegetative cell cultures (panel **A**), 7-day vegetative cell cultures (panel **C**), and the gametes culture (panel **D**). The swimming speed of individual cells was acquired by analyzing the cell moving tracks in two seconds. In panel **A**, sixty cells from each strain were analyzed. In panel **C**, thirty cells from each strain were analyzed. In panel **D**, sixty-nine gametes from *cc125* and seventy-seven gametes from *arl3* were analyzed. In panel **B**, the beating frequency of the 2-day vegetative cell culture was analyzed. No significant difference was shown between *cc125* and *arl3*. In all panels, the error bars represent s.d..

Depletion of ARL3 cause some degree of motility defects

Although the ciliogenesis is not affected (Figure 5-2), we noticed that *arl3* is a slower swimmer than the wild-type *cc125*. We analyzed the swimming paths of the *arl3* mutant cells and *cc125* cells. Results confirmed that both vegetative cells and gametes of *arl3*

had a slower swimming speed than *cc125* (Figure 5-3 A, C, and D). The average swimming speed of the *cc125* vegetative cells taken from the culture in the early log-phase (a two-day culture) was 124 μm/s, which is consistent with previous reports. Under the same conditions, the average swimming speed of the *arl3* vegetative cells was 105 μm/s (Figure 5-3 A). The *arl3* vegetative cells from a seven-day culture and the *arl3* gametes also showed similar reductions in their swimming speed (Figure 5-3 C, D). Then we analyzed the waveforms of the *arl3* mutant cells to figure out why they swim slower than the wild-type cells. However, short-time videos showed that unlike the other two analyzed mutants *ift57-1* and *ift56-2*, the *arl3* mutant cells possess normal flagellar waveforms (Video 5-1 and 5-2) and beating frequency (Figure 5-3 B). However, we noticed that more *arl3* cells showed curved swimming tracks than the wild-type cells, which may explain the reduced swimming speed. Although the percentages and curvature of the curved tracks were not consistent in different batches, it has frequently been shown in the *arl3* culture but rarely seen in *cc125* culture.

ARL3 may affect the ciliogenesis under adverse conditions

Although we have already shown that the ciliogenesis of *arl3* is not affected in standard culture conditions (Figure 5-2), we found that the *arl3* mutant presents ciliogenesis defects under some adverse conditions. We found that when cells were cultured in M1 medium with aeration, both the wild-type *cc125* and the mutant *arl3* assembled normal flagella and swam well. However, when cells were cultured without aeration, cell clumps (a typical phenotype of the ciliogenesis defects) presented in the *arl3* culture but were not detected in the *cc125* culture (Figure 5-4 A). To well document this character,

we kept cells in medium without aeration for 84 hours and took samples at different time points for analysis. Results showed that, under this type of adverse condition, the *arl3* mutant showed much more severe ciliogenesis defects than the wild-type *cc125*, indicating that ARL3 may affect the ciliogenesis in adverse conditions though it is not an essential factor (Figure 5-4 B). Moreover, it is worth noticing that the changing tendency of ciliogenesis defects' level was different between *cc125* and *arl3*. In the wild-type *cc125*, the percentages of cells that have ciliogenesis defects kept increasing in the first three hours. However, after then, the ratio was stabilized. No obvious difference was detected between the samples collected from 3h and 60h. The sample collected from 84h even had fewer cells with ciliogenesis defects than the sample collected at 3h. However, the ciliogenesis defects kept worsening throughout the treatment in the *arl3* mutant (Figure 5-4 B).

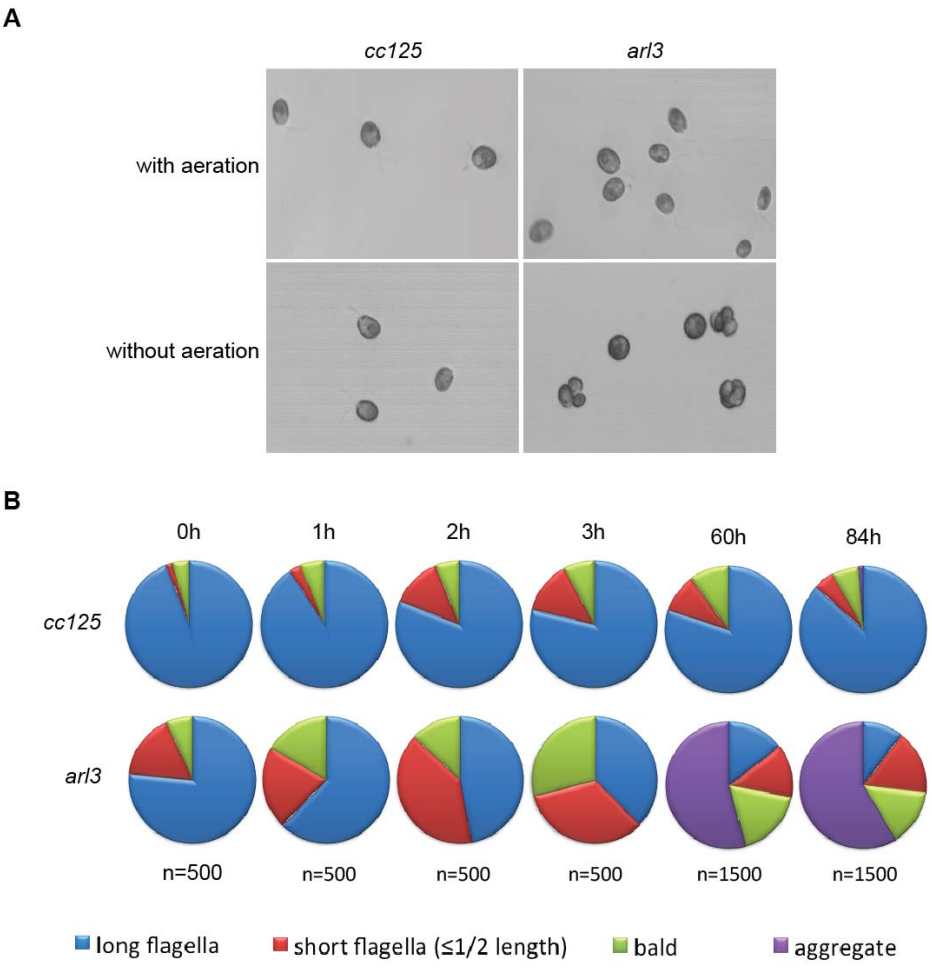

Figure 5-4. The *arl3* mutant presents ciliogenesis defects in adverse conditions.
A. Cell clumps presented in the *arl3* culture but not the *cc125* culture when cells were cultured in M1 medium without aeration. Both strains disperse well in medium with aeration. **B.** The *arl3* mutant presents severer ciliogenesis defects than the wild-type *cc125* after treated in adverse conditions. Cells were cultured in standard conditions before the experiment. Then cells were kept in medium without aeration. Samples were collected at different time points. Randomly picked 500-1500 cells/cell clumps were used for analysis in each sample.

Depletion of ARL3 cause decreased mating efficiency

In figure 5-2 and 5-4, we clearly showed that without ARL3 *Chlamydomonas* cells assemble normal flagella in standard culture conditions but show severe ciliogenesis defects in adverse conditions. Panel B in figure 5-4 revealed that when cells were shifted

to the adverse condition, the ciliogenesis of *arl3* mutant cells worsened steadily throughout the treatment while the *cc125* stabilized the percentage of cells that have ciliogenesis defects after a short period (3 hours) and even got better after then. Considering the possible roles of ARL3 involved in the flagellar enrichment of a subset of lipid-modified proteins [195, 200, 205], which are important in flagellar sensing and signaling transduction, we propose that ARL3 helps *Chlamydomonas* adapt to changing environments.

To test the idea, we first want to verify that the function of ARL3 as a displacement factor for a subset of lipid-modified proteins [195, 200, 205] is conserved in *Chlamydomonas*. A proteomic study of *Chlamydomonas* flagella shows that the flagellar compartment is enriched with myristoylated proteins [22], which is consistent with the role of ARL3 in targeting myristoylated proteins to flagella [195, 200]. In the list of identified *Chlamydomonas* myristoylated flagellar proteins [22], a cGMP-dependent protein kinase CrPKG draws our attention [22]. CrPKG is a peripheral membrane protein and is highly enriched in the flagellar membrane [212]. These characters perfect match the cargos that are released by ARL3, suggesting that ARL3 may be responsible for CrPKG targeting to flagella. It has been reported that CrPKG is involved in the *Chlamydomonas* mating signal pathway [212]. In the mating process, the cells starved for nitrogen differentiate into the gametes. When gametes with different mating types meet, they adhere to each other by their flagella. Then a signaling transduction is activated. Then gametes shed their cell walls and fuse together. The increase of cAMP in flagella and then in the cell body is crucial for the ultimate cell fusion. CrPKG is

responsible for cAMP increase by up-regulating an adenylated cyclase located at the flagellar membrane [213]. If the ARL3's function as a displace factor is conserved in *Chlamydomonas*, the depletion of ARL3 will affect the ciliary localization of CrPKG. If that is the case, the mating efficiency of *arl3* should be compromised.

Thus, we tested the mating efficiency of *arl3*. Gametes were prepared from both mating types of the wild type and *arl3* strains. Then the gametes were divided into four groups: 1); *cc125*(+)×*cc124*(−); 2)*cc124*(−)×*arl3*(+); 3) *cc125*(+)×*arl3*(−); 4) *arl3*(+)×*arl3*(−). Then mating efficiencies of each group, which is represented by the percentage of the zygote, were analyzed. The flagella number can help differentiate gametes and zygotes. Gametes possess two flagella while zygotes have four (Figure 5-5 A, B). Results revealed that group one had the highest mating efficiency whereas the group four had the lowest, indicating that *arl3* has defects in the mating efficiency (Figure 5-5 C).

The reduction in the mating efficiency can be either caused by defects in gametes adhesion or the following signaling transduction. To determine whether *arl3* has defects in the first step (cell adhesion), we observed the aggregation of gametes with different mating types (mt+ and mt-). Results showed that all the four groups form normal "clumps" at a similar level, suggesting that the early steps of the mating process are unaffected (Figure 5-5, D-F). The *arl3* gametes with a lower mating efficiency have issues in the following "fusion" process.

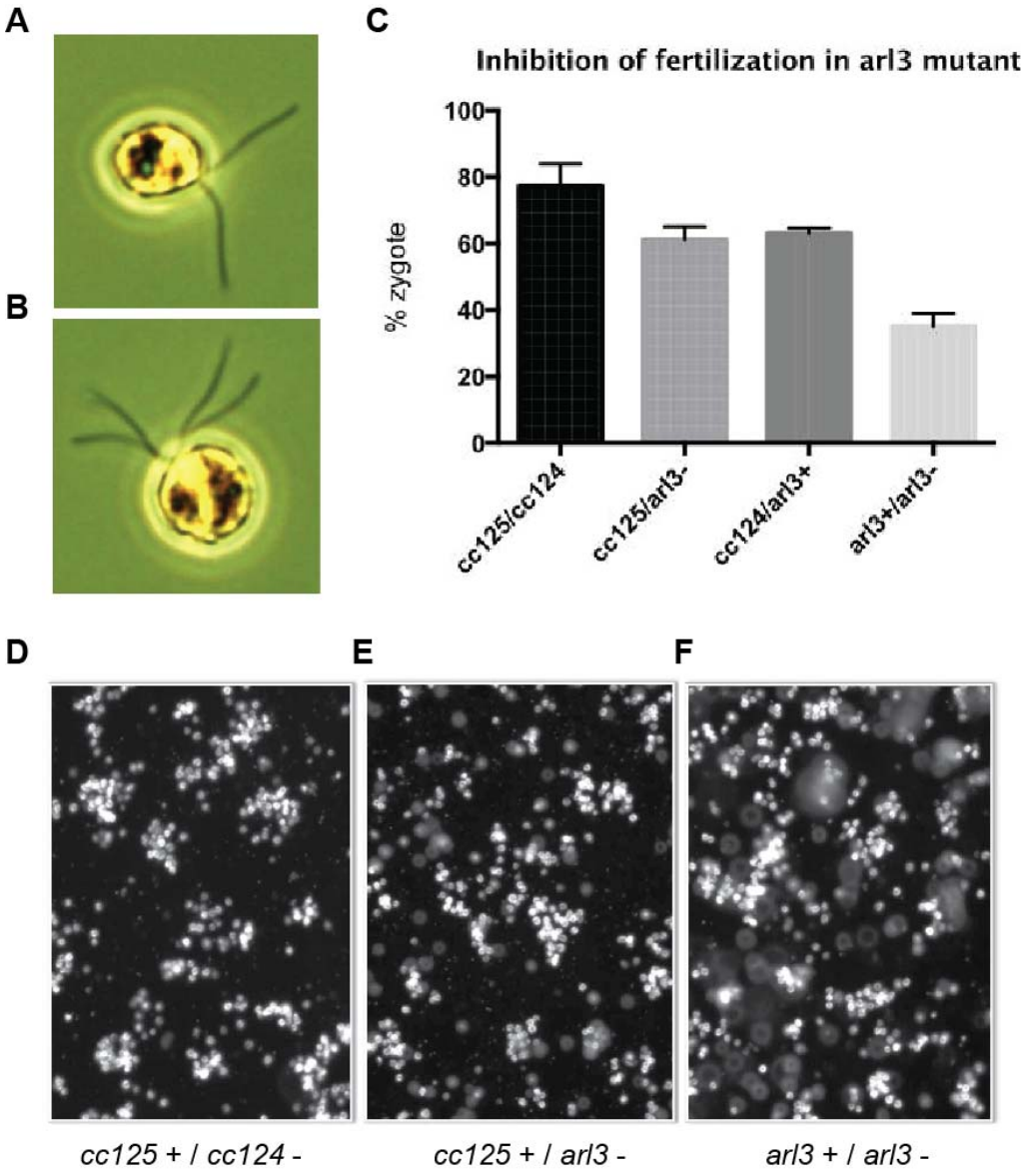

Figure 5-5. The absence of ARL3 leads to a significantly reduced mating defects. **A.** The image of a *Chlamydomonas* gamete, which possesses two flagella. **B.** The image of a *Chlamydomonas* zygote, which possesses four flagella. **C.** The comparison of the mating efficiency among four groups: 1) *cc125* and *cc124*, 2) *cc125* and *arl3* -, 3) *cc124* and *arl3* + and 4) *arl3* + and *arl3* -. *cc125* and *cc124* are wild-type strains with different mating types. The wild-type *cc125* is mating type plus "+" while *cc124* is mating type minus "-". The mating efficiency is represented by the percentage of zygote (% zygote = the number of zygote×2 / (the number of zygote×2 + the number of gametes). One hundred cells from each strain were analyzed. Error bars represent s.d.. **D-F.** Images of the cell aggregations of the group 1) *cc125* and *cc124* (panel **D**), group 2) *cc125* and *arl3*- (panel **E**) and group 4) *arl3*+ and *arl3*- (panel **F**). Group 3) has a similar level of aggregation and is not shown here. The bright white dots in the images are the *Chlamydomonas* gametes.

The depletion of Arl3 alters the flagellar membrane composition

ARL3 plays a crucial role in vesicle trafficking [214] and the ciliary localization of some lipid-modified protein [206]. However, the relative extent to this *Arl3*-dependent pathway contributes to the unique composition of the ciliary membrane remains unknown. *Chlamydomonas* is an ideal organism for analyzing the changes in membrane protein composition because their flagella can be easily isolated, purified, and partitioned. Also, our results about the compromised mating efficiency of *arl3* suggested that the *Arl3*-dependent delivery pathway is likely to be conserved in *Chlamydomonas*. Thus, we compared the protein composition of flagella between *arl3* and *cc125*.

Since axonemal proteins, including tubulin, dynein, and the other high-abundance soluble proteins, dominate the list of the composition of flagellar proteins, we partitioned flagella samples by Triton X-114 to detect the changes in the low abundant flagellar membrane proteins. We compared the band patterns of whole-flagella sample, axoneme samples, and samples from the detergent-rich part and water-soluble part, respectively. Results showed that in the axoneme part and water-soluble part, no obvious difference was detected. However, in the detergent-rich part, several bands show significant differences. We repeated the experiment and identified a few bands that were consistently altered in the *arl3* mutant (Figure 5-6).

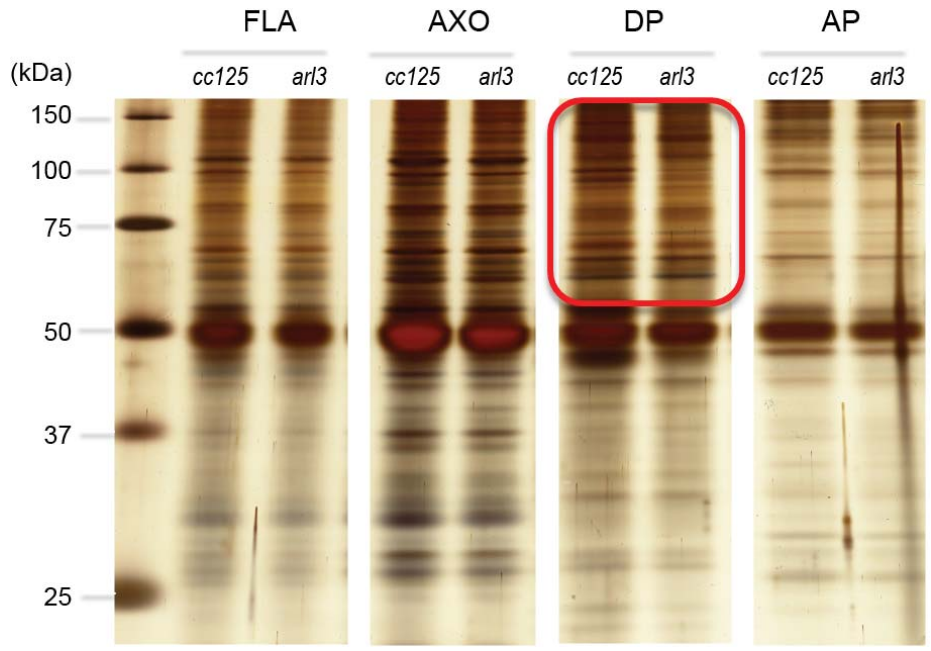

Figure 5-6. Flagellar membrane composition is altered in *arl3*.
A silver-stained 10% SDS-polyacrylamide gel of flagellar partitions. FLA represents the whole flagella. AXO represents the axonemes partition. DP and AP represent detergent partition and aqueous partition, respectively.

The depletion of ARL3 may affect the cell size

Surprisingly, we also noticed that the size of the cell is affected as well. The wild-type cells have a bigger cell size than the *arl3* mutant cells. The size defects are recovered in the *arl3* :: ARL3 (data are now shown).

Rescue arl3 with three forms of ARL3

ARL3 is one of small GTPases, which work as molecular switches. Thus, G-domain, the key part for the "on" and "off" decision, is critical for its physiological functions. To better understand the role of ARL3 in vivo, we expressed three different forms of *ARL3*, normal functioning *ARL3*, constitutively inactive, and constitutively active forms of

ARL3 in the *arl3* mutant. Because ARL3 is highly conserved among ciliated organisms, we were able to identify and mutate the key amino acids in the G-protein domain to manipulate the G-protein activity of ARL3 (Figure 5-7 A). According to previous studies, with a key mutation at the last T (T to N) in GLDNAGK**T**, the GDP/GTP α- and β-phosphate-binding site, the GDP to GTP exchange cannot be made. Thus, a constitutively inactive form can be generated. The constitutively active form was generated by a mutation at last Q (Q to L) in DIGG**Q**, which is a predicted magnesium-andβ-phosphate-binding site. The mutated ARL3 is unable to hydrolyze GTP [195, 198]. The three types of transgenic strains are referred to as *arl3*:: *ARL3*, *arl3*:: *ARL3* (Q70L), and *arl3*:: *ARL3* (T30N). Due to the absence of a specific antibody for ARL3 in *Chlamydomonas*, tags GFP and HA were fused to ARL3 for the expression detection. Results from the immunoblots showed that all three constructs are expressed in the rescued strains (Figure 5-7 B). The rescued strains with a higher expression level were chosen for further analyses. Because the wild-type cells do not have an HA-tag, the expression levels detected by immunoblots cannot be used for comparison with the wild-type strain. Thus, we tested the transcriptional level of ARL3 in rescued strains by qPCR and compared the results with the wild-type strain. Results revealed that at the transcriptional level, the transgene expression was either comparable or higher than the wild-type strain (Figure 5-7 C). The lowest expression was from strain *arl3* :: *ARL3* (Q70L), which is 81.2% of the wild-type strain. The highest level was from the strain *arl3* :: *ARL3* (T30N), which is around forty times of the wild-type strain (Figure 5-7 C). The huge divergence between the expressional level and transcriptional level of ARL3 in

arl3 :: *ARL3* (T30N) is probably due to its instability inside of the cells. By observing living cells under a microscope, we detected GFP signals in flagella from all three types of rescue strains. However, no signals can be detected in the flagella of *arl3*, indicating that both the GDP- and GTP- mutant forms of ARL3 expressed and localized to the flagella as wild-type cells, which is consistent with the data in mammalian cells [206]. Results were confirmed by immunofluorescent stainings (Figure 5-7 D).

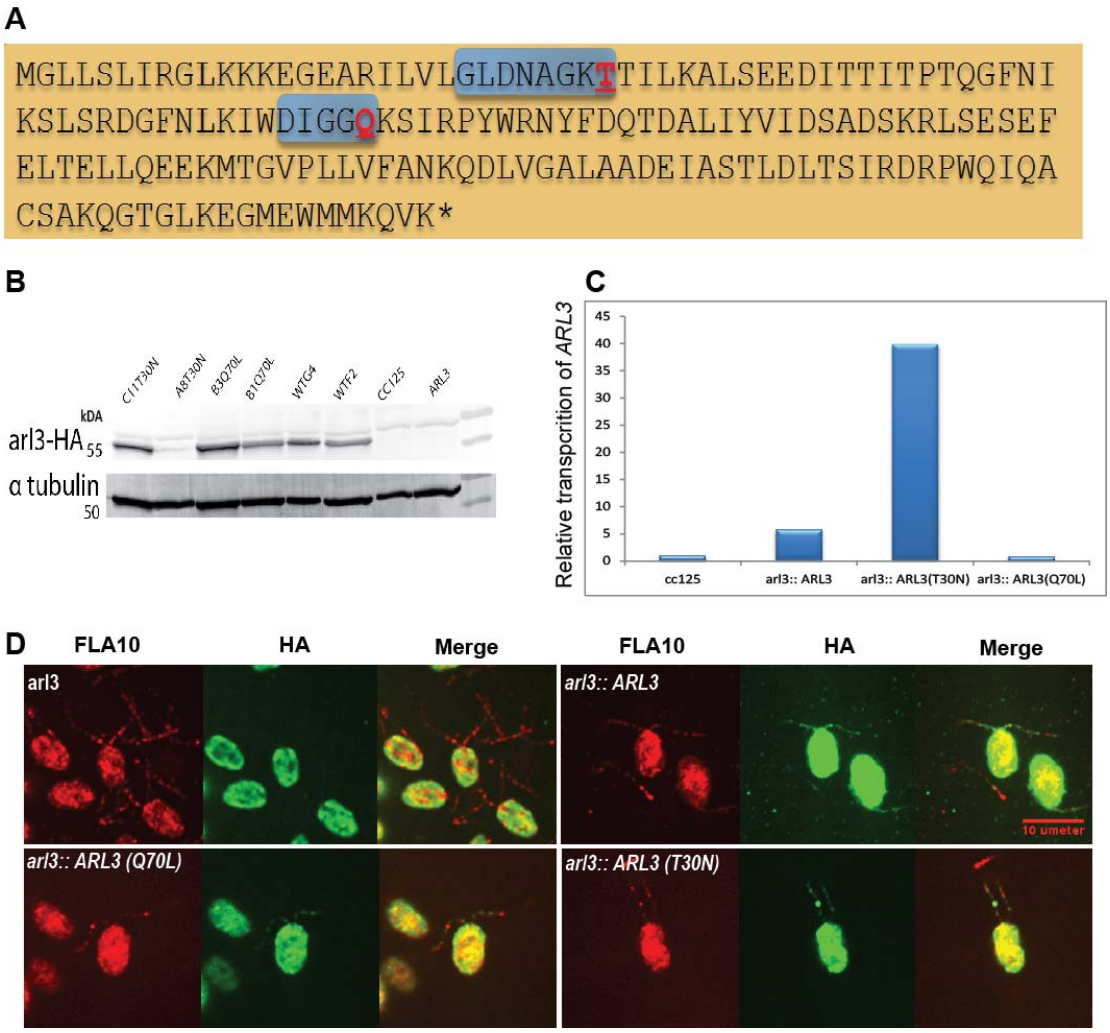

Figure 5-7. The *arl3* mutant was rescued by three forms of ARL3, the wild-type ARL3 (ARL3), the constitutive dominant form of ARL3 (ARL3-Q70L), and the constitutive negative form of ARL3 (ARL3-T30N).

A. Sequence information of the mutated ARL3. GLDNAGKT is the GDP/GTP α- and β-phosphate-binding site. The last T is essential for GDP to GTP exchange. Change T30 to N can produce a constitutive negative ARL3. DIGGQ is the magnesium- and β-phosphate-binding site, which is essential for GTPase activity. Change Q70 to L can produce a constitutive dominant ARL3. **B.** Immunoblots of whole cell lysates showed that normal or mutated ARL3 could be expressed in three types of rescued strains. Antibody against HA was used in the experiment. Antibody against α-tubulin was used as a loading control. **C.** Transcriptional levels of normal or mutated ARL3 in the wild-type *cc125* and three types of rescued strains. qPCR was performed for collecting data. **D.** The immunofluorescent staining of *arl3* and its rescued strains. Antibodies against HA and FLA10 were used in the staining. Scale bar represents 10μm.

Expression of the constitutively active form of ARL3 (ARL3-GTP) cause severe defects in ciliogenesis

We examined the flagellar length of the rescued strains. Results revealed that the average flagellar length of *arl3*:: *ARL3* (Q70L) is significantly shorter than the wild-type *cc125*, indicating that the expression of ARL3-GTP results in ciliogenesis defects (Figure 5-8). The flagellar length of the mutant *arl3* and the other two types of rescue strains was comparable to the wild-type *cc125* (Figure 5-8).

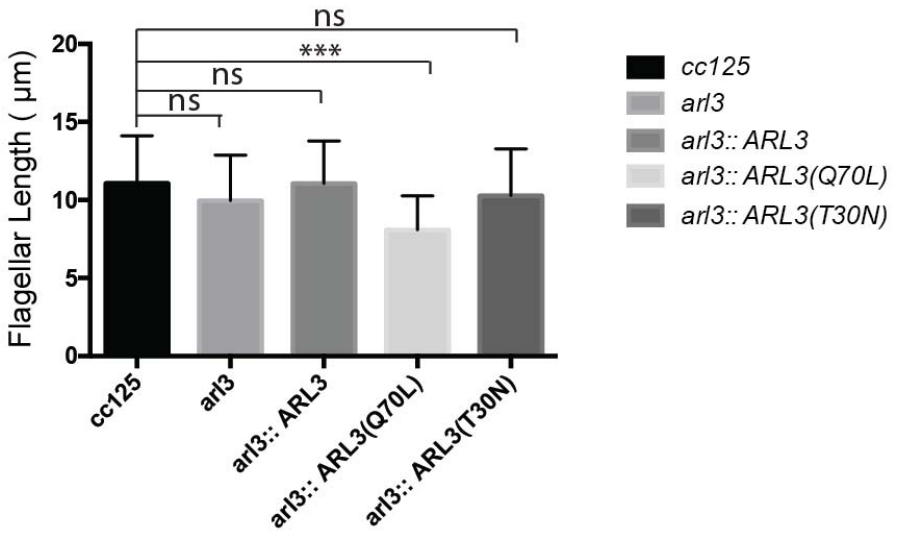

Figure 5-8. Overexpression of the constitutively active form of ARL3 leads to ciliogenesis defects.
The flagellar length of the mutant *arl3* and its three types of rescue strains were measured and compared to the wild-type *cc125*. Only *arl3* :: ARL3 (Q70L) possessed significantly shortened flagella while the other two rescue strains have normal flagellar length. Flagella of fifty randomly picked *Chlamydomonas* cells were measured. Statistical analysis was performed using Student t-test. Error bars represent s.d..

Discussion

Chlamydomonas as an ideal tool to clarify the ARL3-dependent delivery pathway

ARL3 is involved in the ciliary localization of a subset of lipid-modified proteins. ARL3 has been reported to release the myristoylated cargoes into cilia [195, 200], which is consistent with the fact that the myristoylation motif is enriched in cilia, especially in the membrane + matrix fraction [22]. Although it is still controversial, ARL3 also has been shown to play a critical role in the ciliary localization of the farnesylated cargoes [209-211]. It has been proposed that with its GAP and GEF, an ARL3-dependent delivery pathway exists in cilia and is responsible for the delivery of multiple peripheral membrane proteins [194]. In the proposed model, the status of ARL3, GTP-bound or GDP-bound, is critical for the proper function of this type of delivery. ARL3's GEF ARL13 exclusively localizes inside of cilia [194, 215] while the RP2, the specific GAP of ARL3, localizes to the ciliary base [216]. ARL3 can localize to both sides. The different localizations of three key players ensure that an ARL3-GTP gradient is generated across the transition zone of the cilia. Briefly, the GTP-specific binding partners of ARL3, which work as carriers, bind with the delivered cargoes and enter cilia. In cilia, cargoes are released by ARL3-GTP. Then ARL3-GTP-carrier leaves the cilia. At the ciliary base, RP2 assists the switch from the ARL3-GTP to ARL3-GDP and releases the carrier for recycling [195]. However, due to the limitations of the studied organisms, it is hard to verify the predictions at a general level. It is because that the cilia isolation is still challenging in most ciliated organisms. Thus, antibodies and

fluorescence tags are used in related studies. They are good for detecting one specific protein but cannot be used for the proteomic studies.

The fact that the flagella of *Chlamydomonas* can be easily isolated and partitioned makes it a promising model organism to study this ARL3-dependent delivery pathway on a general level. All the key players involved, including UNC119, ARL3, ARL13 and RP2, have homologs or putative homologs in *Chlamydomonas*. Also, the localization information and biochemical evidence showed that they are likely to play conserved roles in *Chlamydomonas* [194, 217, 218]. Moreover, according to our results, the phenotypes of the *arl3* mutant and its rescue strains are similar with the reported phenotypes in other ciliated organisms. These results include 1) ARL3 is not required for ciliogenesis in standard culture conditions (Figure 5-2), 2) The absence of ARL3 cause subtle ciliary defects (Figure 5-3 and 5-4), 3) The myristoylated protein CrPKG is likely to be affected (Figure 5-5), and 4) the overexpression of the constitutive dominant ARL3 (Q70L) results in severe ciliogenesis defects (Figure 5-8). In conclusion, ARL3 is likely to play a conserved role in a wide range of ciliated organisms, from *Chlamydomonas* to mammalians. It is consistent with the fact that ARL3 is a highly-conserved protein among ciliated organisms. For example, although *Chlamydomonas* and human had evolutionarily diverged long time ago, they share a 63.84% identity in ARL3. Analyses of the fractioned flagella samples revealed that the intensity of a few bands consistently altered in *arl3* mutant cells though they cannot be identified due to the high background (Figure 5-6). In the future, two-dimensional gel electrophoresis can be used to identify altered proteins. Moreover, the mass spectrometry-based quantitative proteomic analyses

with a high-resolution, either the label-based or label-free method, had been well established and proven to be successful in subcellular applications [219-222]. Application of these methods can provide more accurate data about the changes in ciliary membrane composition. It is highly possible that findings of ARL3 in *Chlamydomonas* can be extended to the other ciliated organisms due to the extreme evolutionary conservation of ARL3.

Arl3 causes plesiomorphic phenotypes of varying severity

As we mentioned above, ARL3 is a highly conserved small GTPase. However, its mutants show ciliopathy phenotypes of varying severity in different ciliated organisms. In mice, the *arl3* mutants cannot survive longer than three weeks. The newborn knockout mice are small and exhibit typical ciliopathy manifestations [204]. In *Chlamydomonas*, the *arl3* mutant cells show subtle cilia-related defects, including the abnormal phototaxis, a slower swimming speed, and a compromised mating efficiency (Figure 5-3 - 5-5). However, in *C. elegans*, the *arl3* mutants do not show any detectable ciliary defects [215]. The divergence in ciliary defects of the *arl3* mutants might be caused by the specificity of the ARL3 delivery pathway in different ciliated organisms. Protein structural analyses showed that the lipid modifications of the protein, the myristoylation or farnesylation, are essential for the carrier binding. The other parts of proteins cannot affect the binding specificity. Thus, the sets of cargoes delivered by the ARL3-dependent delivery pathway may be partially or even completely distinct in different ciliated organisms or different tissues in the same organism. For example, compare to *C. elegans*, mice have much more complicated signaling pathways. Thus,

this pathway may deliver more signaling related cargoes in mice. It is possible that only the central pathway is conserved among all ciliated organisms. However, the delivered cargoes may be highly versatile, which helps the cilia perform specific functions in different ciliated organisms or different tissues.

ARL3 may play a role in buffering environmental challenges

In our experiments, we noticed that different batches of the *arl3* mutant cells show variations in their phenotypes while the phenotypes of the wild-type *cc125* are consistent in all batches. Our data shows that although *arl3* assembles normal length flagella in standard culture conditions (Figure 5-2), it shows ciliogenesis defects in adverse conditions (Figure 5-4). Also, the comparison of cell tracks between *cc125* and *arl3* revealed the inconsistent performances of the *arl3* mutant. In different motility assay repeats, the wild-type *cc125* cells always swam well under standard culture conditions. However, the *arl3* mutant cells sometimes were immobile or had circular motions while sometimes they had linear motions like wild-type cells. The inconsistent phenotypes of *arl3* were recovered in the rescue strain *arl3* :: ARL3. Our results indicate that ARL3 may play a role in buffering some bad effects caused by environmental changes. It can, at least partially, explain why ARL3 is highly conserved in all ciliated organisms even though the depletion of ARL3 does not cause detectable defects in some of them [215].

The cilium is a sensing and signaling center. ARL3 can affect the composition of its membrane by playing a critical role in the delivery of some lipid-modified cargoes, which may play critical roles in sensing and signaling transduction. Thus, changes in the

composition of the ciliary membrane may cause inappropriate responses to environmental stimuli and cause detrimental results to the cell.

In future experiments, we can examine the effects of specific environmental changes, such as temperature changes, light intensity changes, aeration changes, and medium changes, on the *arl3* mutant. Then we can treat the wild-type *cc125* with screened out environmental changes, which can lead to severe ciliary defects in *arl3*. Then proteomic analyses can be used for detecting the changes in the ciliary membrane partition. Moreover, using FRET-based techniques and the powerful fluorescence reporter, we should be able to detect the ratio changes of ARL3-GDP and ARL3-GTP form *in vivo* during treatments [223, 224]. Due to the conservation of this pathway, the information may be applied in deciphering the disease mechanisms in some human ciliopathies.

Methods and Materials

Assay for Chlamydomonas mating efficiency

Strains for assay were streaked onto TAP plates and kept at room temperature for one week to get a thick layer of growing vegetative cells. Then vegetative cells were collected from TAP plates and transferred to TAP-N plates to induce gametogenesis. After kept on TAP-N for three days, cells were collected again and dispersed in sterile water. Cellometer (Nexcelom) was used to adjust *Chlamydomonas* cell solutions to a suitable concentration (around 10^6 cells/mL). Then cell solutions were transferred to sterile flasks and rotated vigorously on a shaker under a strong light for two hours to produce motile gametes. The flagellation status and motility of gametes were examined

under a microscope to ensure the quality of gametes. Then equal volumes of gametes (mt+, mt-) were mixed and kept under strong light without agitation. Samples were collected after 60 minutes and fixed by LUGOL's Iodine. One hundred randomly picked cells from each strain were analyzed under a microscope. They were divided into two groups, zygote (with four flagella) and gametes (with two flagella). The percentage of zygotes was calculated by the formula: % zygote = the number of zygote×2 / (the number of zygote×2 + the number of the vegetative cells). Few *Chlamydomonas* cells without flagellum were not counted.

Rescue strain construction

Three types of plasmids were used for generating rescue strains. Rescue constructs were created as follows (Figure 5-9). *Chlamydomonas* genomic DNA was extracted from the wild-type strain *cc125* using Genomic DNA Purification Kit from Thermo Scientific. The *ARL3* genomic DNA, including its promoter region, was divided into three smaller parts, fragment 1, 2 and 3, to facilitate the fragments' amplification and mutagenesis. Two enzymes (*Tat*I and *Sac*I), whose cutting sites present inside of the *ARL3*, were used as linkers to ligate three fragments together. The critical base pairs, which need to be mutated for constructing the GTP-dominant and GDP-dominant forms of ARL3, locate in the fragment 2. Three amplified fragments were cloned into a pGEM®-T vector (Promega) and sent out for sequencing. Clones with correct sequence were chosen for further steps. The pGEM-T-fragment 2 was mutated using the site-directed mutagenesis. The mutated pGEM-T-fragment 2 (T30N) and pGEM-T-fragment 2 (Q70L) plasmids were sent out for sequencing to confirm their accuracy. After generating all required

fragments, the intact ARL3 were made by ligating different parts together. Then the intact ARL3 (with or without mutation) were shuttled to the plasmid pBluescript, which contains a paromomycin-resistant gene *aph*8. Then three types of plasmids, pBluescript-ARL3 (wild-type), pBluescript-ARL3 (Q70L), and pBluescript-ARL3 (T30N), were transformed into the *arl3* mutant by electroporation. The rescued strains were first screened out by PCR. Then the expression of *ARL3* was detected using the HA antibody.

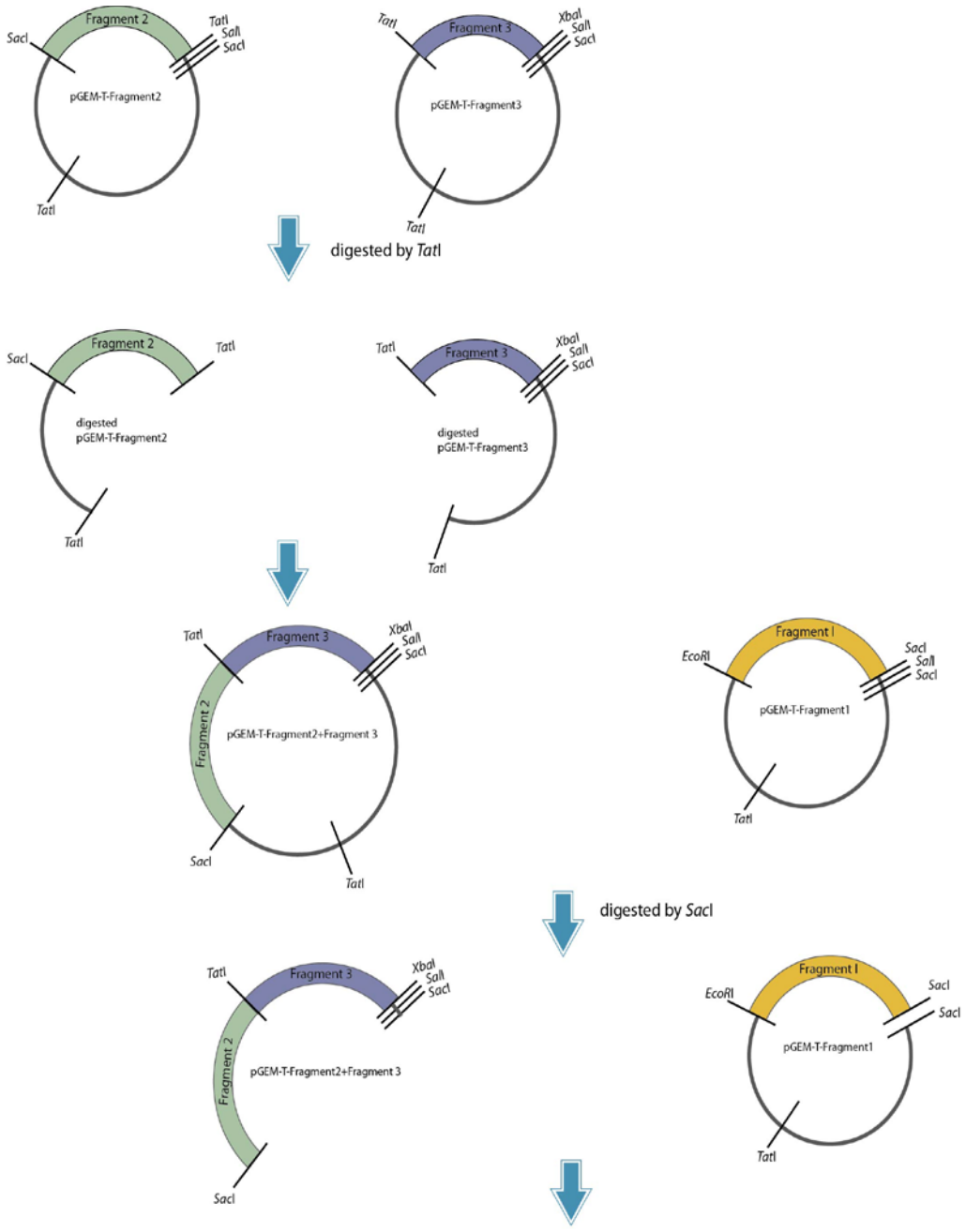

Figure 5-9. The ARL3 construct generation.

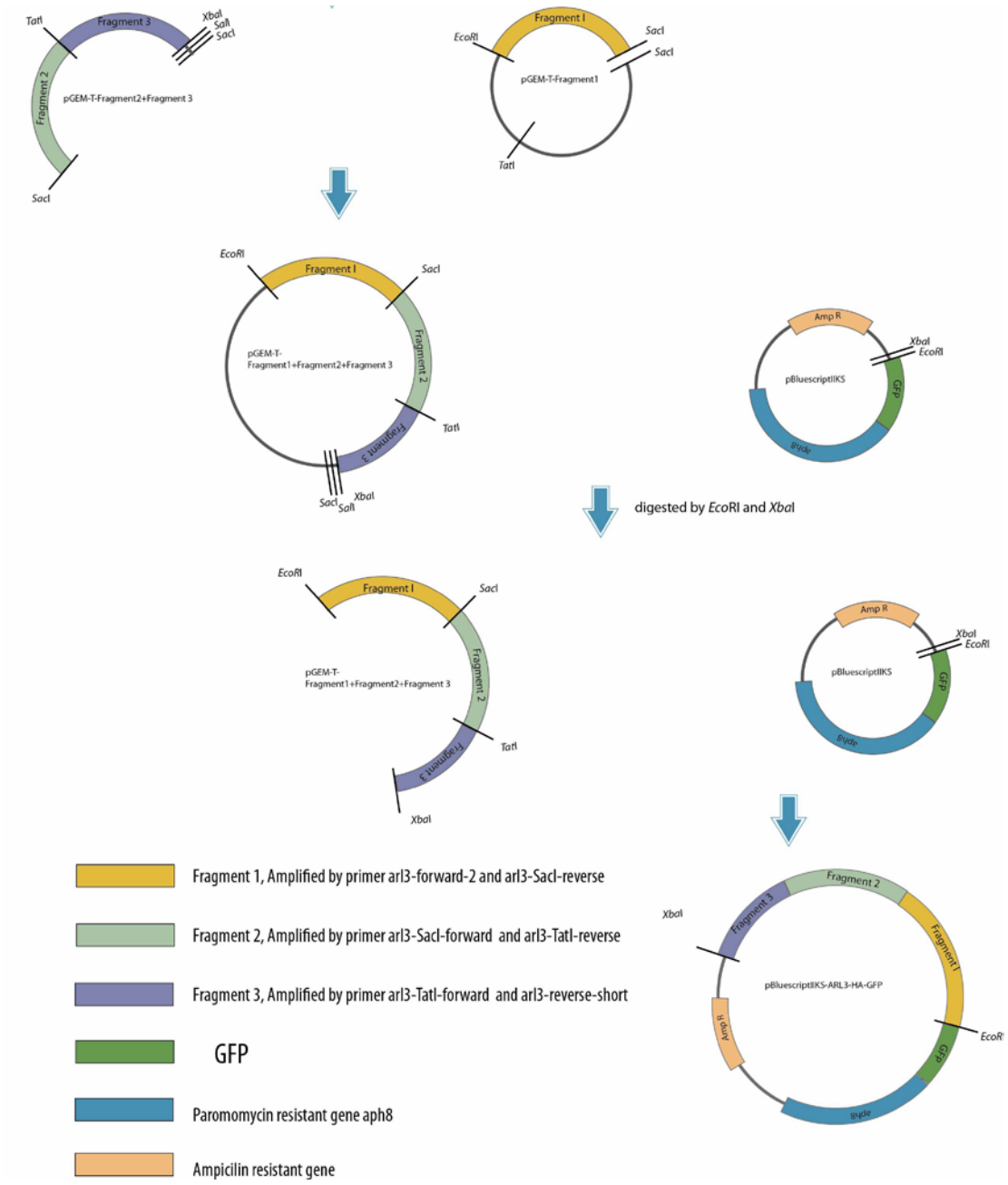

Figure 5-9. Continued.

Triton X-114 partition assay

Flagella were isolated using the method described in Chapter III. Then the Triton X-114 phase-partition was used as previously described [225]. Briefly, flagella samples were solubilized in 1% Triton X-114 for one hour at 4°C, and the insoluble debris (including the axoneme) were removed by centrifugation at 12000 rpm for 10 minutes. To separate the lipophilic/hydrophobic and hydrophilic proteins in the soluble materials, the supernatant was incubated at 37°C for 3 minutes. The solution partitioned into a lower detergent-enriched phase and an upper aqueous phase by centrifugation (12000rpm, 10 minutes, RT). More extraction buffer was used to dilute detergent-enriched phase while extra Triton X-114 was added to the aqueous phase. Then the phase separation was repeated. The detergent was removed from the purified detergent-enriched partition by the standard chloroform/methanol precipitation protocol [226]. The purified detergent-enriched and aqueous partitions along with intact flagella and axoneme samples were used for analysis. Samples were separated on SDS-PAGE gels and stained using SilverXpress® Silver Staining Kit from Invitrogen.

Immunofluorescence

Cells were cultured in TAP medium for three days. The cell staining was carried out as previously described in Chapter II with modifications in fixation and permeabilization steps. The concentrated cells were placed on the glass slides, which were coated with 0.4% PEI for 8 minutes. After removing surface liquid, cells were fixed using freshly made 4% formaldehyde for 30 minutes and washed three times with 0.5×PBS. Then cells were permeabilized with 0.3% TritonX-100 and 3% albumin (in PBS) for 5

minutes, followed by three washes with 0.5×PBS. Then slides were blocked in PBS containing 5% BSA, 1% cold water fish gelatin, and 10% goat serum). Other steps were the same as described in Chapter II.

CHAPTER VI

SUMMARY AND FURTHER DIRECTION

In this study, we identified a few genes that are involved in eukaryotic flagellar assembly using *Chlamydomonas* insertional mutants. Three genes were further analyzed. Two of them encode subunits of Intraflagellar Transport (IFT), IFT57 and IFT56. The other one encodes ARL3, a small GTPase.

Both IFT57 and IFT56 (DYF-13) are IFT-B subunits but play distinct roles. Recent biochemical studies have shown that IFT-B comprises two subcomplexes, IFT-B1 and IFT-B2. IFT57 is an IFT-B2 subunit and lies at the interface between two subcomplexes. Here, we showed that without IFT57 functional IFT-B is still able to assemble but is much less stable than the intact IFT-B. The IFT-B lacking IFT57 mainly exists in the flagella, a compartment that has less protease. These findings indicate that IFT57 does not play an essential structural role in the IFT particle but rather functions to prevent IFT particles from degradation. Moreover, IFT57 depletion disrupted the flagellar waveform and led to cell swimming defects. Further analysis showed that the motility-related protein IC97, a subunit of the inner dynein arm, is reduced in the *ift57-1* mutant flagella. It suggests that beyond its role in ciliogenesis, IFT57 is also involved in transporting specific motility-related proteins. IFT56, on the other side, is an IFT-B1 subunit. In this study, we showed that, unlike IFT57, IFT56 does not contribute to the IFT-B structural stability at all. However, it is required for the complete ciliogenesis. Without IFT56, the flagellar assembly rate is significantly compromised. We also showed that the

ciliogenesis defects caused by the depletion of IFT56 are neither due to the smaller precursor pool for ciliogenesis nor the accelerated axonemal disassembly rate. Tested known regulators are also not affected as well. Further study is needed for figuring out why *ift56-2* has a compromised flagellar assembly rate.

The small GTPase ARL3 has been shown to be involved in ciliogenesis and the flagellar delivery of the lipid-modified cargoes. Here, we showed that without ARL3 *Chlamydomonas* cells present a variety of subtle flagellar defects, especially in adverse conditions. Using the *Chlamydomonas* mating efficiency assay and the comparison of portioned flagella sample, we also showed that the depletion of ARL3 likely altered the composition of flagellar membrane protein. Moreover, we rescued the *arl3* mutant with the wild-type, GTP-dominant, and GDP-dominant forms of ARL3, respectively. Cells rescued with the wild-type ARL3 performed as wild-type cells, while cells rescued with the GTP-dominant form of ARL3 showed worse phenotypes than the *arl3* mutant. Compared to other ciliated organisms, *Chlamydomonas* has a significant advantage – A large amount of isolated and purified flagella can be prepared for the proteomic and other biochemical analyses. This study provides a solid foundation for studying the role of ARL3 in ciliogenesis and lipid-modified protein delivery.

A few intriguing questions arise during the study. One is about how IFT system regulates its cargo loading. It has been shown that the cargo loading can be regulated. Two previously published papers from Dr. Lechtreck's lab showed that the deliveries of two axonemal subunits, tubulin and DRC4, into flagella are tightly controlled. Using the

TIRF microscopy, authors clearly presented that the deliveries of the two subunits are dramatically increased in growing flagella compared to the steady-state flagella [23, 62]. The authors proposed a model in which cells can measure the length of their flagella and then regulate the loading of IFT particles at the ciliary base. Heavily loaded IFT trains bring more cargos and lead to the growth of cilia [23]. However, how the loading of IFT trains can be regulated remains unknown. Based on previous studies, it worth noticing that, in IFT complex, one IFT subunit can play multiple roles while multiple IFT subunits may be responsible for one specific role. A typical example comes from the delivery of the tubulin, which is the main structural unit of the microtubule. It has been shown that two subunits IFT81 and IFT74 cooperate in the tubulin delivery [56, 171]. Moreover, the double mutant with modifications in IFT81 and IFT74 tubulin binding domain is still able to form short flagella, suggesting that there even might be a third tubulin binding subunit. A recently published paper also showed that two IFT subunits IFT46 and IFT56 work together for binding ARL13 [227]. On the other side, the absence of one IFT subunit or binding site, in some cases, can significantly affect but not completely abolish the delivery of the specific cargo. In tubulin delivery, mutants with mutations to either the N-terminus of IFT74 or IFT81 greatly reduced the tubulin delivery. Thus, they have a compromised flagellar assembly rate. However, they are still able to generate full-length or near full-length flagella [56]. Another example comes from the study of IFT56 (also called TTC26 or DYF-13). The absence of IFT56 causes a significant reduction in the specific inner dynein arm delivery instead of a complete stop [53]. In Chapter III, we also showed that the depletion of the IFT57 might not

completely stop the delivery of IC97 (Figure 3-12). Together, it raises a question of why multiple subunits are involved in carrying the same cargo because it seems simpler to have one subunit handles one cargo.

A possible benefit of this many-to-one arrangement is to facilitate the regulation of the cargo loading. When multiple subunits work together in delivering a specific cargo, the binding affinity can be regulated according to the loading requirements. Thus, under challenging conditions in which many cargoes is needed, such as in the growing cilia, all binding-related subunits work together in full capacity to maximum the cargo loading. However, in less challenging situations, such as in the steady-state cilia, some subunits may be inactivated or weakened to reduce the binding affinity to the cargo. Thus, less cargo will be loaded and delivered to the tip of the flagella.

The binding affinity might be adjusted by reversible post-translational modifications. For example, there are different types of kinases and protein phosphatases exist in flagella and around the basal body [22, 228]. Moreover, by now eight IFT subunits were identified as putative phosphoproteins [229-232]. Some have multiple phosphorylation sites (e.g., three high confident phosphosites were identified in IFT46) [230]. Thus, phosphorylation, dephosphorylation, or other reversible modifications may help alter the binding affinity of the IFT trains for specific cargos to control the loading. IFT57 is also one of the identified phosphoproteins. It has one phosphosite [229, 230]. I am curious about the defects might be caused by the mutated IFT57 phosphosite. Unlike many other ciliated organisms, although the flagellar assembly is crucial in *Chlamydomonas*, it is

not essential for the cell survival. Thus, many IFT-related null mutants are available even though they are flagellaless or assemble tiny flagella. Thus, *Chlamydomonas* is a perfect tool to study the modifications in IFT subunits.

A study of the movement of an IFT cargo DRC4 in flagella showed that there are two possible ways for DRC4 to dissociate from the IFT trains. One of them is the DRC4 dissociates from the IFT trains when the trains reach the flagellar tip and start to remodel. In this case, the DRC4 will stop for seconds before it starts to diffuse. The other way is that DRC4 unloads from IFT trains before reaching the flagellar tip. In this case, the DRC4 starts to diffuse immediately after dissociation [62]. The study shows that in the steady-state flagella, a considerable number of DRC4 (around 40%) unload before it reaches the flagellar tip [62]. It is possible that in the steady-state flagella, the DRC4 binds IFT trains with a low affinity. I would like to know, compared to the steady-state flagella, whether in growing cilia there are more DRC4 delivered to flagellar tip.

However, for all these to happen, cells need to "know" the length or the status of their cilia. It has been well known that when one flagellum was amputated from a *Chlamydomonas* cell, the shorter flagellum elongates while the full-length flagellum resorbs until two flagella reach the equal length [21]. Using TIRF microscopy, it had been clearly shown that, in this case, much more tubulin was loaded and delivered to the shorter flagellum [62]. It suggests that cells are aware of the status of their two flagella. Also, it seems like the higher cargo loading cannot be simply explained by a higher

cargo concentration. It has been shown that when cells were treated with a protein synthesis inhibitor cycloheximide and then deflagellated, in which condition cells can only assemble half-length flagella, the cargo delivery kept at a high level even when flagella reach their final length (half-length) under this circumstance. This experiment clearly shows that although the precursor pools in treated cells are consumed and become smaller during flagellar assembly, the cargo delivery rate is not affected [62]. The experiment also showed that the rate examined when treated cell's flagella reach their half-length is comparable to the rate of half-length flagella in untreated cells, indicating that the cargo delivery rate is length-dependent. Although the flagella cannot reach their full-length due to treatment, cells get the message that their flagella are not at the full-length and more cargoes are needed.

Although how cells "know" their flagella status remains unknown, a study about a protein kinase CALK shed light on this process. Its phosphorylation level at T193 correlates with flagellar length [97]. Thus, it can serve as a length indicator. Although by now whether CALK is the key sensor of the length or other key sensors affect it remains unclear [98], it suggests that cells can receive the length-related signals and respond to them. However, the mutant *ift56-2*, which we described in Chapter IV, may have an issue in identifying its flagella status or properly respond to the signals. As we described in Chapter IV, without IFT56, *Chlamydomonas* cells assemble consistent short flagella with a narrow length range. When the flagella are amputated, cells can consistently regenerate flagella as wild type but with a compromised flagellar assembly rate. However, unlike the other IFT mutants with short flagella, the assembly and stability of

the IFT-B are normal. Also, our experimental results supported that the ciliogenesis defects in the *ift56-2* mutant are not due to a limited precursor pool, which differentiate it from some known short flagella mutants like *shf-1*, *shf-2*, and *shf-3* [175]. Our data also showed that the disassembly rate of the flagella is not affected in *ift56-2*. Moreover, the motility of IFT trains, either frequency or speed, is normal as well [53]. Thus, the ciliogenesis defects in *IFT56* mutants are unique. It will be interesting to figure out whether the length indicator CALK still works normally in *ift56-2*. Also, using the described TIRF microscopy technic and related strains [23, 62], we can examine whether cargo can be properly loaded and delivered in *ift56-2* according to the flagellar length, including whether a higher loading can be activated in the growing flagella, whether prematurely down-regulated cargo delivery present as shown in *shf2* mutant, and whether cargo dissociation percentage is similar to the wild-type strains. These data will help us get a better understanding of the IFT system, especially in its regulation.

Another interesting question I want to pursue is that do flagella/cilia need to be over-equipped for handling the changing environment. Cells are constantly exposed to a volatile environment. Either single-cell or multiple-cell organisms, they need to collect the information and respond properly. For example, ciliated cells in the lung, which helps remove mucus, although protected by mucus, they keep exposed to lots of different things, such as inhaled particles, pathogens, irritants, and toxin. Cells have to find a way to maintain their normal functions even in unfavorable conditions.

Cilia, an organelle which protrudes from the cell surface, has a better chance to interact with the outside environment. Indeed, many sensing and signaling proteins are enriched in the cilia. Thus, the cilium serves as a sensing and signaling center. If the cilia are messed up, the cells may lose the communications with the outside environment. Thus, they may be still ok in a stable environment but cannot respond well when the environment changes dramatically.

This question draws my attention due to the *arl3* project, which I described in Chapter V. I had a hard time in the beginning when I tried to characterize the *arl3* mutant because the severity of the *arl3* mutant defects varies from different preparations. It may be caused by slight differences in culture conditions because the repeats from the same batch present consistent phenotypes. In addition, when I carefully repeat all the parameters, such as media, temperature, the amount of the inoculums, and incubation times, I got a more consistent result. In contrast, the phenotypes of the wild-type *cc125* are always consistent. It suggests that wild type cells may be able to adapt well to different environments while the mutant *arl3* cannot.

The ARL3 is involved in ciliogenesis. However, its exact role remains unclear due to the contradictory results presented in different studies. In some cases, no morphological changes in cilia can be detected in *arl3* knockout mutant [215]. However, the absence of ARL3 causes significant ciliogenesis defects in other cases [199]. By now no conclusive explanation has been made. Our data showed that the *arl3* mutant assembles normal length flagella in standard conditions but displays flagellar ciliogenesis defects in

adverse conditions (Figure 5-2 and 5-4), which may help explain the contradictory results. If the cilia are in a position need to adapt to the changing environment and make quick responses, it may show more severe phenotypes. However, if the cilia are in a less challenging position, especially in well-controlled experimental conditions, the cilia may be normal even without ARL3.

We have already discussed in Chapter V that since the ARL3 may be responsible for the delivery of some sensing and signaling -related proteins, the depletion of ARL3 may compromise the sensing and signaling function of cilia. An interesting study from Tilley lab showed that in airway epithelium, cilia were significantly shorter in healthy smokers than nonsmokers. It indicates that environment can affect cilia length and function, and keep normal length functional cilia under unfavorable conditions is a challenge for the cell. Also, they found that in chronic obstructive pulmonary disease (COPD) smokers the cilia are even shorter than healthy smokers [233]. Although whether the cilia sensitivity causes COPD or COPD leads to cilia sensitivity has not been studied yet, it suggests that under some circumstance some cilia can be more sensitive than the normal ones. Thus, the defects in ciliogenesis might be one of the expressions of the decreased ability for adapting to the challenging environment.

Also, when I cultured the *ift56* mutants, *ift56-2* (an insertional mutant generated in the lab) and *ift56-1* (a mutant with point mutations, generated by UV-mutagenesis[53]), I noticed that their motility are varies in different preparations while the wild-type strain *cc125* always swim well (Video 4-3, Video 4-4, Video 4-5, Video 4-6). The similar

phenotype has been documented in a *pf25* mutant lacking an AKAP-binding protein [234]. Biochemical analysis showed that IFT56 is involved in the delivery of a specific set of inner dynein arm [53]. Based on the inconsistent motility performance of the *ift56* mutants, I propose that the binding affinity of the motility-related cargo is weakened in adverse conditions.

In both cases, the *arl3* mutant and the *ift56* mutants, flagella perform fine in some conditions but present obvious defects in some other conditions. It suggests that in an ideal steady condition, many ciliary proteins may be not required for normal ciliary function, but they may play crucial roles in adapting or tolerance in adverse conditions.

REFERENCES

[1] Emmer, B.T., D. Maric, and D.M. Engman, Molecular mechanisms of protein and lipid targeting to ciliary membranes. J Cell Sci, 2010. **123**(Pt 4): p. 529-536.

[2] Rohatgi, R. and W.J. Snell, The ciliary membrane. Curr Opin Cell Biol, 2010. **22**(4): p. 541-546.

[3] Tyler, K.M., et al., Flagellar membrane localization via association with lipid rafts. J Cell Sci, 2009. **122**(Pt 6): p. 859-866.

[4] Nonaka, S., et al., Randomization of left-right asymmetry due to loss of nodal cilia generating leftward flow of extraembryonic fluid in mice lacking KIF3B motor protein (vol 95, pg 829, 95). Cell, 1999. **99**(1).

[5] Satir, P. and S.T. Christensen, Overview of structure and function of mammalian cilia. Annual Review of Physiology, 2007. **69**: p. 377-400.

[6] Banizs, B., et al., Dysfunctional cilia lead to altered ependyma and choroid plexus function, and result in the formation of hydrocephalus. Development, 2005. **132**(23): p. 5329-5339.

[7] Appelbe, O.K., et al., Disruption of the mouse Jhy gene causes abnormal ciliary microtubule patterning and juvenile hydrocephalus. Dev Biol, 2013. **382**(1): p. 172-185.

[8] Pazour, G.J., et al., Polycystin-2 localizes to kidney cilia and the ciliary level is elevated in Tg737(orpk) mice with polycystic kidney disease. Molecular Biology of the Cell, 2002. **13**: p. 326A-327A.

[9] Wheway, G., D.A. Parry, and C.A. Johnson, The role of primary cilia in the development and disease of the retina. Organogenesis, 2014. **10**(1): p. 69-85.

[10] Jenkins, P.M., D.P. McEwen, and J.R. Martens, Olfactory Cilia: Linking Sensory Cilia Function and Human Disease. Chemical Senses, 2009. **34**(5): p. 451-464.

[11] Tasouri, E. and K.L. Tucker, Primary cilia and organogenesis: is Hedgehog the only sculptor? Cell and Tissue Research, 2011. **345**(1): p. 21-40.

[12] Fliegauf, M., T. Benzing, and H. Omran, When cilia go bad: cilia defects and ciliopathies (vol 8, pg 880, 2007). Nature Reviews Molecular Cell Biology, 2008. **9**(1): p. 88-88.

[13] Brown, J.M. and G.B. Witman, Cilia and Diseases. Bioscience, 2014. **64**(12): p. 1126-1137.

[14] van Dam, T.J., et al., Evolution of modular intraflagellar transport from a coatomer-like progenitor. Proc Natl Acad Sci U S A, 2013. **110**(17): p. 6943-6948.

[15] Kozminski, K.G., et al., A motility in the eukaryotic flagellum unrelated to flagellar beating. Proc Natl Acad Sci U S A, 1993. **90**(12): p. 5519-5523.

[16] Kozminski, K.G., P.L. Beech, and J.L. Rosenbaum, The *Chlamydomonas* kinesin-like protein FLA10 is involved in motility associated with the flagellar membrane. J Cell Biol, 1995. **131**(6 Pt 1): p. 1517-1527.

[17] Pazour, G.J., C.G. Wilkerson, and G.B. Witman, A dynein light chain is essential for the retrograde particle movement of intraflagellar transport (IFT). Journal of Cell Biology, 1998. **141**(4): p. 979-992.

[18] Cole, D.G., et al., *Chlamydomonas* kinesin-II-dependent intraflagellar transport (IFT): IFT particles contain proteins required for ciliary assembly in *Caenorhabditis elegans* sensory neurons. J Cell Biol, 1998. **141**(4): p. 993-1008.

[19] Piperno, G. and K. Mead, Transport of a novel complex in the cytoplasmic matrix of *Chlamydomonas* flagella. Proceedings of the National Academy of Sciences of the United States of America, 1997. **94**(9): p. 4457-4462.

[20] Hou, Y., et al., Functional analysis of an individual IFT protein: IFT46 is required for transport of outer dynein arms into flagella. J Cell Biol, 2007. **176**(5): p. 653-65.

[21] Rosenbaum, J.L., J.E. Moulder, and D.L. Ringo, Flagellar elongation and shortening in *Chlamydomonas*. The use of cycloheximide and colchicine to study the synthesis and assembly of flagellar proteins. J Cell Biol, 1969. **41**(2): p. 600-619.

[22] Pazour, G.J., et al., Proteomic analysis of a eukaryotic cilium. J Cell Biol, 2005. **170**(1): p. 103-113.

[23] Craft, J.M., et al., Tubulin transport by IFT is upregulated during ciliary growth by a cilium-autonomous mechanism. J Cell Biol, 2015. **208**(2): p. 223-237.

[24] Stephens, R.E., Differential protein synthesis and utilization during cilia formation in sea urchin embryos. Dev Biol, 1977. **61**(2): p. 311-329.

[25] Guttman, S.D. and M.A. Gorovsky, Cilia regeneration in starved tetrahymena: an inducible system for studying gene expression and organelle biogenesis. Cell, 1979. **17**(2): p. 307-317.

[26] Lefebvre, P.A., et al., Increased levels of mRNAs for tubulin and other flagellar proteins after amputation or shortening of *Chlamydomonas* flagella. Cell, 1980. **20**(2): p. 469-477.

[27] Lefebvre, P.A., et al., Flagellar elongation and shortening in *Chlamydomonas*. IV. Effects of flagellar detachment, regeneration, and resorption on the induction of flagellar protein synthesis. J Cell Biol, 1978. **78**(1): p. 8-27.

[28] Nachury, M.V., E.S. Seeley, and H. Jin, Trafficking to the ciliary membrane: how to get across the periciliary diffusion barrier? Annu Rev Cell Dev Biol, 2010. **26**: p. 59-87.

[29] Kee, H.L., et al., A size-exclusion permeability barrier and nucleoporins characterize a ciliary pore complex that regulates transport into cilia. Nature Cell Biology, 2012. **14**(4): p. 431-438.

[30] Breslow, D.K., et al., An in vitro assay for entry into cilia reveals unique properties of the soluble diffusion barrier. Journal of Cell Biology, 2013. **203**(1): p. 129-147.

[31] Lin, Y.C., et al., Chemically inducible diffusion trap at cilia reveals molecular sieve-like barrier. Nature Chemical Biology, 2013. **9**(7): p. 437-443.

[32] Hu, Q.C., et al., A Septin Diffusion Barrier at the Base of the Primary Cilium Maintains Ciliary Membrane Protein Distribution. Science, 2010. **329**(5990): p. 436-439.

[33] Chih, B., et al., A ciliopathy complex at the transition zone protects the cilia as a privileged membrane domain. Nature Cell Biology, 2012. **14**(1): p. 61-74.

[34] Rosenbaum, J.L. and F.M. Child, Flagellar regeneration in protozoan flagellates. J Cell Biol, 1967. **34**(1): p. 345-364.

[35] Johnson, K.A. and J.L. Rosenbaum, Polarity of flagellar assembly in *Chlamydomonas*. J Cell Biol, 1992. **119**(6): p. 1605-1611.

[36] Ishikawa, H. and W.F. Marshall, Ciliogenesis: building the cell's antenna. Nat Rev Mol Cell Biol, 2011. **12**(4): p. 222-234.

[37] Ou, G., et al., Functional coordination of intraflagellar transport motors. Nature, 2005. **436**(7050): p. 583-587.

[38] Mijalkovic, J., B. Prevo, and E.J. Peterman, Why motor proteins team up - Intraflagellar transport in *C. elegans* cilia. Worm, 2016. **5**(2): p. e1170275.

[39] Stepanek, L. and G. Pigino, Microtubule doublets are double-track railways for intraflagellar transport trains. Science, 2016. **352**(6286): p. 721-724.

[40] Haycraft, C.J., et al., Gli2 and Gli3 localize to cilia and require the intraflagellar transport protein polaris for processing and function. PLoS Genet, 2005. **1**(4): p. e53.

[41] May, S.R., et al., Loss of the retrograde motor for IFT disrupts localization of Smo to cilia and prevents the expression of both activator and repressor functions of Gli. Dev Biol, 2005. **287**(2): p. 378-389.

[42] Qin, H., et al., Intraflagellar transport is required for the vectorial movement of TRPV channels in the ciliary membrane. Curr Biol, 2005. **15**(18): p. 1695-1699.

[43] Qin, H.M., et al., Intraflagellar transport (IFT) cargo: IFT transports flagellar precursors to the tip and turnover products to the cell body. Journal of Cell Biology, 2004. **164**(2): p. 255-266.

[44] Lechtreck, K.F., IFT-Cargo Interactions and Protein Transport in Cilia. Trends Biochem Sci, 2015. **40**(12): p. 765-778.

[45] Taschner, M., S. Bhogaraju, and E. Lorentzen, Architecture and function of IFT complex proteins in ciliogenesis. Differentiation, 2012. **83**(2): p. S12-22.

[46] Piperno, G., et al., Distinct mutants of retrograde intraflagellar transport (IFT) share similar morphological and molecular defects. J Cell Biol, 1998. **143**(6): p. 1591-601.

[47] Cole, D.G., et al., *Chlamydomonas* kinesin-II-dependent intraflagellar transport (IFT): IFT particles contain proteins required for ciliary assembly in *Caenorhabditis elegans* sensory neurons. Journal of Cell Biology, 1998. **141**(4): p. 993-1008.

[48] Behal, R.H., et al., Subunit Interactions and Organization of the *Chlamydomonas reinhardtii* Intraflagellar Transport Complex A Proteins. Journal of Biological Chemistry, 2012. **287**(15): p. 11689-11703.

[49] Lucker, B.F., et al., Characterization of the intraflagellar transport complex B core - Direct interaction of the IFT81 AND IFT74/72 subunits. Journal of Biological Chemistry, 2005. **280**(30): p. 27688-27696.

[50] Taschner, M., et al., Biochemical mapping of interactions within the intraflagellar transport (IFT) B core complex: IFT52 binds directly to four other IFT-B subunits. J Biol Chem, 2011. **286**(30): p. 26344-26352.

[51] Taschner, M., et al., Crystal structures of IFT70/52 and IFT52/46 provide insight into intraflagellar transport B core complex assembly. J Cell Biol, 2014. **207**(2): p. 269-282.

[52] Richey, E.A. and H. Qin, Dissecting the sequential assembly and localization of intraflagellar transport particle complex B in *Chlamydomonas*. PLoS One, 2012. **7**(8): p. e43118.

[53] Ishikawa, H., et al., TTC26/DYF13 is an intraflagellar transport protein required for transport of motility-related proteins into flagella. Elife, 2014. **3**: p. e01566.

[54] Katoh, Y., et al., Overall architecture of the intraflagellar transport (IFT)-B complex containing Cluap1/IFT38 as an essential component of the IFT-B peripheral subcomplex. J Biol Chem, 2016. **291**: p. 10962-10975.

[55] Taschner, M., et al., Intraflagellar transport proteins 172, 80, 57, 54, 38, and 20 form a stable tubulin-binding IFT-B2 complex. EMBO J, 2016. **35**(7): p. 773-790.

[56] Kubo, T., et al., Together, the IFT81 and IFT74 N-termini form the main module for intraflagellar transport of tubulin. J Cell Sci, 2016. **129**(10): p. 2106-2119.

[57] Iomini, C., et al., Retrograde Intraflagellar Transport Mutants Identify Complex A Proteins With Multiple Genetic Interactions in *Chlamydomonas reinhardtii*. Genetics, 2009. **183**(3): p. 885-896.

[58] Tran, P.V., et al., THM1 negatively modulates mouse sonic hedgehog signal transduction and affects retrograde intraflagellar transport in cilia. Nature Genetics, 2008. **40**(4): p. 403-410.

[59] Mukhopadhyay, S., et al., TULP3 bridges the IFT-A complex and membrane phosphoinositides to promote trafficking of G protein-coupled receptors into primary cilia. Genes & Development, 2010. **24**(19): p. 2180-2193.

[60] Liew, G.M., et al., The Intraflagellar Transport Protein IFT27 Promotes BBSome Exit from Cilia through the GTPase ARL6/BBS3. Developmental Cell, 2014. **31**(3): p. 265-278.

[61] Eguether, T.P., et al., IFT27 Links the BBSome to IFT for Maintenance of Ciliary Signaling Compartment. Molecular Biology of the Cell, 2014. **25**.

[62] Wren, K.N., et al., A differential cargo-loading model of ciliary length regulation by IFT. Curr Biol, 2013. **23**(24): p. 2463-2471.

[63] Bhogaraju, S., B.D. Engel, and E. Lorentzen, Intraflagellar transport complex structure and cargo interactions. Cilia, 2013. **2**(1): p. 10.

[64] Brown, J.M., et al., Assembly of IFT trains at the ciliary base depends on IFT74. Curr Biol, 2015. **25**(12): p. 1583-1593.

[65] Ahmed, N.T., et al., ODA16 aids axonemal outer row dynein assembly through an interaction with the intraflagellar transport machinery. J Cell Biol, 2008. **183**(2): p. 313-322.

[66] Bhogaraju, S., et al., Molecular basis of tubulin transport within the cilium by IFT74 and IFT81. Science, 2013. **341**(6149): p. 1009-1012.

[67] Eguether, T., et al., IFT27 links the BBSome to IFT for maintenance of the ciliary signaling compartment. Dev Cell, 2014. **31**(3): p. 279-290.

[68] Pathak, N., et al., The zebrafish fleer gene encodes an essential regulator of cilia tubulin polyglutamylation. Mol Biol Cell, 2007. **18**(11): p. 4353-4364.

[69] Dave, D., et al., DYF-1 Is required for assembly of the axoneme in Tetrahymena thermophila. Eukaryot Cell, 2009. **8**(9): p. 1397-1406.

[70] Tsao, C.C. and M.A. Gorovsky, Different effects of Tetrahymena IFT172 domains on anterograde and retrograde intraflagellar transport. Mol Biol Cell, 2008. **19**(4): p. 1450-1461.

[71] Pedersen, L.B., et al., *Chlamydomonas* IFT172 is encoded by FLA11, interacts with CrEB1, and regulates IFT at the flagellar tip. Current Biology, 2005. **15**(3): p. 262-266.

[72] Pedersen, L.B., et al., The *Chlamydomonas* intraflagellar transport protein IFT172 is encoded by FLA11 and interacts with the microtubule plus end-tracking protein EB1. Molecular Biology of the Cell, 2004. **15**: p. 359A-360A.

[73] Pedersen, L.B., et al., The microtubule plus end-tracking protein EB1 is localized to the flagellar tip and basal bodies in *Chlamydomonas reinhardtii*. Current Biology, 2003. **13**(22): p. 1969-1974.

[74] Zhu, B., et al., Functional exploration of the IFT-A complex in intraflagellar transport and ciliogenesis. PLoS Genet, 2017. **13**(2): p. e1006627.

[75] Chemes, H.E., J.L. Morero, and J.C. Lavieri, Extreme asthenozoospermia and chronic respiratory disease: a new variant of the immotile cilia syndrome. Int J Androl, 1990. **13**(3): p. 216-222.

[76] Basten, S.G. and R.H. Giles, Functional aspects of primary cilia in signaling, cell cycle and tumorigenesis. Cilia, 2013. **2**(1): p. 6.

[77] Marley A, v.Z.M., A simple cell-based assay reveals that diverse neuropsychiatric risk genes converge on primary cilia. Plos One, 2012. **7**(10).

[78] Niggemann, B., et al., Abnormal length of cilia--a cause of primary ciliary dyskinesia--a case report. Eur J Pediatr, 1992. **151**(1): p. 73-75.

[79] Smith, L.A., et al., Development of polycystic kidney disease in juvenile cystic kidney mice: insights into pathogenesis, ciliary abnormalities, and common features with human disease. J Am Soc Nephrol, 2006. **17**(10): p. 2821-2831.

[80] Verghese, E., et al., Renal cilia display length alterations following tubular injury and are present early in epithelial repair. Nephrol Dial Transplant, 2008. **23**(3): p. 834-841.

[81] Mokrzan, E.M., J.S. Lewis, and K. Mykytyn, Differences in renal tubule primary cilia length in a mouse model of Bardet-Biedl syndrome. Nephron Exp Nephrol, 2007. **106**(3): p. e88-96.

[82] Tuxhorn, J., T. Daise, and W.L. Dentler, Regulation of flagellar length in *Chlamydomonas*. Cell Motil Cytoskeleton, 1998. **40**(2): p. 133-146.

[83] McVittie, A., Flagellum mutants of *Chlamydomonas reinhardii*. J Gen Microbiol, 1972. **71**(3): p. 525-540.

[84] Barsel, S.E., D.E. Wexler, and P.A. Lefebvre, Genetic analysis of long-flagella mutants of *Chlamydomonas reinhardtii*. Genetics, 1988. **118**(4): p. 637-648.

[85] Asleson, C.M. and P.A. Lefebvre, Genetic analysis of flagellar length control in *Chlamydomonas reinhardtii*: a new long-flagella locus and extragenic suppressor mutations. Genetics, 1998. **148**(2): p. 693-702.

[86] Tam, L.W., N.F. Wilson, and P.A. Lefebvre, A CDK-related kinase regulates the length and assembly of flagella in *Chlamydomonas*. J Cell Biol, 2007. **176**(6): p. 819-829.

[87] Berman, S.A., et al., A novel MAP kinase regulates flagellar length in *Chlamydomonas*. Curr Biol, 2003. **13**(13): p. 1145-9.

[88] Tam, L.W., P.T. Ranum, and P.A. Lefebvre, CDKL5 regulates flagellar length and localizes to the base of the flagella in *Chlamydomonas*. Mol Biol Cell, 2013. **24**(5): p. 588-600.

[89] Sharma, N., et al., Soluble levels of cytosolic tubulin regulate ciliary length control. Mol Biol Cell, 2011. **22**(6): p. 806-816.

[90] Engel, B.D., W.B. Ludington, and W.F. Marshall, Intraflagellar transport particle size scales inversely with flagellar length: revisiting the balance-point length control model. J Cell Biol, 2009. **187**(1): p. 81-89.

[91] Kozminski, K.G., P.L. Beech, and J.L. Rosenbaum, The *Chlamydomonas* Kinesin-Like Protein Fla10 Is Involved in Motility Associated with the Flagellar Membrane. Journal of Cell Biology, 1995. **131**(6): p. 1517-1527.

[92] Ludington, W.B., et al., Avalanche-like behavior in ciliary import. Proc Natl Acad Sci U S A, 2013. **110**(10): p. 3925-3930.

[93] Hilton, L.K., et al., The kinases LF4 and CNK2 control ciliary length by feedback regulation of assembly and disassembly rates. Curr Biol, 2013. **23**(22): p. 2208-2214.

[94] Pan, J. and W.J. Snell, *Chlamydomonas* shortens its flagella by activating axonemal disassembly, stimulating IFT particle trafficking, and blocking anterograde cargo loading. Dev Cell, 2005. **9**(3): p. 431-438.

[95] Avasthi, P. and W.F. Marshall, Ciliary regulation: disassembly takes the spotlight. Curr Biol, 2013. **23**(22): p. R1001-3.

[96] Luo, M., et al., The phosphorylation state of an aurora-like kinase marks the length of growing flagella in *Chlamydomonas*. Curr Biol, 2011. **21**(7): p. 586-591.

[97] Cao, M., et al., Activation loop phosphorylation of a protein kinase is a molecular marker of organelle size that dynamically reports flagellar length. Proc Natl Acad Sci U S A, 2013. **110**(30): p. 12337-12342.

[98] Pan, J. and W.J. Snell, Organelle Size: A Cilium Length Signal Regulates IFT Cargo Loading. Curr Biol, 2014. **24**(2): p. R75-78.

[99] Pazour, G.J., et al., *Chlamydomonas* IFT88 and its mouse homologue, polycystic kidney disease gene tg737, are required for assembly of cilia and flagella. J Cell Biol, 2000. **151**(3): p. 709-718.

[100] Aldahmesh, M.A., et al., IFT27, encoding a small GTPase component of IFT particles, is mutated in a consanguineous family with Bardet-Biedl syndrome. Hum Mol Genet, 2014. **23**(12): p. 3307-3315.

[101] Huynh Cong, E., et al., A homozygous missense mutation in the ciliary gene TTC21B causes familial FSGS. J Am Soc Nephrol, 2014. **25**(11): p. 2435-2443.

[102] Gervais, F.G., et al., Recruitment and activation of caspase-8 by the Huntingtin-interacting protein Hip-1 and a novel partners Hippi. Nature Cell Biology, 2002. **4**(2): p. 95-105.

[103] Richey, E.A., H. Qin, and Texas A & M University, *Probing the Roles that Intraflagellar Transport B Protiens Play on Stability, Assembly, and Localization of Complex B in Chlamydomonas ReinhardtII*. 1 online resource.

[104] Thevenon, J., et al., Autosomal Recessive IFT57 hypomorphic mutation cause ciliary transport defect in unclassified oral-facial-digital syndrome with short stature and brachymesophalangia. Clin Genet, 2016. **90**(6): p. 509-517.

[105] Sakamoto, K., et al., Homer1c interacts with Hippi and protects striatal neurons from apoptosis. Biochemical and Biophysical Research Communications, 2007. **352**(1): p. 1-5.

[106] Majumder, P., et al., Interactions of HIPPI, a molecular partner of Huntingtin interacting protein HIP1, with the specific motif present at the putative promoter sequence of the caspase-1, caspase-8 and caspase-10 genes. Febs Journal, 2007. **274**(15): p. 3886-3899.

[107] Starich, T.A., et al., Mutations affecting the chemosensory neurons of *Caenorhabditis elegans*. Genetics, 1995. **139**(1): p. 171-188.

[108] Blacque, O.E., S. Cevik, and O.I. Kaplan, Intraflagellar transport: from molecular characterisation to mechanism. Front Biosci, 2008. **13**: p. 2633-2652.

[109] Franklin, J.B. and E. Ullu, Biochemical analysis of PIFTC3, the Trypanosoma brucei orthologue of nematode DYF-13, reveals interactions with established and putative intraflagellar transport components. Mol Microbiol, 2010. **78**(1): p. 173-186.

[110] Follit, J.A., et al., Characterization of mouse IFT complex B. Cell Motil Cytoskeleton, 2009. **66**(8): p. 457-468.

[111] Perrault, I., et al., IFT81, encoding an IFT-B core protein, as a very rare cause of a ciliopathy phenotype. Journal of Medical Genetics, 2015. **52**(10): p. 657-665.

[112] Gonzalez-Ballester, D., et al., Restriction enzyme site-directed amplification PCR: A tool to identify regions flanking a marker DNA. Analytical Biochemistry, 2005. **340**(2): p. 330-335.

[113] Walsh, P.S., D.A. Metzger, and R. Higuchi, Chelex-100 as a Medium for Simple Extraction of DNA for Pcr-Based Typing from Forensic Material. Biotechniques, 1991. **10**(4): p. 506-513.

[114] Dutcher, S.K., et al., Whole-Genome Sequencing to Identify Mutants and Polymorphisms in *Chlamydomonas reinhardtii*. G3 (Bethesda), 2012. **2**(1): p. 15-22.

[115] Lin, H., et al., Whole genome sequencing identifies a deletion in protein phosphatase 2A that affects its stability and localization in *Chlamydomonas reinhardtii*. PLoS Genet, 2013. **9**(9): p. e1003841.

[116] Tulin, F. and F.R. Cross, A microbial avenue to cell cycle control in the plant superkingdom. Plant Cell, 2014. **26**(10): p. 4019-4038.

[117] Jinkerson, R.E. and M.C. Jonikas, Molecular techniques to interrogate and edit the *Chlamydomonas* nuclear genome. Plant J, 2015. **82**(3): p. 393-412.

[118] Cong, L., et al., Multiplex Genome Engineering Using CRISPR/Cas Systems. Science, 2013. **339**(6121): p. 819-823.

[119] Horvath, P. and R. Barrangou, CRISPR/Cas, the immune system of bacteria and archaea. Science, 2010. **327**(5962): p. 167-170.

[120] Jiang, W.Z., et al., Successful Transient Expression of Cas9 and Single Guide RNA Genes in *Chlamydomonas reinhardtii*. Eukaryotic Cell, 2014. **13**(11): p. 1465-1469.

[121] Shin, S.E., et al., CRISPR/Cas9-induced knockout and knock-in mutations in *Chlamydomonas reinhardtii*. Scientific Reports, 2016. **6**: p. 27810.

[122] Pigino, G., et al., Electron-tomographic analysis of intraflagellar transport particle trains in situ. J Cell Biol, 2009. **187**(1): p. 135-148.

[123] Badano, J.L., et al., The ciliopathies: an emerging class of human genetic disorders. Annu Rev Genomics Hum Genet, 2006. **7**: p. 125-148.

[124] Behal, R.H., et al., Subunit interactions and organization of the *Chlamydomonas reinhardtii* intraflagellar transport complex A proteins. J Biol Chem, 2012. **287**(15): p. 11689-11703.

[125] Katoh, Y., et al., Overall Architecture of the Intraflagellar Transport (IFT)-B Complex Containing Cluap1/IFT38 as an Essential Component of the IFT-B Peripheral Subcomplex. J Biol Chem, 2016. **291**(21): p. 10962-10975.

[126] Lucker, B.F., et al., Characterization of the intraflagellar transport complex B core: direct interaction of the IFT81 and IFT74/72 subunits. J Biol Chem, 2005. **280**(30): p. 27688-27696.

[127] Baker, S.A., et al., IFT20 links kinesin II with a mammalian intraflagellar transport complex that is conserved in motile flagella and sensory cilia. J Biol Chem, 2003. **278**(36): p. 34211-8.

[128] Pazour, G.J., B.L. Dickert, and G.B. Witman, The DHC1b (DHC2) isoform of cytoplasmic dynein is required for flagellar assembly. J Cell Biol, 1999. **144**(3): p. 473-481.

[129] Pazour, G.J., C.G. Wilkerson, and G.B. Witman, A dynein light chain is essential for the retrograde particle movement of intraflagellar transport (IFT). J Cell Biol, 1998. **141**(4): p. 979-992.

[130] Porter, M.E., et al., Cytoplasmic dynein heavy chain 1b is required for flagellar assembly in *Chlamydomonas*. Mol Biol Cell, 1999. **10**(3): p. 693-712.

[131] Rosenbaum, J.L. and G.B. Witman, Intraflagellar transport. Nat Rev Mol Cell Biol, 2002. **3**(11): p. 813-825.

[132] Gao, C., et al., Oda16/Wdr69 is essential for axonemal dynein assembly and ciliary motility during zebrafish embryogenesis. Dev Dyn, 2010. **239**(8): p. 2190-2197.

[133] Haycraft, C.J., et al., Identification of CHE-13, a novel intraflagellar transport protein required for cilia formation. Exp Cell Res, 2003. **284**(2): p. 251-263.

[134] Perkins, L.A., et al., Mutant sensory cilia in the nematode *Caenorhabditis elegans*. Dev Biol, 1986. **117**(2): p. 456-487.

[135] Cao, Y., A. Park, and Z. Sun, Intraflagellar transport proteins are essential for cilia formation and for planar cell polarity. J Am Soc Nephrol, 2010. **21**(8): p. 1326-1333.

[136] Houde, C., et al., Hippi is essential for node cilia assembly and Sonic hedgehog signaling. Dev Biol, 2006. **300**(2): p. 523-533.

[137] Yanagisawa, H.A., et al., FAP20 is an inner junction protein of doublet microtubules essential for both the planar asymmetrical waveform and stability of flagella in *Chlamydomonas*. Mol Biol Cell, 2014. **25**(9): p. 1472-1483.

[138] Wood, C.R., et al., IFT proteins accumulate during cell division and localize to the cleavage furrow in *Chlamydomonas*. PLoS One, 2012. **7**(2): p. e30729.

[139] Kubo, T., et al., The *Chlamydomonas* hatching enzyme, sporangin, is expressed in specific phases of the cell cycle and is localized to the flagella of daughter cells within the sporangial cell wall. Plant Cell Physiol, 2009. **50**(3): p. 572-583.

[140] Deane, J.A., et al., Localization of intraflagellar transport protein IFT52 identifies basal body transitional fibers as the docking site for IFT particles. Curr Biol, 2001. **11**(20): p. 1586-1590.

[141] Walther, Z., M. Vashishtha, and J.L. Hall, The *Chlamydomonas* FLA10 gene encodes a novel kinesin-homologous protein. J Cell Biol, 1994. **126**(1): p. 175-188.

[142] Engel, B.D., et al., Total internal reflection fluorescence (TIRF) microscopy of *Chlamydomonas* flagella. Methods Cell Biol, 2009. **93**: p. 157-177.

[143] Lechtreck, K.F., et al., The *Chlamydomonas reinhardtii* BBSome is an IFT cargo required for export of specific signaling proteins from flagella. J Cell Biol, 2009. **187**(7): p. 1117-1132.

[144] Bower, R., et al., IC138 defines a subdomain at the base of the I1 dynein that regulates microtubule sliding and flagellar motility. Mol Biol Cell, 2009. **20**(13): p. 3055-3063.

[145] Perrone, C.A., et al., The *Chlamydomonas* IDA7 locus encodes a 140-kDa dynein intermediate chain required to assemble the I1 inner arm complex. Mol Biol Cell, 1998. **9**(12): p. 3351-3365.

[146] Yang, P. and W.S. Sale, The Mr 140,000 intermediate chain of *Chlamydomonas* flagellar inner arm dynein is a WD-repeat protein implicated in dynein arm anchoring. Mol Biol Cell, 1998. **9**(12): p. 3335-3349.

[147] King, S.M., Integrated control of axonemal dynein AAA(+) motors. J Struct Biol, 2012. **179**(2): p. 222-228.

[148] Yang, P., et al., Radial spoke proteins of *Chlamydomonas* flagella. J Cell Sci, 2006. **119**(Pt 6): p. 1165-1174.

[149] Tam, L.W. and P.A. Lefebvre, The *Chlamydomonas* MBO2 locus encodes a conserved coiled-coil protein important for flagellar waveform conversion. Cell Motil Cytoskeleton, 2002. **51**(4): p. 197-212.

[150] Wirschell, M., et al., IC97 is a novel intermediate chain of I1 dynein that interacts with tubulin and regulates interdoublet sliding. Mol Biol Cell, 2009. **20**(13): p. 3044-3054.

[151] Krock, B.L. and B.D. Perkins, The intraflagellar transport protein IFT57 is required for cilia maintenance and regulates IFT-particle-kinesin-II dissociation in vertebrate photoreceptors. J Cell Sci, 2008. **121**(11): p. 1907-1915.

[152] Mukhopadhyay, S., et al., TULP3 bridges the IFT-A complex and membrane phosphoinositides to promote trafficking of G protein-coupled receptors into primary cilia. Genes Dev, 2010. **24**(19): p. 2180-2193.

[153] Viswanadha, R., et al., The ciliary inner dynein arm, I1 dynein, is assembled in the cytoplasm and transported by IFT before axonemal docking. Cytoskeleton (Hoboken), 2014. **71**(10): p. 573-586.

[154] Pollock, S.V., et al., The *Chlamydomonas reinhardtii* proteins Ccp1 and Ccp2 are required for long-term growth, but are not necessary for efficient photosynthesis, in a low-CO2 environment. Plant Mol Biol, 2004. **56**(1): p. 125-132.

[155] Fan, Z.C., et al., *Chlamydomonas* IFT70/CrDYF-1 is a core component of IFT particle complex B and is required for flagellar assembly. Mol Biol Cell, 2010. **21**(15): p. 2696-2706.

[156] Qin, H., et al., Intraflagellar transport (IFT) cargo: IFT transports flagellar precursors to the tip and turnover products to the cell body. J Cell Biol, 2004. **164**(2): p. 255-266.

[157] Diener, D.R., L.H. Ang, and J.L. Rosenbaum, Assembly of flagellar radial spoke proteins in *Chlamydomonas*: identification of the axoneme binding domain of radial spoke protein 3. J Cell Biol, 1993. **123**(1): p. 183-190.

[158] Hendrickson, T.W., et al., IC138 is a WD-repeat dynein intermediate chain required for light chain assembly and regulation of flagellar bending. Mol Biol Cell, 2004. **15**(12): p. 5431-5442.

[159] Benashski, S.E., R.S. Patel-King, and S.M. King, Light chain 1 from the *Chlamydomonas* outer dynein arm is a leucine-rich repeat protein associated with the motor domain of the gamma heavy chain. Biochemistry, 1999. **38**(22): p. 7253-7264.

[160] Silva, D.A., et al., The RABL5 homolog IFT22 regulates the cellular pool size and the amount of IFT particles partitioned to the flagellar compartment in *Chlamydomonas reinhardtii*. Cytoskeleton (Hoboken), 2012. **69**(1): p. 33-48.

[161] DiPetrillo, C.G. and E.F. Smith, The Pcdp1 complex coordinates the activity of dynein isoforms to produce wild-type ciliary motility. Mol Biol Cell, 2011. **22**(23): p. 4527-4538.

[162] Sager, R. and S. Granick, Nutritional studies with *Chlamydomonas reinhardtii*. Annals of the New York Academy of Science, 1953. **56**(5): p. 831-838.

[163] Mueller, J., et al., The FLA3 KAP subunit is required for localization of kinesin-2 to the site of flagellar assembly and processive anterograde intraflagellar transport. Mol Biol Cell, 2005. **16**(3): p. 1341-1354.

[164] Kuchka, M.R. and J.W. Jarvik, Short-Flagella Mutants of *Chlamydomonas reinhardtii*. Genetics, 1987. **115**(4): p. 685-691.

[165] Khona, D.K., et al., Anomalies in the motion dynamics of long-flagella mutants of *Chlamydomonas reinhardtii*. Journal of Biological Physics, 2013. **39**(1): p. 1-14.

[166] Chemes, H.E., J.L. Morero, and J.C. Lavieri, Extreme Asthenozoospermia and Chronic Respiratory-Disease - a New Variant of the Immotile Cilia Syndrome. International Journal of Andrology, 1990. **13**(3): p. 216-222.

[167] Keady, B.T., et al., IFT25 links the signal-dependent movement of Hedgehog components to intraflagellar transport. Dev Cell, 2012. **22**(5): p. 940-951.

[168] Schafer, J.C., et al., IFTA-2 is a conserved cilia protein involved in pathways regulating longevity and dauer formation in *Caenorhabditis elegans*. J Cell Sci, 2006. **119**(Pt 19): p. 4088-4100.

[169] Yang, N., et al., Intraflagellar transport 27 is essential for hedgehog signaling but dispensable for ciliogenesis during hair follicle morphogenesis (vol 142, pg 2194, 2015). Development, 2015. **142**(16): p. 2860-2860.

[170] Deane, J.A., et al., Localization of intraflagellar transport protein IFT52 identifies basal body transitional fibers as the docking site for IFT particles. Current Biology, 2001. **11**(20): p. 1586-1590.

[171] Bhogaraju, S., et al., Molecular Basis of Tubulin Transport Within the Cilium by IFT74 and IFT81. Science, 2013. **341**(6149): p. 1009-1012.

[172] Blacque, O.E., et al., Functional genomics of the cilium, a sensory organelle. Curr Biol, 2005. **15**(10): p. 935-941.

[173] Absalon, S., et al., Intraflagellar transport and functional analysis of genes required for flagellum formation in trypanosomes. Mol Biol Cell, 2008. **19**(3): p. 929-944.

[174] Avasthi, P., et al., Actin Is Required for IFT Regulation in *Chlamydomonas reinhardtii*. Current Biology, 2014. **24**(17): p. 2025-2032.

[175] Kuchka, M.R. and J.W. Jarvik, Short-Flagella Mutants of Chlamydomonas-Reinhardtii. Genetics, 1987. **115**(4): p. 685-691.

[176] Shogo Nakamura, H.T.a.M.K.K., Effect of Lithium on Flagllar Length in *Chlamydomonas reinhardtii*. Cell Structure and Function, 1987. **12**: p. 369-374.

[177] Jiang, X. and D. Stern, Mating and tetrad separation of *Chlamydomonas reinhardtii* for genetic analysis. J Vis Exp, 2009(30).

[178] Hayashi, I. and M. Ikura, Crystal structure of the amino-terminal microtubule-binding domain of end-binding protein 1 (EB1). J Biol Chem, 2003. **278**(38): p. 36430-36434.

[179] Cole, D.G., The intraflagellar transport machinery of *Chlamydomonas reinhardtii*. Traffic, 2003. **4**(7): p. 435-442.

[180] Blatch, G.L. and M. Lassle, The tetratricopeptide repeat: a structural motif mediating protein-protein interactions. Bioessays, 1999. **21**(11): p. 932-939.

[181] Das, A.K., P.W. Cohen, and D. Barford, The structure of the tetratricopeptide repeats of protein phosphatase 5: implications for TPR-mediated protein-protein interactions. EMBO J, 1998. **17**(5): p. 1192-1199.

[182] D'Andrea, L.D. and L. Regan, TPR proteins: the versatile helix. Trends Biochem Sci, 2003. **28**(12): p. 655-662.

[183] Allan, R.K. and T. Ratajczak, Versatile TPR domains accommodate different modes of target protein recognition and function. Cell Stress Chaperones, 2011. **16**(4): p. 353-367.

[184] Zhang, Q., et al., Knockdown of ttc26 disrupts ciliogenesis of the photoreceptor cells and the pronephros in zebrafish. Mol Biol Cell, 2012. **23**(16): p. 3069-78.

[185] Ishikawa, H., et al., Proteomic analysis of mammalian primary cilia. Curr Biol, 2012. **22**(5): p. 414-419.

[186] Liu, Q., et al., The proteome of the mouse photoreceptor sensory cilium complex. Mol Cell Proteomics, 2007. **6**(8): p. 1299-1317.

[187] Efimenko, E., et al., Analysis of xbx genes in *C. elegans*. Development, 2005. **132**(8): p. 1923-1934.

[188] Mukhopadhyay, S., et al., Trafficking to the primary cilium membrane. Mol Biol Cell, 2017. **28**(2): p. 233-239.

[189] Avidor-Reiss, T., et al., Decoding cilia function: defining specialized genes required for compartmentalized cilia biogenesis. Cell, 2004. **117**(4): p. 527-539.

[190] Li, J.B., et al., Comparative genomics identifies a flagellar and basal body proteome that includes the BBS5 human disease gene. Cell, 2004. **117**(4): p. 541-552.

[191] Grayson, C., et al., Localization in the human retina of the X-linked retinitis pigmentosa protein RP2, its homologue cofactor C and the RP2 interacting protein Arl3. Hum Mol Genet, 2002. **11**(24): p. 3065-3074.

[192] Veltel, S., et al., Specificity of Arl2/Arl3 signaling is mediated by a ternary Arl3-effector-GAP complex. FEBS Lett, 2008. **582**(17): p. 2501-2507.

[193] Zhang, Q., et al., GTP-binding of ARL-3 is activated by ARL-13 as a GEF and stabilized by UNC-119. Scientific Reports, 2016. **6**.

[194] Gotthardt, K., et al., A G-protein activation cascade from Arl13B to Arl3 and implications for ciliary targeting of lipidated proteins. Elife, 2015. **4**: p. e11859.

[195] Wright, K.J., et al., An ARL3-UNC119-RP2 GTPase cycle targets myristoylated NPHP3 to the primary cilium. Genes & Development, 2011. **25**(22): p. 2347-2360.

[196] Lokaj, M., et al., The Interaction of CCDC104/BARTL1 with Arl3 and Implications for Ciliary Function. Structure, 2015. **23**(11): p. 2122-2132.

[197] Linari, M., M. Hanzal-Bayer, and J. Becker, The delta subunit of rod specific cyclic GMP phosphodiesterase, PDE delta, interacts with the Arf-like protein Arl3 in a GTP specific manner. Febs Letters, 1999. **458**(1): p. 55-59.

[198] Cuvillier, A., et al., LdARL-3A, a Leishmania promastigote-specific ADP-ribosylation factor-like protein, is essential for flagellum integrity. J Cell Sci, 2000. **113 (Pt 11)**: p. 2065-2074.

[199] Hanke-Gogokhia, C., et al., Arf-like Protein 3 (ARL3) Regulates Protein Trafficking and Ciliogenesis in Mouse Photoreceptors. Journal of Biological Chemistry, 2016. **291**(13): p. 7142-7155.

[200] Ismail, S.A., et al., Structural basis for Arl3-specific release of myristoylated ciliary cargo from UNC119. EMBO J, 2012. **31**(20): p. 4085-4094.

[201] Caviglia, S., et al., Staccato/Unc-13-4 controls secretory lysosome-mediated lumen fusion during epithelial tube anastomosis. Nature Cell Biology, 2016. **18**(7): p. 727-739.

[202] Long, H., et al., Comparative Analysis of Ciliary Membranes and Ectosomes. Curr Biol, 2016. **26**(24): p. 3327-3335.

[203] Li, Y.J., et al., The small GTPases ARL-13 and ARL-3 coordinate intraflagellar transport and ciliogenesis. Journal of Cell Biology, 2010. **189**(6): p. 1039-1051.

[204] Schrick, J.J., et al., ADP-ribosylation factor-like 3 is involved in kidney and photoreceptor development. Am J Pathol, 2006. **168**(4): p. 1288-1298.

[205] Zhang, Q., J. Hu, and K. Ling, Molecular views of Arf-like small GTPases in cilia and ciliopathies. Exp Cell Res, 2013. **319**(15): p. 2316-2322.

[206] Wright, K.J., et al., An ARL3-UNC119-RP2 GTPase cycle targets myristoylated NPHP3 to the primary cilium. Genes Dev, 2011. **25**(22): p. 2347-2360.

[207] Ismail, S.A., et al., Arl2-GTP and Arl3-GTP regulate a GDI-like transport system for farnesylated cargo. Nat Chem Biol, 2011. **7**(12): p. 942-949.

[208] Watzlich, D., et al., The interplay between RPGR, PDEdelta and Arl2/3 regulate the ciliary targeting of farnesylated cargo. EMBO Rep, 2013. **14**(5): p. 465-472.

[209] Humbert, M.C., et al., ARL13B, PDE6D, and CEP164 form a functional network for INPP5E ciliary targeting. Proc Natl Acad Sci U S A, 2012. **109**(48): p. 19691-19696.

[210] Thomas, S., et al., A Homozygous PDE6D Mutation in Joubert Syndrome Impairs Targeting of Farnesylated INPP5E Protein to the Primary Cilium. Human Mutation, 2014. **35**(1): p. 137-146.

[211] Fansa, E.K., et al., PDE6 delta-mediated sorting of INPP5E into the cilium is determined by cargo-carrier affinity. Nature Communications, 2016. **7**.

[212] Wang, Q., J. Pan, and W.J. Snell, Intraflagellar transport particles participate directly in cilium-generated signaling in *Chlamydomonas*. Cell, 2006. **125**(3): p. 549-562.

[213] Huang, K., et al., Function and dynamics of PKD2 in *Chlamydomonas reinhardtii* flagella. Journal of Cell Biology, 2007. **179**(3): p. 501-514.

[214] Jiang, L., S.L. Rogers, and S.T. Crews, The Drosophila Dead end Arf-like3 GTPase controls vesicle trafficking during tracheal fusion cell morphogenesis. Dev Biol, 2007. **311**(2): p. 487-499.

[215] Li, Y., et al., The small GTPases ARL-13 and ARL-3 coordinate intraflagellar transport and ciliogenesis. J Cell Biol, 2010. **189**(6): p. 1039-1051.

[216] Hurd, T.W., S.L. Fan, and B.L. Margolis, Localization of retinitis pigmentosa 2 to cilia is regulated by Importin beta 2. Journal of Cell Science, 2011. **124**(5): p. 718-726.

[217] Keller, L.C., et al., Proteomic analysis of isolated *chlamydomonas* centrioles reveals orthologs of ciliary-disease genes. Curr Biol, 2005. **15**(12): p. 1090-8.

[218] Evans, R.J., et al., The retinitis pigmentosa protein RP2 links pericentriolar vesicle transport between the Golgi and the primary cilium. Hum Mol Genet, 2010. **19**(7): p. 1358-67.

[219] Bantscheff, M., et al., Quantitative mass spectrometry in proteomics: a critical review. Analytical and Bioanalytical Chemistry, 2007. **389**(4): p. 1017-1031.

[220] Latosinska, A., et al., Comparative Analysis of Label-Free and 8-Plex iTRAQ Approach for Quantitative Tissue Proteomic Analysis. Plos One, 2015. **10**(9).

[221] Wiese, S., et al., Protein labeling by iTRAQ: A new tool for quantitative mass spectrometry in proteome research. Proteomics, 2007. **7**(3): p. 340-350.

[222] Qattan, A.T., et al., Quantitative Organelle Proteomics of MCF-7 Breast Cancer Cells Reveals Multiple Subcellular Locations for Proteins in Cellular Functional Processes. Journal of Proteome Research, 2010. **9**(1): p. 495-508.

[223] Nakamura, T., K. Aoki, and M. Matsuda, Monitoring spatio-temporal regulation of Ras and Rho GTPases with GFP-based FRET probes. Methods, 2005. **37**(2): p. 146-153.

[224] Lam, A.J., et al., Improving FRET Dynamic Range with Bright Green and Red Fluorescent Proteins. Biophysical Journal, 2013. **104**(2): p. 683A-683A.

[225] Lechtreck, K.F., et al., Cycling of the signaling protein phospholipase D through cilia requires the BBSome only for the export phase. J Cell Biol, 2013. **201**(2): p. 249-61.

[226] Wessel, D. and U.I. Flugge, A Method for the Quantitative Recovery of Protein in Dilute-Solution in the Presence of Detergents and Lipids. Analytical Biochemistry, 1984. **138**(1): p. 141-143.

[227] Nozaki, S., et al., Regulation of ciliary retrograde protein trafficking by the Joubert syndrome proteins ARL13B and INPP5E. J Cell Sci, 2017. **130**(3): p. 563-576.

[228] Diener, D.R., P. Lupetti, and J.L. Rosenbaum, Proteomic analysis of isolated ciliary transition zones reveals the presence of ESCRT proteins. Curr Biol, 2015. **25**(3): p. 379-84.

[229] Pan, J., et al., Protein phosphorylation is a key event of flagellar disassembly revealed by analysis of flagellar phosphoproteins during flagellar shortening in *Chlamydomonas*. J Proteome Res, 2011. **10**(8): p. 3830-9.

[230] Wang, H.X., et al., The Global Phosphoproteome of *Chlamydomonas reinhardtii* Reveals Complex Organellar Phosphorylation in the Flagella and Thylakoid Membrane. Molecular & Cellular Proteomics, 2014. **13**(9): p. 2337-2353.

[231] Wang, Z., et al., Intraflagellar transport (IFT) protein IFT25 is a phosphoprotein component of IFT complex B and physically interacts with IFT27 in *Chlamydomonas*. PLoS One, 2009. **4**(5): p. e5384.

[232] Boesger, J., et al., Analysis of flagellar phosphoproteins from *Chlamydomonas reinhardtii*. Eukaryot Cell, 2009. **8**(7): p. 922-32.

[233] Hessel, J., et al., Intraflagellar transport gene expression associated with short cilia in smoking and COPD. PLoS One, 2014. **9**(1): p. e85453.

[234] Yang, C. and P. Yang, The flagellar motility of *Chlamydomonas* pf25 mutant lacking an AKAP-binding protein is overtly sensitive to medium conditions. Mol Biol Cell, 2006. **17**(1): p. 227-38.

APPENDIX

Table A-1. Antibodies used in this study

Antibody	Dilution		Reference or source
	WB	IF	
Anti-BBS4	1:1,500	NA	(Lechtreck et al., 2009)
Anti-CrDYF-3	1:1,000	NA	This Study
Anti-IFT172	1:50	1:10	(Cole et al., 1998)
Anti-IFT139	1:50	1:20	(Cole et al., 1998)
Anti-IFT122	1:1,000	1:100	(Behal et al., 2012)
Anti-IFT81	1:100	1:10	(Cole et al., 1998)
Anti-IFT74	1:8,000	NA	(Qin et al., 2004)
Anti-IFT70	1:1,000	NA	(Fan et al., 2010)
Anti-IFT57	1:50	NA	(Cole et al., 1998)
Anti-IFT56	1:1,000	NA	(Ishikawa et al., 2014)
Anti-IFT46	1:20,000	1:1,000	(Hou et al., 2007)
Anti-IFT20	1:500	NA	(Hou et al., 2007)
Anti-FLA10	1:5,000	1:1,000	(Cole et al., 1998)
Anti-FAP20	1:1,000	NA	(Yanagisawa et al., 2014)
Anti-MBO2	1:1,000	NA	(Tam and Lefebvre, 2002)
Anti-IC140	1:10,000	NA	(Yang and Sale, 1998)
Anti-IC138	1:20,000	NA	(Hendrickson et al., 2004)
Anti-IC97	1:2,000	NA	(Wirschell et al., 2009)
Anti-LC1	1:200	NA	(Benashski et al., 1999)
Anti-RSP3	1:200	NA	(Diener et al., 1993)
Anti-β-F1-ATPase	1:5,000	NA	Agrisera (AS05 085)
Anti-IC69	1:10,000	NA	Sigma (D6168)

IF, immunofluorescence; NA, not application; WB, Western blot.